Quantitative Modeling of the Rheology of Surfactant Wormlike Micelles

by

Grace X. Tan

A dissertation submitted in partial fulfillment
of the requirements for the degree of
Doctor of Philosophy
(Chemical Engineering)
in the University of Michigan
2022

Doctoral committee:

Professor Ronald G. Larson, Chair
Professor Emeritus Erdogan Gulari
Professor Emeritus Alan Wineman
Professor Robert Ziff

Grace X. Tan

gxtan@umich.edu

ORCID iD: 0000-0003-0876-8295

Dedication

To my family and friends, who heard everything they never knew

they wanted to know about my micelles

Acknowledgements

Firstly, I would like to thank my advisor, Professor Ronald G. Larson, for his guidance over the past five years. He may have gotten quite possibly the only person in my program who already knew Fortran, but I got to learn from his years of knowledge and experience, and I'll leave the doctoral program a much better researcher than when I began. I would also like to thank the other members of my committee, Professor Erdogan Gulari, Professor Alan Wineman, and Professor Robert Ziff for their support throughout my degree.

Additionally, I would like to thank the researchers I've had the pleasure of collaborating with. Thank you to Dr. Weizhong Zou for first teaching me about the pointer algorithm code in the Larson group; Mike Weaver at P&G for supporting our work and generating several of the experimental rheology data sets used in this thesis; Dr. Takeshi Sato at Kyoto University for his work validating the pointer algorithm, an effort that has helped to improve my thesis; and Anukta Datta and Tanmay Velidanda for letting me help out with their project one summer so I could say I didn't graduate without putting something in the rheometer. You were all great to work with; thank you for sharing your expertise with me.

I would also like to thank the members of the Larson group past and present for making the office a great place to work, especially my coworkers in the corner office, Dr. Sabina Wilkanowicz, Nisha Hollingsworth, and Alyssa Travitz. I'll miss our courtyard lunch breaks, field trips for snacks, and getting to hear about all your different areas of research.

Finally, thank you to the family and friends who have been with me throughout this process, from starting out as a chemical engineer learning to draw process diagrams to

graduating with my doctorate. To the classmates and roommates who sat through lectures, toiled through problem sets, and spent midnights in Olin with me, I wouldn't be here today if you hadn't kept my enjoyment of chemical engineering alive. To all the bands I've played with, most recently the Ann Arbor Concert Band, thank you for always being a space to step away from engineering for a while so that I would be ready to get back to work the next morning. Thank you to the friends who have followed me along this journey, for being there to listen from afar and for joining me on various adventures when we're together. Lastly, thank you to my parents and brother, for your continual support and for providing a place to call home.

Table of Contents

List of Tables

List of Figures

List of Appendices

Abstract

The use of surfactants in a variety of consumer and industrial products makes them an important class of molecules. Surfactants self-assemble, at high enough concentrations forming long wormlike micelles that impart a distinct viscoelasticity to solutions containing them. Understanding the rheology of such solutions is of interest from both an industrial and academic standpoint. Connecting the flow behavior of wormlike micellar solutions to the solution composition is done by modeling the underlying physics using a mesoscopic model previously developed in the Larson lab, the "pointer algorithm." The pointer algorithm has been shown to be capable of fitting experimental linear rheological data and extracting micelle parameters, such as the average micelle length and breakage time, from the data. Because of the self-assembled nature of micelles, direct measurement of their features, necessarily performed on diluted or modified solutions, changes the micelle properties. Thus, the only way to infer these properties in a non-diluted solution is from the rheology.

Here, the pointer algorithm is first validated using the more highly resolved slip-spring model and comparisons between the two simulation methods show good agreement at low numbers of entanglements. Next, the rheology of a series of surfactant solutions is fit and the extracted micelle parameters used to calculate scaling laws that describe how the micelle parameters change as a function of the surfactant concentration. Correlations that relate experimental rheological features to micelle parameters are also developed, providing a relatively fast and simple way to estimate micelle parameters directly from experimental data. These correlations, along with the pointer algorithm, are finally applied to a variety of surfactant

solutions from literature. In general, both using a pointer algorithm simulation to extract micelle parameters from the experimental rheology and estimating the micelle parameters from the correlations give good results, producing parameters consistent with the high viscosity and viscoelasticity of the solutions and predicted rheology that matches the experimental data well. The results show that the pointier algorithm is able to describe the linear rheology of a general wormlike micellar solution and that these surfactant solutions exhibit universality in their rheological behavior. The thesis also contains a user manual to help users learn to run the pointer algorithm software, which is made publicly available.

Chapter 1: Introduction

Introduction to surfactant solutions

Surfactants are a class of molecules that have important applications in areas ranging from biology to drug delivery, personal care products, and oil flow in pipelines [1]. They are amphiphilic, having a long hydrophobic tail and a hydrophilic head group. This property of surfactants means that in solution, they self-assemble into micelles that are spherical at low surfactant concentration and grow into rodlike, then wormlike micelles as concentration increases. It is generally understood that this change in microstructure is reflected in the viscosity of the solution. For example, a graph of the zero-shear viscosity plotted against salt concentration, a so-called "salt curve," shows the viscosity first increase as salt concentration increases, then reach a peak and decrease. Electron micrographs of sample solutions along the salt curve have shown imaging of spherical micelles at low concentration, followed by rodlike micelles, long wormlike micelles, branching past the viscosity peak, and finally vesicles at high salt concentration [2–4]. What is not as well understood is the quantitative effect of salt, or surfactant, concentration on the solution's viscosity and other macroscopic flow properties, e.g. the rheology of such solutions, particularly at concentrations where entangled wormlike micelles are present. This is an important area of study for the formulation of commercial personal care products such as shampoos and detergents where understanding the relation between a solution's composition and its flow behavior is beneficial for product design and development.

One way to make the connection between solution composition and rheology is by modeling these solutions at the microstructural scale. If the model correctly captures the

underlying physics of surfactant micellar solutions, it can be used to determine the relationship between composition and microscopic properties such as the length of the micelles, which can then predict the rheology of solutions at different salt or surfactant concentrations. There are, however, multiple challenges in modelling micellar solutions. Firstly, the relevant length scales in surfactant solutions span several orders of magnitude. At the surfactant level, the tail length of a surfactant molecule sets the radius of the micelles, which is usually found to be around 2 nm. Overall, wormlike micelles are flexible, but locally, the micelles behave like elastic rods or beams. The micelle stiffness is quantified by the persistence length, l_p, where at lengths less than l_p the micelle is like a rigid rod and at lengths greater than l_p the micelle can bend. The persistence length depends on the identities and concentrations of the surfactant and salt and varies from 20-100 nm. As wormlike micelles grow, they entangle with each other like strands of spaghetti in a bowl; the entanglements can be described by an entanglement length, l_e, that is the average distance between entanglements along a micelle, and is typically 100s of nanometers. Finally, the longest length scale to consider is the contour length of the micelle (the average micelle length is denoted as $\langle L \rangle$), which can be several microns or longer.

From a computational perspective, the range in length scales creates difficulties in simulating these solutions. In general, the smaller the length scale that needs to be simulated, the smaller the simulation time step. For example, an all-atom molecular dynamics simulation, in which every atom is individually modeled on a scale of 0.1 nm (10^{-10} m), has a time step on the order of a femtosecond, or 10^{-15} seconds, making it very difficult to reach even a second of real time. Wormlike micellar solutions, with contour lengths on the order of a micron (10^{-6} m) or greater, can take several seconds to relax, so it is evident that some level of coarse-graining or a mesoscopic model is necessary to model these solutions. This model, however, will still need to

be able to account for relaxation processes apparent in experimental rheological measurements that result from the smaller length scales in the system.

Physically, the different lengths result in surfactant wormlike micellar solutions exhibiting somewhat complex rheology that cannot fully be described by simple viscoelastic models such as the Maxwell model. Figure 1.1 shows the linear oscillatory shear rheology of a typical wormlike micellar solution, including several features that a model will need to capture. At low frequency, the micelles relax similarly to a Maxwell fluid, with the storage modulus G'(ω) and loss modulus G"(ω) having terminal slopes (on a log-log plot) of 2 and 1 respectively. At intermediate frequency, the loss modulus exhibits a minimum, marked as G''_{min} in Figure 1.1, while the storage modulus grows slowly and is approximately constant. At high frequency, both G' and G" eventually reach a slope of 3/4. Additionally, there are two crossover frequencies, one at low frequency and one at high frequency, ω_{c1} and ω_{c2}, where G' and G" intersect. A model for wormlike micelle solutions will need to be able to describe all of these rheological features.

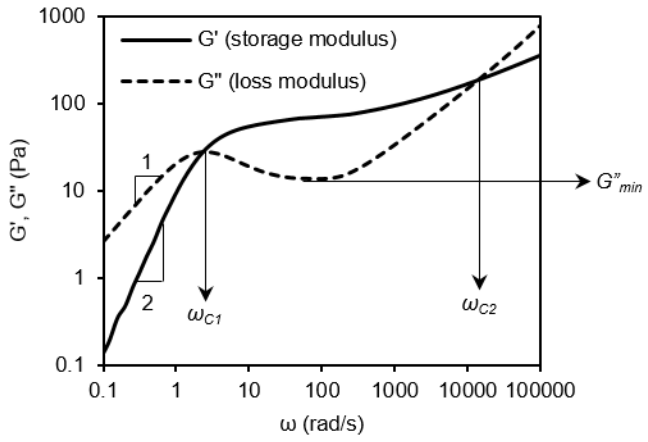

Figure 1.1: Example surfactant rheology curves with rheological features denoted.

Modeling surfactant solutions

To construct a simulation capable of modeling the rheology of surfactant solutions, we first see if there is an existing model that we can modify or add features to. We already determined that the Maxwell model, one of the simplest models for a viscoelastic fluid, does not describe surfactant solution rheology across the entire frequency range. The addition of a viscous term to the storage modulus introduces a minimum in G", but the high-frequency rheology is still not modeled correctly. Furthermore, the fitting parameters of the Maxwell model are chosen solely to best fit the experimental data and are unrelated to the physical microstructural properties like the contour and persistence lengths of the micelles.

Instead, we take advantage of the similarity between surfactant micelles and polymers and adapt more well established polymer theory to micelles. Like polymers, surfactant micelles are long and flexible and entangle with each other, resulting in viscoelastic solutions whose rheology often share several qualitative features, including low-frequency Maxwell fluid-like relaxation, a minimum in G", and two crossover frequencies. On the other hand, unlike monomers that chemically bond to form polymers, surfactant molecules self-assemble in a reversible process depending on hydrophobic and electrostatic interactions. Surfactant micelles can therefore reversibly break and rejoin while polymers are fixed in length. Polymers can also be synthesized to create an ensemble with a single, or close to single, molecular weight while the thermodynamic equilibrium length distribution for micelles is exponential. The aim is then to find a model for polymer rheology to which reversible breakage and rejoining and an exponential length distribution can be added.

The Cates theory is one such model [5]. Reptation theory was originally developed by de Gennes to describe the mobility of a polymer chain surrounded by fixed obstacles. de Gennes hypothesized that the surrounding obstacles would confine the polymer chain to a tube so that the polymer would relax by diffusing, i.e. reptating, in one dimension along the tube [6]. Doi and Edwards later expanded on the reptation theory to develop constitutive equations for the rheology of polymer melts or concentrated solutions containing entangled polymers [7,8]. Further modifications to the Doi and Edwards tube theory have been shown to be able to model rheological behaviors of polymer solutions such as steady shear, shear startup, and uniaxial elongation [9]. Cates took the reptation theory, accounted for an exponential length distribution of micelles, and added reversible breakage and rejoining. He was then able to generate viscosity and stress relaxation curves at varying breakage to reptation time ratios consistent with the multiexponential relaxation expected of micelles with a distribution of lengths [5]. Later, Turner and Cates used the model to perform numerical simulations and produced a series of stress relaxation curves that agreed qualitatively with experimental data [10]. Additional work by Granek and Cates then allowed the development of a semi-quantitative equation that could be used to estimate the micelle length from rheological data [11]. This result is important for the characterization of surfactant solutions because the microscopic micelle parameters are difficult to measure directly and must be inferred from rheology.

Unlike polymers, which have a fixed length after synthesis and can be diluted or change temperature without being physically altered, the self-assembled nature of micelles means that changing the experimental conditions changes the micelles themselves, in particular their average length. This indicates that any experimental method that requires modifying the surfactant solution unavoidably changes the micelles in the solution. For example, small-angle

neutron scattering (SANS) experiments have been used to determine micelle lengths, but the experiments are best performed on dilute solutions where the micelles are short and do not overlap. Once the micelles overlap, screening makes it difficult to differentiate micelle contour lengths, especially micelles that are longer than the maximum resolution of SANS, which is usually a couple hundred nanometers. Surfactant solutions with measurable rheology are typically at concentrations high enough that the micelles are entangled and overlap significantly, so that the options are to either dilute the solution, in which case the micelles decrease in length and are no longer representative of their length in the original solution, or perform SANS on solutions with a high degree of screening that obscures the full micelle contour length. Similarly, direct visualization of the micelles through cryo-TEM requires the formation of a thin film, so the micelles are no longer in solution when viewed. While cryo-TEM can provide some qualitative information on the micelle structure and length, it is difficult to make any quantitative conclusions about their properties. Thus, rheological models seem to be the best way to infer micelle properties in surfactant solutions containing entangled micelles.

The Cates theory is still a promising basis for a model of surfactant micelle rheology, but it has several limitations that need to be considered when adapting it. Firstly, the scaling relation developed by Granek and Cates is semiquantitative; the prefactor is assumed to be 1. The scaling relation is also based on the limit where the breakage time for a micelle of average length is much longer than the Rouse time of a micelle segment as long as the entanglement length ($\tau_{br} >> \tau_e$), which Granek and Cates suggest is usually true when the micelles are long and strongly entangled and the ratio G_0/G''_{min} of the plateau modulus to the value of G" at its local minimum is high. [11] This makes the scaling relation most accurate for more concentrated solutions while less concentrated solutions may not be able to be described as precisely. However, even for fairly

concentrated solutions expected to contain well-entangled micelles, the scaling relation with prefactor unity sometimes estimates the micelle length to be under a micron, which seems too short considering the high viscosity of some of these surfactant solutions [12–14]. The micelle lengths calculated from the Cates scaling relation also can be predicted to decrease as surfactant concentration increases, the opposite of what is expected to happen [15]. An example of this can be seen below in Table 2.1. Additionally, the micelles are assumed to be loosely entangled, i.e. the entanglement length l_e is longer than the persistence length l_p, which may not always be true, and we may want to be able to model tightly entangled micelles ($l_e < l_p$) as well. Finally, the high-frequency rheology predicted by the Cates theory shows G' and G" coinciding at high frequency (see Figure 6 in Granek and Cates [11]), but experimental data such as in Figure 1.1 do not show G' and G" overlapping at high frequency. When we modify the Cates model, we therefore look for ways to model a range of concentrations encompassing weakly to well-entangled micelles, better match the predicted high-frequency rheology to experimental data, and model both loosely and tightly entangled micelles. After developing this model, we can determine if we recover a Cates-like scaling relation for the micelle length, perhaps with a prefactor differing from unity.

The Pointer Algorithm

Previously in the Larson lab, a mesoscopic simulation, the "pointer algorithm," was developed to address the points above and model the rheology of surfactant micellar solutions. Full details of the simulation can be found in [16,17]; here the key features of the pointer algorithm will be summarized. A mesoscopic simulation in which an ensemble of micelles, but not individual surfactant molecules, is generated, was chosen to access the time scale of several

seconds necessary to model low-frequency rheology. To model the different relaxation processes over the length scales of the micelles, multiple additional relaxation modes were included in the simulation.

At low frequency, where reptation is the main relaxation mechanism, the Cates theory was adapted into the simulation. When the simulation starts, the micelles are unrelaxed; the simulation runs until the micelles are relaxed. At each simulation time step, every micelle in the ensemble randomly moves a calculated distance left or right within its confining tube. The unrelaxed percentage of the micelle still in its original tube is tracked. At time steps where breakage or rejoining, determined by the breakage time, occurs, either a micelle is chosen to break at a random point along its length or two micelles are chosen to combine. During the reptation portion of the simulation, the micelle ends further relax because of contour length fluctuations (CLF), which are calculated and added to the reptation distance. While individual micelles reptate and relax, all the surrounding micelles are also moving, a process that speeds up relaxation known as constraint release (CR). Constraint release is accounted for in the pointer algorithm by double reptation, so the contribution to relaxation from reptation is squared. The stress relaxation curve can then be constructed from the unrelaxed fraction of micelles as a function of time and converted into the frequency domain to determine the impact of reptation on the rheology of the solution.

After reptation with CLFs and CR is simulated, the contributions from higher frequency relaxation modes are added analytically. These relaxation modes, Rouse and bending modes, are again borrowed from polymer theory. Rouse modes were originally derived for a single polymer chain (or a polymer chain in a dilute solution) relaxing in solution [18]. However, for polymer melts or concentrated solutions where the chains are entangled and can no longer move freely,

the Rouse modes become fractionated into relaxation parallel to the tube and relaxation perpendicular to the tube [19,20]. Because of entanglements slowing down motion along the tube, the perpendicular relaxation modes are known as "fast Rouse modes" and the slower parallel relaxation modes as "longitudinal Rouse modes." Since micelles experience similar entanglement to polymers, we expect Rouse modes to also be relevant to our surfactant solutions and add the fast Rouse modes to the simulation, assuming that there are enough entanglements that they damp out the effects of the longitudinal Rouse modes. [16] The fast Rouse modes are given by Eq. 1.1, and can be calculated from the values of the micelle parameters.

$$G'(\omega) = G_0 \frac{5}{4} \sum_i \frac{\phi_i}{Z_i} \sum_{p=Z_i}^{N_e Z_i} \frac{(\omega\tau_e)^2}{(\omega\tau_e)^2 + 4(p/Z_i)^4}$$

$$G'(\omega) = G_0 \frac{5}{4} \sum_i \frac{\phi_i}{Z_i} \sum_{p=Z_i}^{N_e Z_i} \frac{(\omega\tau_e)^2}{(\omega\tau_e)^2 + 4(p/Z_i)^4} \qquad (1.1)$$

where ϕ_i is the volume fraction of micelles of length i, τ_e is the Rouse time of a micelle between entanglements, and Z_i is the number of entanglements in a micelle of length i.

Rouse modes contribute to relaxation on a length scale around the entanglement length; at even shorter length and higher frequency, bending modes become important. Similarly to the Rouse modes, they are calculated from an equation (Eq. 1.2) and added analytically to the simulation. [21] Bending modes describe the relaxation of a rigid rod, which micelles behave like at lengths smaller than the persistence length. While Rouse modes were considered by the Cates theory, the effects of bending modes were not, and this addition improves the rheology modeling at high frequency.

$$G'(\omega) = Re\left[i^{3/4}\right] \frac{\rho}{15} \frac{2^{3/4} k_B T}{l_p} \left(\omega\tau_p\right)^{3/4}$$

$$G^{"}(\omega) = Im\left[i^{3/4}\right]\frac{\rho}{15}\frac{2^{3/4}k_BT}{l_p}\left(\omega\tau_p\right)^{3/4} + \omega\eta_s \qquad (1.2)$$

where τ_p is the relaxation time for a micelle segment as long as the persistence length.

To further account for relaxation processes from short, unentangled micelles (in Eqs. 1.1 and 1.2 micelles shorter than the entanglement length make no contribution to relaxation), a later modification to the pointer algorithm, Rouse, bending, and rotary relaxation modes for unentangled micelles were added analytically. These relaxation modes are similar to Eqs. 1.1 and 1.2 and their equations are given fully in [17].

Once all the contributions to relaxation have been simulated and calculated, the final rheology curves can be calculated and compared to experimental data. Based on the difference between the predicted simulation and experimental curves, the micelle parameters are adjusted. For example, if the ratio of G'_{min} to G''_{min} is smaller for the simulation rheological curves than in the experimental data, that indicates that the micelles in the simulation are too short and not entangled enough, so the micelle length is increased for the next iteration. Iterations of the simulation are run, modifying the micelle parameters at the end of each iteration based on a comparison to the experimental data, until the simulation rheology curves match the experimental data to within a pre-set error. In this way, the pointer algorithm is able to extract micelle parameters from experimental rheological data.

Overview

In this work, we apply the pointer algorithm toward the goal of understanding the relationship between surfactant solution composition and rheology. Chapter 2 begins by first comparing pointer algorithm simulations to slip-spring simulations. Because of the difficulties of directly measuring micelle properties in solution as discussed above, alternate means of

validating the pointer algorithm must be used. The slip-spring model, developed by Likhtman [22], has been shown to be able to describe the rheology of entangled polymer solutions well. It was modified to model surfactant solutions by adding reversible breakage and rejoining [23]. When we compare these slip-spring simulations with pointer algorithm results at a variety of numbers of entanglements and breakage to reptation time ratios, we find good agreement between the two simulation methods, helping to validate the rheological predictions of the pointer algorithm and the micelle parameters that we extract from rheology. Once the pointer algorithm has been validated, we study a series of surfactant solutions at constant counterion concentration and varying surfactant concentration. After using the pointer algorithm to fit the rheology of these solutions, we calculate scaling relations that describe how the micelle parameters vary with surfactant concentration and compare them to theoretically predicted scalings. We also construct correlations that allow micelle parameters to be directly estimated from rheological data, which we use in chapter 3 to investigate other surfactant systems in literature.

Chapter 3 considers solutions of a variety of different salts and surfactants found in literature. The pointer algorithm and the correlations derived from it are used to fit the rheology of these solutions and directly predict micelle parameters from the experimental data. The correlations allow the pointer algorithm to be applied to a greater range of solutions, including solutions with weakly entangled micelles that have rheology without enough features to fit and solutions with very highly entangled micelles that are too long to run iterative pointer algorithm simulations. Our results, showing that the pointer algorithm can describe the rheology of a variety of salt and surfactant systems, demonstrates some universality in surfactant solution rheology and that the relaxation modes considered are independent of surfactant or salt identity.

In chapter 4, the pointer algorithm code is documented with a user manual. Instructions for running pointer algorithm simulations are given so that other researchers can use the pointer algorithm in their own work and example simulations are provided as a guide. Chapter 5 summarizes and concludes this work.

Chapter 2: Determining Threadlike Micelle Lengths from Rheometry

Abstract: We show that the average length $\langle L \rangle$ of threadlike micelles in surfactant solutions predicted by fitting results of a mesoscopic simulation, the "pointer algorithm," to experimental G'(ω), G"(ω) data, is longer than, and more accurate than, that from a scaling law that equates $\langle L \rangle / l_e$ to the modulus ratio G_0/G''_{min}. Here G_0 is the plateau modulus, G''_{min} is obtained at the local minimum in G", and l_e is the entanglement length. The accuracy of the pointer algorithm is supported by the agreement of its predictions with results from a recent application of the slip-spring simulation method to threadlike micelles. Improved fits of the pointer algorithm to the slip-spring results are obtained for weakly entangled micelles (with average number of entanglements $Z < 15$) if the full spectrum of Rouse modes is included in the description rather than just the high-frequency modes included in an earlier version. For sodium laureth-1 sulfate (SLE1S) and cocamidopropyl betaine (CAPB) in NaCl solutions, we find scaling relations for micelle length, the plateau modulus, and the persistence length that are in rough agreement with the predictions of mean field theory and with the modified scaling relation in which $\langle L \rangle / l_e$ is raised to the 0.82 power, rather than unity, that we recommend as an improvement to the original scaling law.

Introduction

Surfactant molecules are used in a variety of industrial and personal care products due to their drag-reduction properties and ability to encapsulate and solubilize hydrophobic molecules

in water [1,24]. In solution, they self-assemble, at high enough concentrations forming long wormlike micelles that impart a distinct viscoelastic behavior to the solutions. Understanding the relationship between the microscopic and macroscopic features of these micellar solutions, for example between the average micelle length and the macroscopic rheology, has remained a problem of particular interest, especially since such properties are very hard to measure except through their influence on rheology.

The first proposed method for determining the micelle length from rheology is the *Cates method* [12–14], which is based on *Cates theory* [5] for the dynamics and linear rheology of entangled threadlike micelles. The Cates theory, adapted from the reptation theory for entangled polymers, takes the micelles to be contained in a "tube" formed by surrounding micelles, and to relax by diffusing (or "reptating") along, and eventually out of, the tube. However, unlike polymers, micelles can also reversibly break and rejoin, and the Cates theory adds this mechanism to reptation to obtain its predictions of rheology.

The pointer algorithm is a numerical implementation of the Cates theory that simulates an ensemble of breaking and rejoining micelles with the exponential length distribution expected from random breakage [17]. It allows predictions to be obtained from the Cates theory over a broader range of conditions than allowed by the earlier analyses of the theory, and allows some additional physics to be introduced. In the pointer algorithm, at each simulation time step, a micelle can slide randomly a pre-calculated distance along its tube, and the fraction of the micelle that remains unrelaxed is then updated. A fraction of these micelles will also randomly break or re-join at each time step, as determined by the breakage/re-joining rate. The reptation process accounts for relaxation at low frequencies. At higher frequencies, other mechanisms become important, including Rouse and bending modes, which are added analytically to the

relaxation modulus determined by the simulation. Given measured storage and loss moduli versus frequency, G'(ω) and G"(ω), micelle parameters, including the micelle length, can be determined from the pointer algorithm by iteratively adjusting them to give a best fit to G'(ω) and G"(ω). Full details of the pointer algorithm and the method of fitting its predictions to rheological data can be found in previous work [16,17].

In this work, we show that micelle lengths estimated from fits of the pointer algorithm to linear rheology significantly improve upon those obtained from the *Cates method,* which gives highly approximate estimates of lengths from the Cates theory. The Cates method uses a scaling law that relates the micelle average length $\langle L \rangle$ to the ratio G_0/G''_{min} where G_0 is the plateau modulus, and G''_{min} is G" at the frequency ω_{min} at which G" is a local minimum. We argue here that the micelle length estimates from the pointer algorithm are superior to those from the Cates method, in the following ways: 1) the longer micelle lengths from the pointer algorithm are more consistent with the high viscoelasticity and viscosity exhibited by the surfactant solutions; 2) lengths from the pointer algorithm are more consistent with extrapolations of lengths obtained from dilute solution rheometry of the same surfactant; and 3) predictions of the pointer algorithm agree better with those from a more microscopic slip-spring simulation model. We also give a modification of the Cates scaling law that matches more closely the predictions of the pointer algorithm and that can be used to obtain more accurate estimates of micelle length.

Details of Cates Method and Pointer Algorithm

In the Cates theory, the stress relaxation of "living polymers," such as surfactant micelles, is modeled using equations that account for reptation and reversible breakage and rejoining of micelles [5]. Later work [11] also considered the effect of contour-length fluctuations, or

"breathing," as well as Rouse modes, on the stress relaxation. In addition, Cates developed from his theory a scaling relationship linking rheology to average micelle length, namely $\frac{G_0}{G''_{min}} \sim \frac{\langle L \rangle}{l_e}$ where l_e is the "entanglement length," the length of the micelle per entanglement, and other parameters are defined above. Since G_0 and G''_{min} are reasonably easy to obtain experimentally, if l_e is known, and if we take the prefactor to be unity, this scaling relation provides a way to estimate the average micelle length, a property that can otherwise be difficult to determine. In a good solvent, the entanglement length is approximated by $l_e \cong \xi^{\frac{5}{3}}/l_p^{\frac{2}{3}}$ where ξ is the correlation length and l_p is the persistence length. For "loosely entangled" micelles $(l_e/l_p > 1)$, ξ can be estimated by $\xi \sim \left(\frac{k_B T}{G_0}\right)^{\frac{1}{3}}$ [12], where, again, the prefactor is typically taken to be unity. Thus, if the persistence length is known from another experimental method, such as small-angle neutron scattering (SANS) [25], diffusing wave spectroscopy (DWS) [26], or rheo-optics [27], and G_0 and G''_{min} are determined from rheology, then $\langle L \rangle$ can be calculated using the relationships above. Here, the use of the above scaling formulas for micelles lengths and other parameters will be referred to as the "*Cates method*," distinguishing it from the more general "Cates theory," which gives a comprehensive model of dynamics and linear rheology of worm-like micelles.

Alternatively to the Cates *method*, the pointer algorithm (which is itself based on the Cates *theory*) can give the average micelle length through an iterative fitting procedure, as mentioned above. In this method, reptation, breakage, and rejoining are simulated for an ensemble of micelles, and then high-frequency relaxation mechanisms – Rouse and bending modes – are added analytically. Iterating to minimize the error between the simulated experimental G' and G" curves, micelle parameter values are determined that best fit experimental data. The pointer algorithm offers the following advantages over the Cates method:

1) The average micelle length $\langle L \rangle$ is not calculated directly from a single rheological feature (i.e., G_0/G''_{min}) at a single frequency ω_{min}, but is obtained by fitting the entire frequency dependence of the rheology, making the result less sensitive to errors in either experimental data or the Cates theory at this frequency. Since the micelle length should have its greatest influence in the terminal region well below the frequency ω_{min}, fitting the rheology over the entire frequency range should be a more robust method of extracting $\langle L \rangle$.

2) The plateau modulus G_0 is also a fitting parameter whose value is determined simultaneously with $\langle L \rangle$ from the same fitting of the pointer-algorithm predictions to data. This differs from work by Cates and Turner [10], where G_0 was estimated by extrapolating the linear region of a "Cole-Cole" plot to high frequency. Other methods used in the literature to obtain G_0 include fitting the semi-circular region of a Cole-Cole plot [28], fitting G' and G" to one or two Maxwell elements [14], or using the value of G' at the frequency where G" has its minimum [26]. However, for moderately- to lightly-entangled micelles where G' never clearly flattens but continuously increases with frequency, these methods likely underestimate G_0.

3) In the pointer algorithm the plateau modulus is related to the correlation length by a "crossover formula" [16] that allows for consideration of both tightly and loosely entangled micelles and the intermediate region between these limits. Since most solutions of entangled micelles are in this crossover region while the Cates method assumes that the micelles are in the loosely entangled region, the pointer algorithm treats entanglements more realistically than does the Cates method. Even in the loosely entangled region, the pointer algorithm introduces a prefactor A (discussed later) into the scaling law $\xi \sim A(k_B T/G_0)^{\frac{1}{3}}$, whose value is derived from well-established correlations for polymer solutions and melts [16].

4) If data are available at high enough frequency to encompass a second crossover of G' and G", the persistence length can also be determined as a fitting parameter in the pointer algorithm simulations; otherwise, the persistence length is an input parameter. The frequency required to reach the second crossover is typically up to 10^5 rad/s, usually obtained from diffusing-wave spectroscopy (DWS).

5) The accuracy of the pointer algorithm can be validated by showing (in what follows) that its predictions of G' and G" match, using the same parameter values, the results from a more microscopic slip-spring simulation, details of which can be found elsewhere [23].

Experimental Materials and Methods

The experimental data are for mixed surfactant solutions containing sodium laureth-1 sulfate (SLE1S) and cocamidopropyl betaine (CAPB) of varying concentration with added NaCl, such that the total sodium ion concentration, including the counterions of SLE1S, is held constant at $[Na^+] = 0.70$ M. The weight ratio of SLE1S to CAPB is 8.65 and the total volume fraction of surfactant lies in the range $\varphi = 0.015$-0.09. These solutions were prepared in D_2O with 0.5 wt% of 630 nm polystyrene latex beads for DWS analysis for the high frequency portion of the rheological spectrum. The added beads do not measurably affect the zero shear viscosity. The high frequency data measured using DWS are shifted vertically to merge smoothly with the mechanical rheology [17].

A second set of data contains only SLE1S ($\varphi = 0.067$-0.14) and NaCl (3.1 wt%) in D_2O. The rheology for these solutions are obtained from mechanical rheometry and no high frequency data are available. All data for both sets of solutions are taken at 25 C.

Experimental values for the specific viscosity (defined as $\eta_{sp} = \frac{\eta_0 - \eta_s}{\eta_s}$, where η_0 is the zero-shear solution viscosity and η_s is the viscosity of the pure solvent) is also obtained along with the modulus curves. At low concentrations, when the viscosity is low, the zero shear viscosity η_0 is found by steady-state shear using a single-wall, Couette geometry and shear rates from 20 to 0.05 s^{-1}. The zero shear viscosity is extracted in the limit of the low-shear viscosity plateau. At high enough concentrations, η_0 is extracted from the complex viscosity plateau in the low frequency limit of a frequency sweep experiment. The solvent viscosity is determined using a rolling ball rheometer.

Results and Discussion

Anomalously Small Micelle Lengths from Rheology Using the Cates Method

Although the simplicity of the Cates method makes it a relatively fast way to determine the micelle length, in some cases, as discussed below, the calculated length is much shorter than might be expected based on the viscosity of the solution. Even more suspiciously, the micelle lengths predicted by the Cates method can sometimes actually decrease as the surfactant concentration increases, the opposite of the expected behavior predicted by simple laws of mass action (unless somehow concentration-dependent electrostatic interactions reverse this dependence). This anomalous inverted relationship between micelle length and concentration can be seen for our series of solutions containing mixed SLE1S and CAPB surfactants. Figure 2.1a shows the rheological data for a few of these solutions. As the surfactant concentration increases, G' and G" increase and the minimum in G" (which is used in the Cates method) appears and becomes deeper; the terminal relaxation time, calculated as the inverse of the first crossover frequency, increases. All of these features indicate that wormlike micelles are present that, at 5%

and 10% concentrations, have become long and entangled. This conclusion is reinforced by a plot of the specific viscosity η_{sp} versus volume fraction φ in Figure 2.2. Figure 2.2 shows data for SLE1S solutions, without CAPB, and with constant added NaCl concentration (3.1 wt%), but the rheology for these solutions, shown in Figure 2.1b, is similar to that of the mixed surfactant solutions (Figure 2.1a), for which wormlike micelles are also expected to be present. Notice in Figure 2.2 that η_{sp} rises slowly with φ at low concentrations below about 1%, followed by a much steeper rise at higher concentrations. Figure 2.2 has a very similar appearance to corresponding plots of viscosity versus concentration for polymers solutions, such as that shown in Figs. 8.11 and 9.10 of Rubinstein and Colby [29]. For polymers, the region of steep increase in viscosity corresponds to a regime of well entangled micelles, suggesting that the micelles are long enough to be entangled at concentrations above 1%, and become longer still at concentrations approaching 10%.

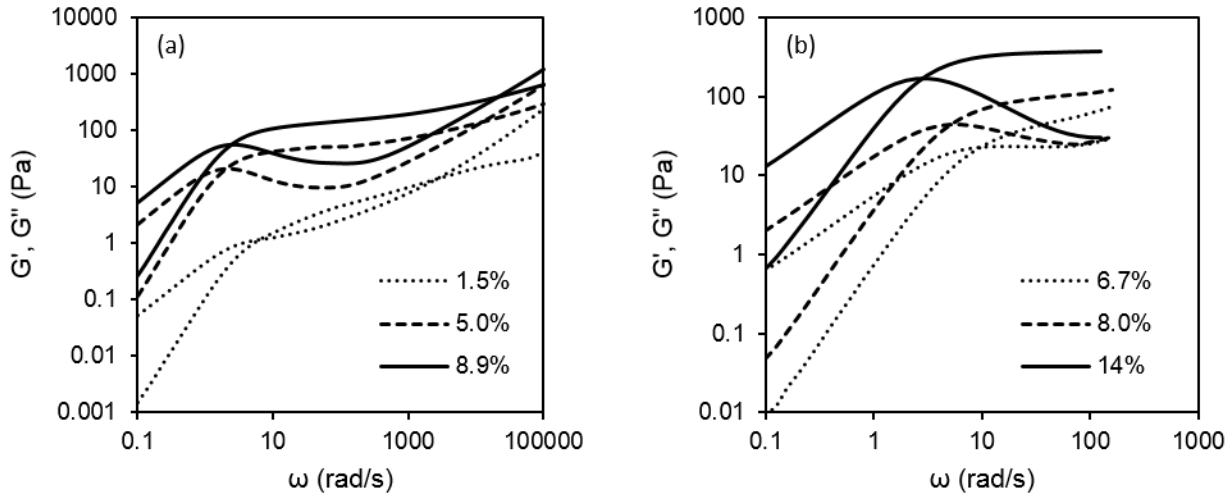

Figure 2.1: Example rheological data at various surfactant volume fractions shown in the legends. (a) SLE1S/CAPB at constant sodium ion concentration, $[Na^+]$ = 0.7 M and (b) SLE1S at constant added salt, NaCl = 3.1 wt%.

However, Table 2.1a shows that the micelle lengths calculated from the mixed surfactant data in Figure 2.1a using the Cates method are very short, ≤ 200 nm, and decrease to a length ≈ 100 nm, with increasing concentration. We use in these calculations a previously determined persistence length of 70 nm [30], and approximate the plateau modulus as G'_{min}, the value of G' at the minimum in G". The resulting micelle lengths are shorter than expected, having, on average, only $Z = \langle L \rangle / l_e$ = 3-6 entanglements, which would make them lightly entangled, and in entangled polymers, the rapid 3.4 power-law increase in viscosity with Z typically occurs only for Z > 2-4 [29]. Given that the zero-shear viscosities are thousands of times higher than the viscosity of water, and that the inverse of the low-frequency cross-over frequency indicates a relaxation time near 1 s, it seems unlikely that micelles would be that short and still show such high values of the solution viscosity and relaxation time.

To make these arguments more quantitative, we note firstly, that, the reptation times for the SLE1S/CAPB micelles predicted by the Cates method are approximately 0.001 s, much shorter than the relaxation times (~1 s) indicated by the terminal crossover frequency. The reptation time is calculated from $\tau_{rep} = \frac{2<L>^3}{\pi^2 \alpha D_0}$, where $\alpha \equiv l_e/l_p$ is the ratio of entanglement length to persistence length, the diffusivity is given by $D_0 = \frac{k_B T}{\varsigma}$ with the drag coefficient for a cylinder given by $\varsigma = \frac{2\pi\eta_s}{\ln(\xi/d)}$, and η_s the solvent viscosity (around 1 cP), d the micelle diameter (4 nm), and ξ the correlation length (30-80 nm). Additionally, the experimental zero-shear viscosities at high concentrations in Table 2.1a are orders of magnitude higher than the viscosities we infer for solutions with micelles less than a micron in length from the slip-spring model, as shown later. The slip-spring model has been well validated by Likhtman for slightly and densely entangled polymers, and so estimates of viscosity from the slip-spring model should

be reasonably accurate, and yet are much lower than the experimental values if micelles are less than a micron in length. For example, in one of our comparisons with the slip-spring model, a solution with 0.84 μm-long micelles at a surfactant volume fraction of 0.01, has a predicted zero-shear viscosity of 0.075 Pa·s, about an order of magnitude smaller than that of even the most dilute solution in Table 2.1a. While perhaps not definitive, these arguments strongly suggest that the micelle lengths estimated by the Cates method are too short.

Table 2.1a: Experimental rheological parameters and micelle lengths calculated from the Cates method for SLE1S/CAPB at $[Na^+]$ = 0.7 M.

ϕ	$G_0 \approx G'_{min}$ (Pa)	G''_{min} (Pa)	l_e (nm)	$\langle L \rangle$ (μm)	η_0 (Pa·s)
0.015*					0.526
0.020*					1.14
0.025	8.48	3.55	84.9	0.202	2.82
0.030	13.0	5.07	66.9	0.172	4.43
0.040	28.0	7.60	43.7	0.161	10.5
0.050	47.3	10.7	32.7	0.145	17.0
0.050	49.9	9.72	31.7	0.163	21.7
0.060	69.9	13.8	26.3	0.133	26.1
0.070	95.9	16.6	22.1	0.127	38.5
0.075	106	18.9	20.8	0.117	41.2
0.079	125	22.7	19.0	0.105	43.3
0.089	150	26.2	17.2	0.098	52.9

*These data sets have no minimum in G" (see 1.5% solution in Figure 2.1).

Table 2.1b: Experimental rheological parameters and micelle lengths calculated from the Cates method for SLE1S at NaCl = 3.1 wt%.

ϕ	$G_0 \approx G'_{min}$ (Pa)	G''_{min} (Pa)	l_e (nm)	$\langle L \rangle$ (μm)	η_0 (Pa·s)
0.067	45.6	23.2	33.3	0.066	5.45
0.080	105.2	25.0	20.9	0.088	17.5
0.11	248.1	27.3	13.0	0.118	67.1
0.14	370.3	30.4	10.4	0.127	113

In fact, Granek and Cates [11] first proposed the relationship $\frac{G_0}{G''_{min}} \sim \frac{\langle L \rangle}{l_e}$ as a scaling relationship and simply chose a prefactor of unity to estimate specific values of the micelle length from literature data. They also remarked that micelle lengths will be underestimated if the timescale for micelle breakage and rejoining is on the same order of magnitude as the entanglement time, as seems to be the case for the experimental data discussed above.

Exploiting the similarity between Figure 2.2 and the corresponding data for polymer solutions, we can use the known scaling laws relating polymer length to viscosity, along with neutron scattering data in the dilute regime, to help estimate the lengths of threadlike micelles. Of course, threadlike micelles dynamically break and fuse, while polymers do not. Since for fixed average micelle length, breakage/scission *decreases* the viscosity of the micellar solution, by neglecting breakage/scission, the micelle length estimated from the measured viscosity without accounting for breakage/scission will be shorter than the actual length, and thus will be a *lower bound* on micelle length. The actual micelle length will be significantly longer especially at higher concentrations.

First, note that at low concentrations below around 1%, the observed scaling of viscosity with concentration in Figure 2.2 is $\eta_{sp} \propto \varphi^{1.7}$ while at concentrations above around 2%, the scaling is $\eta_{sp} \propto \phi^{5.0}$. From dilute polymer theory, we expect $\eta_{sp} \propto \nu R_g^3$, where ν is the micelle number density and R_g is the average radius of gyration of the micelle. For dilute polymers, the chain length is constant and so $\eta_{sp} \propto \nu \propto \varphi$. However, micelle length is expected to increase with surfactant concentration. Assuming a mean-field scaling of $\langle L \rangle \propto \varphi^{0.5}$, and a good solvent scaling of $R_g \propto \langle L \rangle^{0.6}$, we obtain $R_g \propto \varphi^{0.3}$. Since $\nu \propto \varphi / \langle L \rangle \propto \varphi^{0.5}$, $\eta_{sp} \propto \nu R_g^3$ implies that $\eta_{sp} \propto \varphi^{1.4}$, somewhat weaker than the scaling observed in Figure 2.2, $\eta_{sp} \propto \phi^{1.7}$. A scaling

closer to the observed scaling $\eta_{sp} \propto \phi^{1.7}$ would be obtained if the non-mean-field, excluded-volume, scaling [31] $\langle L \rangle \propto \varphi^{0.6}$ holds, which leads to $\eta_{sp} \propto \varphi^{1.6}$.

At high concentrations, the predicted viscosity scaling from the Cates model in the fast-breakage limit, with $\langle L \rangle \propto \varphi^{0.5}$, is $\eta_{sp} \propto \phi^{3.5}$ [12], which is lower than seen in Figure 2.2, $\eta_{sp} \propto \phi^{5.0}$. The higher power law of the scaling in Figure 2.2 is likely to be partly due to micelles lying outside the fast-breakage limit, and perhaps partly due to more rapid growth of micelle length than $\langle L \rangle \propto \varphi^{0.5}$. The average micelle length for the SLE1S solutions, at the same salt concentration (3.1 wt%), and at the lowest surfactant concentrations of 0.1-0.25%, was determined from small angle neutron scattering (SANS) to be around 200 nm [25]. Assuming a constant scaling law $\langle L \rangle \propto \phi^{0.5}$ across the range of surfactant concentrations, at the concentration 1% where the viscosity shows a transition from dilute to entangled, the micelle length should be 400-600 nm, and at 10% it should be 1-2 μm. For surfactant concentrations usually studied rheologically (around 10%), this again indicates that the micelles should be on the order of microns, not hundreds of nanometers or less. We also note from Table 2.1b that while the Cates method correctly predicts increasing micelle lengths as surfactant concentration increases, the lengths are much less than a micron and are shorter than the lengths from SANS (~ 200 nm), even at concentrations 100 times higher than those at which SANS measurements were made.

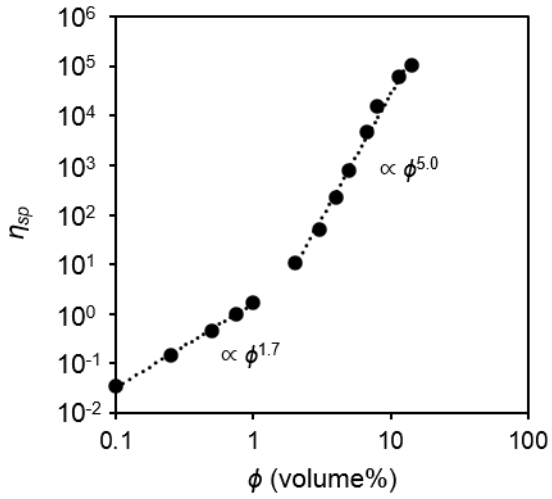

Figure 2.2: Specific viscosity versus concentration of SLE1S surfactant and 3.1 wt% NaCl showing different power law dependencies in dilute vs. semi-dilute concentration ranges at 25°C.

Review of Selected Literature Measurements of Micelle Length

In other work, micelle lengths were estimated over a range of surfactant concentrations through the use of SANS, cryo-TEM, and rheology. Afifi *et al.* [32] measured the linear rheology and a zero shear viscosity of 10-100 Pa·s, or $\eta_{sp} \approx 10^4$-10^5 for a wormlike micellar solution of 10 wt% poly(oxyethylene) cholesteryl ether ($ChEO_{10}$) and varying amounts of lipophilic monoglycerides. They then imaged micelles in a 5-fold dilution of this solution using cryo-TEM and performed SANS experiments on a 10-fold dilution. From SANS, the micelles were inferred to be ellipsoids or cylinders with elliptical cross-section and "lengths" between 16 and 80 nm, which, according to the authors, may be either contour lengths or persistence lengths, indicating either small micellar aggregates or semi-flexible wormlike micelles of unknown length. For the 5-fold dilution from this concentration, cryo-TEM revealed long wormlike micelles greater than 1 μm in length, although it must be acknowledged that the disruptive preparation methods for cryo-TEM could distort micelle length distributions. As we argued above for SLE1S/CAPB

micelles, the high viscosity of the 10% solution (i.e., or $\eta_{sp} \approx 10^4$-10^5) suggests that micelle lengths for this solution are likely significantly longer than the SANS estimates for the diluted sample. Given the combined findings from multiple experimental methods, it seems possible that small ellipsoidal or short wormlike micelles exist at low surfactant concentrations, then grow into long wormlike micelles with lengths around 1 μm or more at higher surfactant concentration.

In an unusually thorough study, Helgeson *et al.* [14] found good agreement between micelle contour lengths from rheology and those from SANS for solutions of CTAB from 40 to 100 mM (i.e., around 1-3% by volume) in $NaNO_3$ at three mole ratios (1, 2, and 3) of salt to surfactant and temperatures ranging from 25-45 C. Other micelle parameters were also obtained. Importantly, the persistence length for each solution l_p was obtained from the stress-optic coefficient in flow birefringence. The micelle breakage time $\tau_{br} = 1/\omega_{min}$ was taken as the inverse of the frequency at which G" reached a local minimum (which we find from the pointer algorithm not to be a very accurate estimate). The modulus G_0 was obtained from Maxwell fits to the rheology, and this combined with l_p was used to calculate the entanglement length l_e. To do so, the formula $\xi = (k_B T/G_0)^{1/3}$ for the mesh size was combined with the expression $\xi = l_e^{3/5} l_p^{2/5}$, allowing l_e to be obtained. The Granek and Cates expression $\frac{G_0}{G''_{min}} \sim \frac{\langle L \rangle}{l_e}$ was then used to obtain $\langle L \rangle$. The micelle lengths were obtained from SANS for many solutions and also from rheology for a half dozen of them; agreement between the two measurement was within 10%, and included lengths ranging from 200 to 900 nm, with the highest values at high surfactant and salt concentrations and low temperature, as expected. Based on the rheology and viscosities of these solutions, and our experience inferring lengths from the pointer algorithm, these lengths seem too short. The dependence of specific viscosity on concentration for these solutions showed

three scaling regimes corresponding to dilute, semi-dilute, and concentrated (fully entangled) solutions, very similar to those for polymers, again implying that the micelles are quite long in the entangled regime.

Additionally, the requirement of multiple Maxwell modes to approximate the data at lower salt and surfactant concentrations indicates that the micelles are not in the fast breakage limit. In that case, $\tau_{br} > \tau_{rep}$ and $\underline{\tau_R} \approx \tau_{rep}$, where τ_{br} is the breakage time, τ_{rep} the reptation time, and $\underline{\tau_R}$ the terminal relaxation time, all for a micelle of average length. But for a 60 mM CTAB and 120 mM $NaNO_3$ solution studied by Helgeson *et al.*, it is found that $\tau_R = \omega_{c1}^{-1} = 0.04$ s and $\tau_{rep} = 1.4 \times 10^{-4}$ s, as calculated from the reported parameters ($\langle L \rangle = 225$ nm, $l_e = 221.5$ nm, $l_p = 32$ nm). The terminal relaxation time $\underline{\tau_R}$ is the inverse of the first crossover frequency, ω_{c1}, and the reptation time is calculated from $\tau_{rep} = \frac{2\langle L \rangle^3}{\pi^2 \alpha D_0}$, where the diffusivity is given by $D_0 = \frac{k_B T}{\varsigma}$ with the drag coefficient for a cylinder given by $\varsigma = \frac{2\pi\eta_s}{\ln(\xi/d)}$ [16]. This gives a reptation time two orders of magnitude shorter than the relaxation time from rheology, suggesting again that the micelle length used to estimate this reptation time is too short.

For this solution, the micelle length of 225 nm comes from fitting SANS data, but the actual micelle length for this and more concentrated solutions is likely longer than what that can be accurately resolved by SANS. The smallest q value for which Helgeson *et al.* report SANS data is about $q_{min} = 0.03$ nm^{-1}, corresponding to $r_{max} = \frac{\pi}{0.03\ nm^{-1}} = 105\ nm$. Even when micelle radii of gyration fall within this restriction, overlap of micelles leads to screening of scattering signal, making longer micelle lengths hard to infer by SANS. Others who have performed SANS measurements on non-dilute surfactant solutions have concluded that the micelles are too long for their lengths to be accurately determined from SANS. Work by Francisco *et al.* [33] that examined the effect of co-solutes on CTAB/NaSal micelles found a large variation in the

rheology and zero-shear viscosity, up to two orders of magnitude in the crossover frequency and viscosity. The SANS results, however, superimpose exactly for all co-solutes, and the authors comment that for micelles greater than a few hundred nanometers in length, a change in length would not be detectable by SANS. A different study of saponin micelles came to a similar conclusion. There Peixoto *et al.* [34] found relaxation times greater than 100 s from rheology but determined from SANS only that the micelle length was greater than the q range of their SANS experiments. Finally, Croce *et al.* [3,35], studying erucyl bis(hydroxyethyl) methylammonium chloride (EHAC) micelles, measured viscosities in the range of what is typically reported for solutions of wormlike micelles (1-100 Pa·s). At these concentrations they note that the micelles are longer than can be measured within their q range and that there was no model to usefully fit the whole scattering curve.

As an example of the longer micelle length extracted from our experimental data using the pointer algorithm than is obtained from the Cates' scaling law, Figure 2.3 shows a fit of rheology data for ϕ = 0.05 SLE1S/CAPB, [Na^+] = 0.7 M, giving a micelle length of $\langle L \rangle$ = 3.0 μm in contrast to the length of 0.145 μm calculated from the Cates method (Table 2.1a). A length of 3.0 μm seems reasonable considering that a) the solution viscosity is high, indicating that the micelles are well entangled, that b) extrapolation of micelle lengths from SANS yields lengths well over 1 μm, and that c) long ~1 μm micelle lengths are observed in cryo-TEM results on other solutions with similarly high viscosities discussed above. All of these considerations suggest micelle lengths that are on the order of microns for surfactant solutions at our experimental concentrations.

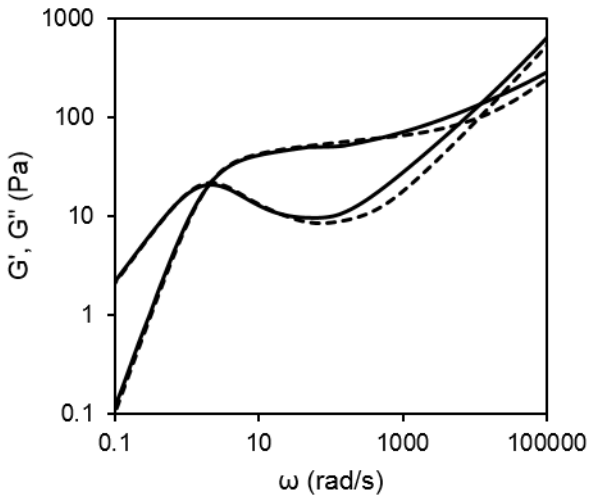

Figure 2.3: Fits of original pointer algorithm with only fast Rouse modes (dashed lines) to an example experimental data set (solid lines) for which ϕ = 0.05, [Na^+] = 0.7 M, and T = 25°C, resulting in the following "best fit" micelle parameters: G_0 = 76 Pa, $\langle L \rangle$ = 3.0 μm, τ_{br} = 0.73 s, l_p = 76 nm, and l_e = 140 nm.

Comparisons with Slip-Spring Simulations

To further validate the micelle length obtained from the pointer algorithm, we next compare rheology generated by the pointer algorithm to results from a more highly resolved slip-spring simulation model. The slip-spring model, originally developed for solutions of entangled polymers as an alternative to the tube model, and which is regarded as quantitatively accurate for polymer solutions and melts, treats each polymer as a bead-spring Rouse chain with entanglements represented by slip-links attached to the chain [19,22]. To adapt this model to micelles, chains were allowed to reversibly break and rejoin [23]. To make the slip-spring simulations numerically tractable, the micelles must be relatively short and therefore only weakly entangled with an average number of entanglements Z = 3 or 5. Stresses in this limit are often too low to be measurable for experimental solutions, but since the slip-link simulations have proved to be quite accurate for entangled polymers, they can serve to test the accuracy of

the rheological predictions of the pointer algorithm, thus justifying their use for estimating micelle length.

The slip-spring model naturally captures reptation, contour length fluctuations, constraint release, and Rouse modes. The pointer algorithm imposes the effects of these phenomena on rheology in a coarser-grained way, but only the short range (fast) Rouse modes were originally included. Slower, "longitudinal" Rouse modes were omitted from the original pointer algorithm because they were assumed to be negligible relative to the stresses produced by entanglements. (Additionally, in the comparisons to the slip-spring model, bending modes usually present in the pointer algorithm are dropped since the slip-spring simulations do not have bending modes.) In previous work [23], we found good agreement between the predictions of the slip-spring and the original pointer algorithm at low frequency, but pronounced deviation starting at intermediate and high frequencies; this deviation could be alleviated by inclusion of the full spectrum of Rouse modes rather than just the high-frequency ones. The inclusion of the full spectrum of Rouse modes can be justified by the weakness of the entanglements in the slip-spring simulations, since $Z = 3$ or $Z = 5$ represents only 3 or 5 entanglements, which is not enough to create a distinct "tube" able to suppress the slow Rouse modes.

Even for a highly entangled solution, there should be slower, longer-range modes present, but restricted by the tube to one-dimensional relaxation and hence having reduced amplitude. Within the tube model, the one dimensionality of these modes is imposed by reducing their amplitude by a factor of 5 relative to their original amplitude in the absence of the tube. These reduced-modulus slow Rouse modes are called "longitudinal" Rouse modes. Thus, for weakly entangled micelles with $Z = 3$ or 5 (where we use "Z" as a shorthand for the average value $\langle Z \rangle$), we found in previous work that the full Rouse spectrum of modes should be added to the

predictions of the pointer algorithm to be able to match results from the slip-link model. For high degrees of entanglement, the longitudinal Rouse modes, with their reduced magnitude, should theoretically be included, but were assumed to have negligible effect and so were neglected in the original pointer algorithm. However, because we found that these slower modes are clearly important for weakly entangled micelles and must be included, we wish to check whether the longitudinal Rouse modes (i.e., with reduced amplitude) need to be included even for higher levels of entanglement. Thus, there are three options for choice of Rouse modes, shown mathematically below in Eqs. 2.1 and 2.2 respectively, where the first terms in Eq. 2.1 are the longitudinal Rouse modes. In these equations, ϕ_i and Z_i are the volume fraction and number of entanglements respectively of micelles of length i, p is the mode number, and τ_e is the entanglement time.

$$G'(\omega) = G_0 \sum_i \frac{\phi_i}{Z_i}\left[\frac{1}{4}\sum_{p=1}^{Z_i-1}\frac{(\omega\tau_e)^2}{(\omega\tau_e)^2 + (p/Z_i)^4} + \frac{5}{4}\sum_{p=Z_i}^{N_iZ_i}\frac{(\omega\tau_e)^2}{(\omega\tau_e)^2 + 4(p/Z_i)^4}\right] \quad (2.1a)$$

$$G''(\omega) = G_0 \sum_i \frac{\phi_i}{Z_i}\left[\frac{1}{4}\sum_{p=1}^{Z_i-1}\frac{(\omega\tau_e)(p/Z_i)^2}{(\omega\tau_e)^2 + (p/Z_i)^4} + \frac{5}{4}\sum_{p=Z_i}^{N_iZ_i}\frac{2(\omega\tau_e)(p/Z_i)^2}{(\omega\tau_e)^2 + 4(p/Z_i)^4}\right] \quad (2.1b)$$

$$G'(\omega) = \frac{5}{4}G_0 \sum_i \frac{\phi_i}{Z_i}\sum_{p=1}^{N_iZ_i}\frac{(\omega\tau_e)^2}{(\omega\tau_e)^2 + 4(p/Z_i)^4} \quad (2.2a)$$

$$G''(\omega) = \frac{5}{4}G_0 \sum_i \frac{\phi_i}{Z_i}\sum_{p=1}^{N_iZ_i}\frac{2(\omega\tau_e)(p/Z_i)^2}{(\omega\tau_e)^2 + 4(p/Z_i)^4} \quad (2.2b)$$

Figure 2.4 compares results from slip-spring simulations to those from the pointer algorithm, using each of the three options for Rouse modes, namely 1) fast Rouse modes only (second term only in Eqs. 2.1a and 2.1b), 2) a "fractionated" Rouse spectrum including fast and longitudinal Rouse modes (both terms in Eqs. 2.1a and 2.1b), or 3) full Rouse modes (Eqs. 2.2a and 2.2b). The calculations are carried out for solutions of micelles with mean length of 0.84 or 1.4 μm, containing, respectively, 3 or 5 entanglements with an entanglement length l_e of 280 nm; a micelle persistence length of 20 nm, resulting in a semi-flexibility parameter $\alpha = l_e/l_p$ of 14; and ratio of breakage to reptation time $\zeta = 100$. These comparisons show that adding longitudinal Rouse modes improves the comparison marginally, but using a full Rouse spectrum gives us good agreement with the slip-spring simulations across the whole frequency range. It therefore seems that at low numbers of entanglements, the entanglement network is not fully formed and at short length scales, the tube has no confining effect, leading to relaxation by unfractionated Rouse modes. Thus full Rouse modes give the best overall agreement to the slip-spring model. Similar results are obtained when $Z < 5$ for other values of ζ.

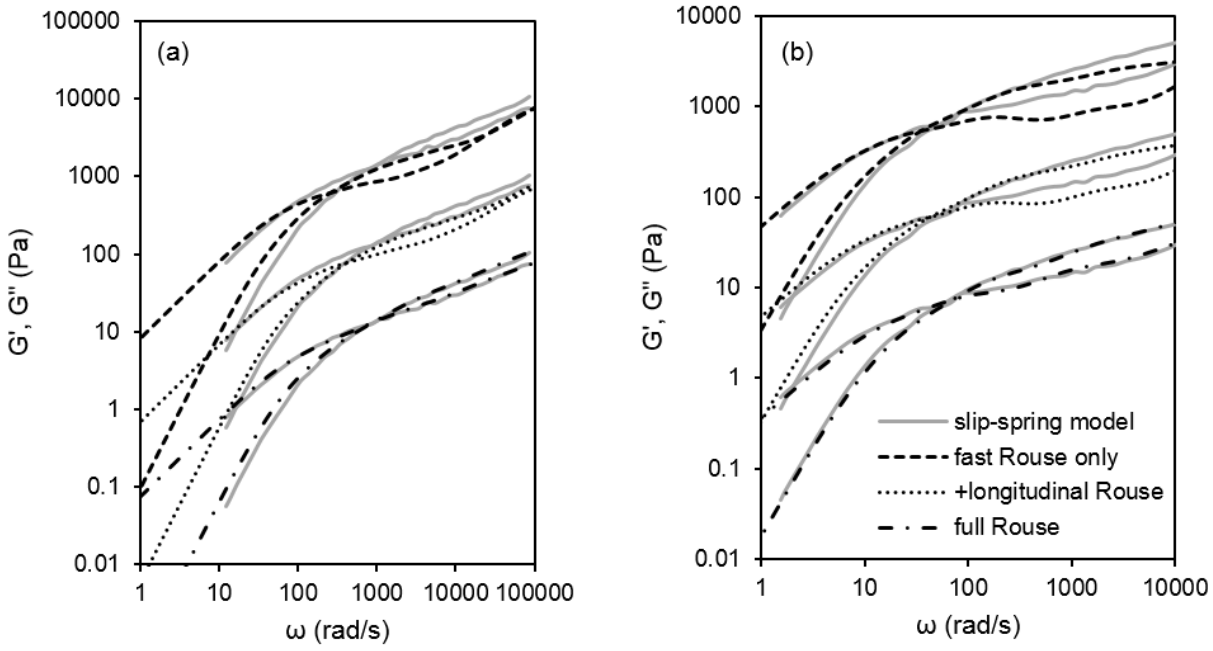

Figure 2.4: Comparison of G' and G" between the slip-spring model and the pointer algorithm at (a) $Z = 3$ and (b) $Z = 5$. In each sub-plot the curves for the three cases are separated by shifting the upper two cases upwards by either one or two decades.

We next investigate at what point the tube has enough entanglements to suppress the longitudinal Rouse modes, as originally assumed. To do this, we compare fits of pointer algorithm predictions to SLE1S/CAPB experimental data using our three different options for Rouse modes discussed above. Two sample experimental data sets are fit by the pointer algorithm predictions in Figure 2.5, with bending modes included. We find that for all solutions, adding additional Rouse modes results in better fits to the experimental data, particularly beyond the maximum in G", where fits with only fast Rouse motion tend to underestimate the moduli. By modifying the Rouse modes, we can fit the experimental data well across all frequencies. At lower concentrations where $Z = 7$ (Figure 2.5a), adding full Rouse modes improves the predictions at frequencies above the first cross-over. At a higher concentration with $Z = 30$ (Figure 2.5b), including full Rouse modes no longer results in a good fit to the experimental data,

which can be seen particularly near the minimum in G". From the slip-spring simulation data, with Z = 3 and 5, we determined that simulations with full Rouse modes best represent the high-frequency relaxation for small Z. All these results taken together are consistent with the progressive formation of a confining tube as the number of entanglements per micelle increases. Based on our fits, the transition from full to fractionated (fast and longitudinal) Rouse modes seems to occur at or slightly below around 15 entanglements per micelle. At no point does it appear that the tube entirely suppresses the influence of longitudinal Rouse modes, contrary to the original pointer algorithm model.

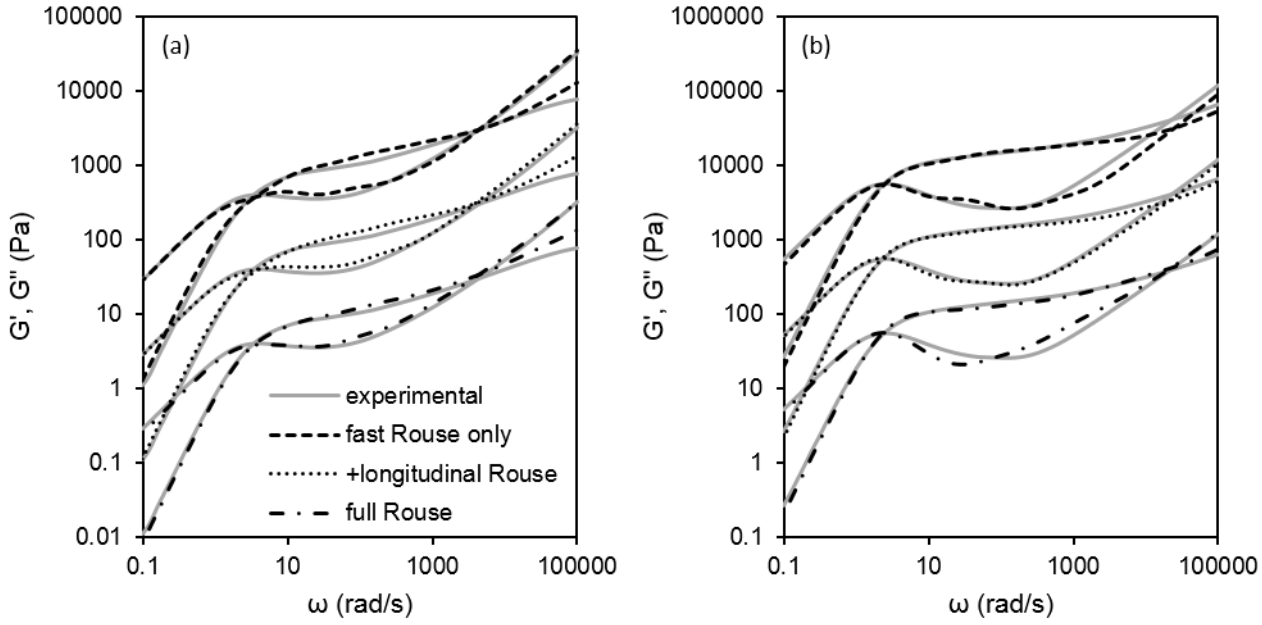

Figure 2.5: Fits of pointer algorithm predictions to rheological data for SLE1S/CAPB and [Na^+] = 0.7 M at (a) lower concentration (ϕ = 0.025, Z = 7) and (b) higher concentration (ϕ = 0.089, Z = 30) with different treatments of Rouse modes. The topmost two sets of curves in both graphs have been shifted upwards for readability.

Micelle Parameters Obtained by Pointer Algorithm

By fitting a series of experimental data sets using the pointer algorithm, we can determine how the micelle parameters vary with the surfactant concentration. The data we consider here are for the SLE1S and CAPB solutions with NaCl added to maintain a constant sodium ion concentration (while the surfactant concentration varies). Example fits can be found in Figure 2.3 andFigure *2.5* above. Figure 2.6 shows selected micelle parameters extracted from the experimental data using our various treatments of the Rouse modes. From *Figure 2.6*, the parameters most sensitive to the treatment of the Rouse modes are τ_{br}, which varies by about a factor of three, and $\langle L \rangle$, which varies by a factor of two. However, in all cases, the micelle lengths obtained are on the order of microns, not hundreds of nanometers or less. Thus, the conclusion that micelle lengths are on the order of microns is robust to the choice of how the Rouse modes are treated. We note that fits are better when we include the slower Rouse modes. *Table 2.2* gives our calculated scaling laws along with their mean-field theoretical values in the fast-breakage limit and literature values drawn primarily from experimental correlations. For the case in *Table 2.2* labeled "full ($Z < 15$) to fractionated Rouse modes," (third column), when calculating scaling laws we assume a transition from full Rouse modes at low $Z < 15$ to a combination of fast and longitudinal Rouse modes for $Z \geq 15$. Overall, we find that the scaling exponents (except the one for τ_{br}) agree fairly well with their theoretical values as well as with literature values. Scaling exponents for the plateau modulus similar to those obtained by our fitting have been reported in the literature – 1.85 for CTAB and KBr [12], 2.18 for CPyCl/NaSal and NaCl [28], and 2.12 for CTAC/NaSal and NaCl [36]. For the micelle length, Berret *et al.* [28] used a combination of rheology and light scattering to find a scaling relation with a power of 0.24 or 0.36, though they did not explicitly determine the micelle length. Re-analysis of their

data resulted in a power law of 0.60 [37]. These values are similar to the theoretical value as well as to the range of values calculated from fits of our data by the pointer algorithm. The greatest deviation from theory occurs for the breakage time, where the theoretical scaling exponent is simply the negative of the exponent for micelle length, based on the assumption that the product $\tau_{br}\langle L\rangle$ is constant (an assumption not made when using the pointer algorithm). The persistence length from fits by the pointer algorithm is approximately constant at high concentrations, as shown in *Figure 2.6*d, consistent with theory, but then appears to decrease at lower concentration. Previous work [17] at lower surfactant concentrations reports persistence lengths of around 20-30 nm, which is consistent with our finding of a lower persistence length at low concentration.

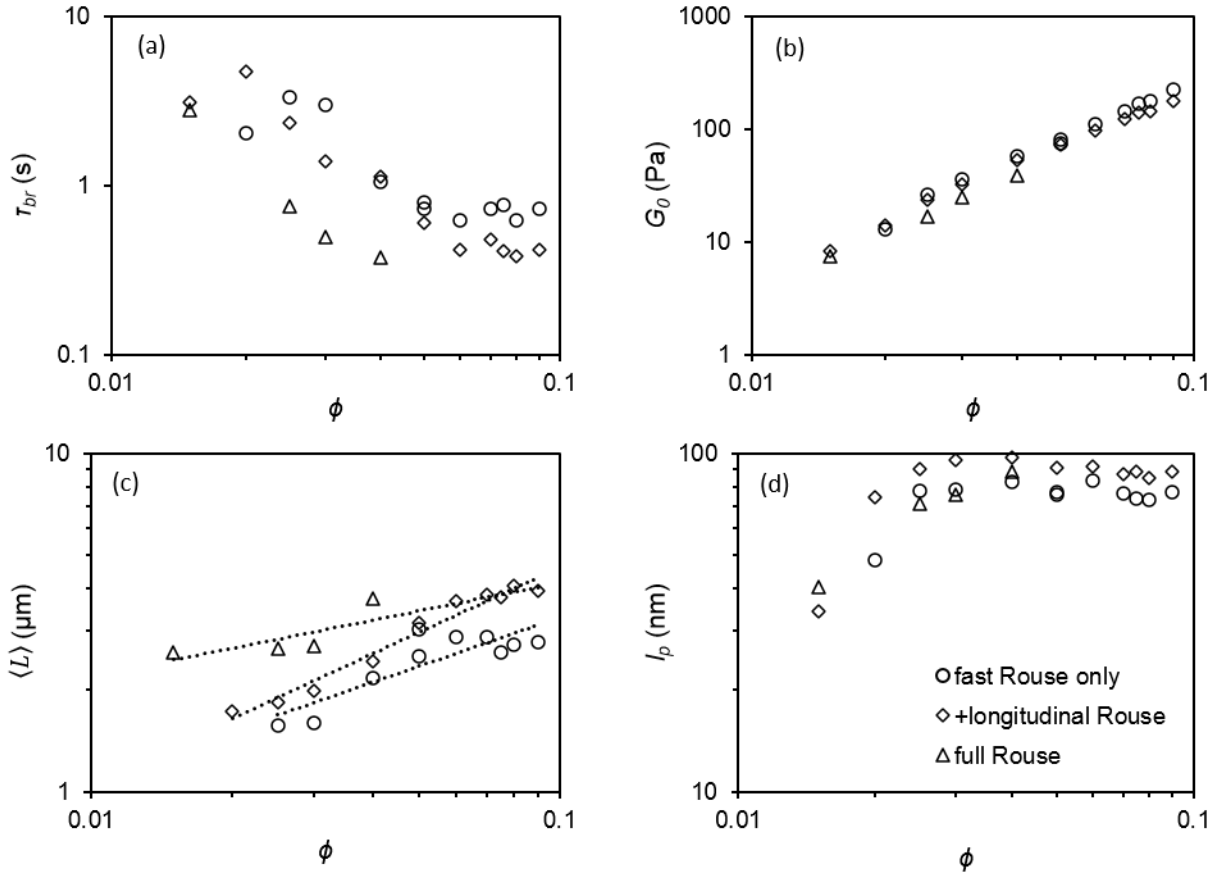

Figure 2.6: Micelle parameters extracted from rheological data for SLE1S/CAPB at $[Na^+]$ = 0.7 M, using the pointer algorithm with varying choices for Rouse modes described in the legend of (d). Figure 2.6(c) also contains linear fits to the $\langle L \rangle$ values on a log-log plot from which different values of the scaling exponent are obtained and tabulated in Table 2.2, for the different treatments of the Rouse modes.

Table 2.2: Scaling-law exponents for surfactant-concentration dependencies

parameter	fast Rouse modes only	full ($Z < 15$) to fractionated Rouse modes	fractionated Rouse modes	mean field [12]	literature [12,28,36,38,39]
τ_{br}	-1.1	-0.84	-1.5	-0.5	
$\langle L \rangle$	0.48	0.28	0.64	0.5	0.24-0.6
G_0	1.77	1.83	1.69	2.2	1.5-2.18
l_p	~0	~0	~0	0	
l_e	-0.57	-0.65	-0.56	-0.75	-0.65 – -0.72
η_0	2.9	2.9	2.9	3.5	2.42-5

A New Cates-like Correlation for Micelle Length

Finally, we attempt to recover a Cates-like scaling for the micelle length, i.e., resembling $\frac{G_0}{G''_{min}} \sim \frac{\langle L \rangle}{l_e}$, but matching our micelle lengths fitted from the pointer algorithm. Fitting rheological data for a variety of mixed SLE1S/CAPB and pure SLE1S solutions with NaCl using the pointer algorithm with only fast Rouse modes, we find that by plotting the experimental values for G'_{min}/G''_{min} rather than G_0/G''_{min} against $\langle L \rangle / l_e$ (Figure 2.7), we obtain a best-fit relationship $\frac{G'_{min}}{G''_{min}} = 0.225 \left(\frac{\langle L \rangle}{l_e}\right)^{0.99 \pm 0.03}$, which is essentially the Cates scaling with a prefactor less than unity and that uses the experimental value of G'_{min} instead of an estimated plateau modulus. If we use results from full Rouse modes for $Z < 15$ and from fast and longitudinal Rouse modes for $Z > 15$, we obtain $\frac{G'_{min}}{G''_{min}} = 0.317 \left(\frac{\langle L \rangle}{l_e}\right)^{0.82 \pm 0.05}$, which more closely resembles a refinement of the Cates scaling law by Granek [37] that includes contour length fluctuations as well as Rouse modes and predicts a 0.8 power-law exponent. The similarity between our exponent of 0.82 and the 0.8 power-law exponent derived by Granek may be significant since the Granek correction includes contour length fluctuations which are also part of the pointer algorithm. However, the pointer algorithm also includes constraint release and bending modes, which are lacking from the Granek calculation, and so the similarity of the exponents may be fortuitous.

When we used the original Cates scaling law to calculate average micelle lengths for our experimental data in Table 2.1a and b, we found that the lengths were too short and for the data in Table 2.1a, the micelles were predicted to shrink as surfactant concentration increased. Our modified Cates scaling relation derived from the pointer algorithm, however, is consistent with micelles growing as surfactant concentration increases and yields micelles that are at least 10-20 times longer than calculated from the original Cates method. Both the micelle growth and

lengths given by the modified scaling better agree with the high solution viscosities. For the solutions with a constant concentration of added salt (Figure 2.1b and Table 2.1b), the micelle lengths are also longer than the lengths determined from SANS at lower concentrations, not shorter as is found from the Cates scaling law.

The increased micelle lengths come partially from the crossover formula in the pointer algorithm which accounts for a transition between loosely and tightly entangled micelles and an additional factor of 9.75 in the formula $G_0 = 9.75\, k_B T/\xi^3$ for loosely entangled micelles, rather than the simple scaling law $G_0 = k_B T/\xi^3$ typically used along with the Cates scaling law to determine micelle length. The factor of 9.75 is based on equations for the packing of polymer chains in good solvent, with the full derivation given in [16]. Inclusion of the prefactor 9.75 increases ξ by $9.75^{1/3} = 2.14$, which in turn increases l_e and thus $\langle L \rangle$ by $2.14^{5/3} = 3.5$. For more tightly entangled micelles, the effect of the prefactor lessens. The additional prefactor of 0.317 in the modified Cates relationship further increases the micelle length by $(0.317^{-1})^{1/0.82} = 4.1$. Assuming loosely entangled micelles, the cumulative effect is to increase the micelle length by a factor of about 15 compared to the original Cates method.

The Cates model in the "fast breakage limit" also allows derivation of a relationship for the terminal relaxation time – $\tau_R = \left(\tau_{br}\tau_{rep}\right)^{0.5}$. If we allow the exponents for τ_{br} and τ_{rep} to vary separately but constrain them to sum to unity so that the expression remains dimensionally correct, we calculate $\tau_R = 0.48\tau_{br}^{0.58}\tau_{rep}^{0.42}$ and $\tau_R = 0.48\tau_{br}^{0.63}\tau_{rep}^{0.37}$ for simulations with fast Rouse modes only and modified Rouse modes respectively. These scaling laws indicate that the pointer algorithm results are in general agreement with the Cates model scaling for the relaxation time, but have a stronger dependence on the breakage time. Thus, for both the micelle length $\langle L \rangle$

and time scale τ_R, we recover scaling relationships that are similar with those from the Cates theory, but with somewhat different exponents and prefactors.

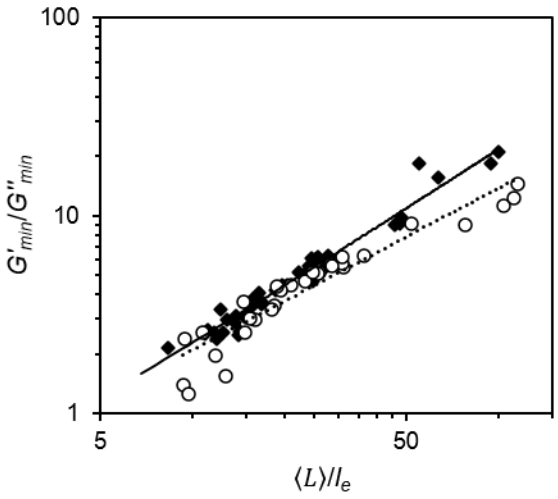

Figure 2.7: Scaling relation between G'_{min}/G''_{min} and $\langle L\rangle/l_e$ with fast Rouse modes only (filled diamonds), slope = 0.99 ± 0.03, or a transition from unfractionated to a combination of fast and longitudinal Rouse modes (open circles), slope = 0.82 ± 0.05.

We now use the correlations established above, in particular the new Cates-like scaling law

$$\frac{G'_{min}}{G''_{min}} = 0.317\left(\frac{\langle L\rangle}{l_e}\right)^{0.82} \quad (2.3)$$

to predict the micelle length for the 60 mM CTAB/120 mM $NaNO_3$ solution from Helgeson *et al.* [14]. This prediction enables us to further test the pointer algorithm and compare the micelle lengths obtained from the pointer algorithm with the published value. The input parameters for the pointer algorithm are taken to be G_0 = 22.2 Pa, $\langle L\rangle$ = 1.2 μm, l_p = 32 nm, and ζ = 200. The micelle length is obtained using Eq. 2.3, and details of how the other parameters are estimated for this solution, from information provided in the paper of Helgeson *et al.*, can be found in

Appendix A. Figure 2.8 compares experimental data to predictions of the pointer algorithm obtained from the above micelle parameters and from those published in Helgeson *et al.* The most significant difference is that our correlation in Eq. 2.3 gives a micelle length of 1.2 μm, while in Helgeson *et al.*, the reported length is 225 nm, obtained from the Cates correlation.

We can see in *Figure 2.8* that the published parameter values, when used in the pointer algorithm, result in G' and G" curves that relax 1-2 orders of magnitude more quickly than in the experiments, as might have been expected from the calculation of the reptation time above. Furthermore, using the published values, the shapes of the relaxation curves do not match the experimental data, and no crossover between G' and G" is observed, all of which signifies that the micelle length of 225 nm is too short. Alternately, the results from the micelle length obtained from Eq. 2.3, with other parameters given in Appendix A, match the experimental data fairly well. The micelle length from Eq. 2.3, 1.2 μm, corresponds to about five entanglements. Since our new parameters for this solution were themselves obtained from the predictions of the pointer algorithm, it is no great surprise that the rheology predicted by the pointer algorithm using these same parameters agrees with the data. However, recall that the predictions of our pointer algorithm also agree well with those from the slip-spring model, where this model has proved able to predict well the effects of entanglements in polymers, and so is likely quite accurate. This, plus the fact that the micelle length we estimate from Eq. 2.3 is consistent with the relatively high solution viscosity, strongly indicates that the micelle lengths we obtain from the pointer algorithm are more accurate than those estimated from the original Cates scaling law.

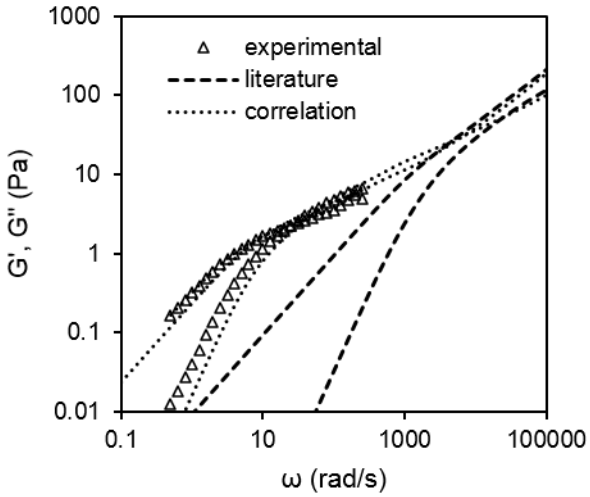

Figure 2.8: Experimental data for 60 mM CTAB/120 mM $NaNO_3$ solution from Helgeson *et al.* [14] (symbols) compared to results from pointer algorithm using both micelle parameters given in Helgeson *et al.* (dashed lines) and those calculated from the new Cates-like scaling law, Eq. 2.3, for micelle length with other parameters estimated in Appendix A.

While the modification of the Cates method by Granek results in somewhat longer micelle lengths and a scaling exponent (0.8) in closer agreement to what we obtain from the pointer algorithm, the Granek modification does not change predictions of decreasing micelle length with increasing surfactant concentration obtained from the Cates method, and the micelle lengths remain much smaller than those inferred from the pointer algorithm, unless the prefactor of the scaling law is changed to a value suggested by fits to results from the pointer algorithm. Although most of the fits and our proposed scaling laws are based on the SLE1S + CAPB/NaCl system, the pointer algorithm should be generally applicable to solutions of entangled wormlike micelles. Our prediction of the experimental data from Helgeson *et al.* indicates that this true, but to verify that the pointer algorithm and the derived scaling laws are applicable to any given surfactant solution with entangled micelles, more pointer algorithm fits with different systems would need to be run. Further comparisons of the pointer algorithm with predictions of the slip-

spring model for more highly entangled wormlike micelles should also help determine the general accuracy of the pointer algorithm.

Conclusions

Using a mesoscopic simulation, the pointer algorithm, we have extracted surfactant micelle parameters from linear rheology data for entangled wormlike micellar solutions for a series of solutions of sodium laureth-1 sulfate (SLE1S) and cocamidopropyl betaine (CAPB) in NaCl solutions. In particular, the extracted average micelle lengths $\langle L \rangle$ are more consistent with the high solution viscosities, in excess of 10^2 Pa·s, measured for these solutions, than are the values extracted from the Cates method in which $\frac{G_0}{G''_{min}} \sim \frac{\langle L \rangle}{l_e}$ where l_e is the entanglement length, G_0 is the plateau modulus, and G''_{min} is the local minimum value of G" as a function of frequency. Similar data in the literature also give sub-micron micelle lengths despite high solution viscosities, again suggesting underprediction of micelle lengths by the Cates method.

To further validate the micelle lengths from the pointer algorithm, we compared G' and G" curves generated by the pointer algorithm to results from a slip-spring simulation model adapted to breakable chains and found good agreement between the two methods after modifying the Rouse modes in the pointer algorithm to include low-frequency modes. By modifying the pointer algorithm by switching to an unfractionated Rouse spectrum at low concentrations and adding longitudinal Rouse modes to the high-frequency modes at higher concentrations where the number of entanglements per micelle exceeds Z = 15, we also improved our fits to experimental data. From the fits to experimental data by this and the original version of the pointer algorithm, we calculated scaling laws for the micelle parameters that generally agree with theoretical and literature values, and that do not depend severely on the choice of which Rouse

modes to include. Additionally, the micelle lengths from fits of the pointer algorithm to experimental data for a variety of surfactant solutions follow a scaling law, $\frac{G'_{min}}{G''_{min}} = 0.317\left(\frac{\langle L\rangle}{l_e}\right)^{0.82}$, similar to the scaling law $\frac{G_0}{G''_{min}} \sim \frac{\langle L\rangle}{l_e}$, of Cates and even more similar to the scaling law $\frac{G_0}{G''_{min}} \sim \left(\frac{\langle L\rangle}{l_e}\right)^{0.8}$ of Granek. But, because of the smaller prefactor (0.317), the new scaling law is more consistent with the longer micelle lengths obtained from the pointer algorithm. Thus, the pointer algorithm allows extraction of micelle parameters, in particular the average micelle length, that are consistent with the high solution viscosities of these solutions, and gives dependencies of micelle parameters on surfactant concentration that are generally in agreement with theoretical scaling laws. In the future, we recommend use of either the pointer algorithm or the scaling law $\frac{G'_{min}}{G''_{min}} = 0.317\left(\frac{\langle L\rangle}{l_e}\right)^{0.82}$, rather than the Cates scaling law, to extract average micelle lengths from rheological data.

Acknowledgements: Funding was provided by Procter and Gamble, as well as the National Science Foundation under grant CBET-1907517. Any opinions, findings, and conclusions or recommendations expressed in this material are those of the authors and do not necessarily reflect the views of NSF.

Note: This chapter in its entirety has been published as a peer-reviewed publication with the permission of the authors and publisher.

Chapter 3: Quantitative Modeling of Threadlike Micellar Solution Rheology

Abstract: A mesoscopic simulation method, the "pointer algorithm," is here shown to capture accurately the rheology of a variety of surfactant solutions, including CTAB/$NaNO_3$, CPyCl/NaSal, and CTAB/NaSal, at different salt and surfactant concentrations presented in the literature. In addition, correlations derived from this method are shown to allow the average micelle length $\langle L \rangle$ to be estimated from $\frac{G'_{min}}{G''_{min}} = 0.317\left(\frac{\langle L \rangle}{l_e}\right)^{0.82}$ where G'_{min}/G''_{min} is the ratio of storage to loss modulus at the frequency where G" exhibits a local minimum, and l_e is the entanglement length, which can be estimated from the modulus. We also obtain from the pointer algorithm a formula whereby the micelle breakage time τ_{br} can be estimated from the longest relaxation time τ_R. The pointer algorithm's predictions are also shown to match those of a more microscopic slip-spring model, which had been previously validated by comparison to polymer rheological data. Thus, the work provides both a method and example estimates of these parameters as functions of surfactant and salt concentration, filling a major gap in characterization of these solutions. Finally, we investigate the determination of the micelle persistence length from high frequency data.

Introduction

Over the past forty years, starting with the work of Cates [5], a theory for the rheology of surfactant solutions containing wormlike micelles has been developed by borrowing from entangled polymer theory the relaxation processes of reptation, contour length fluctuations, and

constraint release (e.g. double reptation), and adding to these micelle reversible breakage and rejoining [16]. In addition, to model the rheology at high frequencies, Rouse and bending modes have been included [20,21]. Granek and Cates [11,37] derived from a simplified version of the model an empirical scaling relation (with prefactor assumed to be unity) that allowed the average micelle length to be estimated from experimental linear rheology, specifically from the ratio of the plateau modulus to the loss modulus at the frequency where G" exhibits a local minimum, G_0/G''_{min}. Such a method is much needed, given that length (or molecular weight) is perhaps the most basic characterization of polymeric materials, and cannot be readily obtained in entangled solutions of wormlike micelles, because the latter are the result of self-assembly. This points to the general difficulty that micelle parameters, especially their length and average time to break, cannot be obtained readily except by fitting to rheological models. But these models themselves need to be tested against experimental data from which the parameters are obtained, thus introducing circularity in model building and testing.

More recently, the core ideas of Cates, and the above relaxation mechanisms, were incorporated with greater precision into the "pointer algorithm," a mesoscopic simulation method, and used to extract micelle parameters, including the average micelle length and breakage time, by fitting linear rheology data over the entire frequency range (and not relying on matching data at a single frequency, for example) [16,17]. In particular, in previous work, we used the pointer algorithm to obtain micelle parameters for various sodium laureth-1 sulfate (SLE1S) + cocoamidopropyl betaine (CAPB)/NaCl solutions, and showed that and predictions of the pointer algorithm were consistent with a correlation linking micelle length to G'_{min}/G''_{min} similar to what Cates found, *but with prefactor significantly different from unity* [15], as discussed below. We also previously derived a novel correlation (discussed below) for the

micelle breakage time, which is another critical micelle parameter not easily determined except through rheology.

While the above represents significant progress, the theory for entangled wormlike micelles remains much less developed than that for entangled linear polymers, from which the former was derived. For entangled polymers, standard sets of reference data have accumulated, for which theory works relatively well at least in the linear viscoelastic regime, while such data sets remain either unavailable, or at least unrecognized, for wormlike micelles. Moreover, rheological data for different polymer chemistries have been shown to behave essentially identically with each other, as long as the relevant parameters, especially the number of entanglements per polymers Z, are the same, and the effects of other parameters, such as frictional time and plateau modulus, are scaled out. No such "universality" in the linear rheology of wormlike micelles that self assemble from solutions of various surfactants and salts has been identified, although the rheological data do show common features. As alluded to above, a key problem is the lack of accurate *characterization* of the self-assembled micelles that form in such solutions.

We here address this problem in two different ways. The first is a comparison of the predictions of the pointer algorithm with predictions of a more microscopic model, the slip-spring model, which has already been validated by previous comparisons of its predictions against the linear rheology of well-characterized entangled polymer solutions and melts. Initial comparisons of the pointer algorithm against the slip-spring model were presented in our previous work [15], and here we extend these comparisons to more densely entangled micellar solutions.

The second validation method is to fit the predictions of the pointer algorithm to rheological data for multiple wormlike micelle solutions in the literature, thereby extracting fitted micelle parameters, and simultaneously testing the consistency of the quality of the fit. We can also use our scaling laws derived from the pointer algorithm that link micelle length and breakage time to simple rheological properties, to set our micelle parameters in advance, and then use these parameters to see how well predictions of the pointer algorithm fit the experimental rheology. While this method remains circular (since it uses a correlation derived from the pointer algorithm itself to obtain the parameters needed to make predictions using the pointer algorithm), this strategy does check the self-consistency of the method.

Additionally, as part of the project to investigate the "universality" of the rheology of entangled micellar rheology, we survey some of the methods used to obtain surfactant rheology and determine micelle parameters, including the extraction of the persistence length from high-frequency diffusing wave spectroscopy (DWS) data and methods of estimating the micelle diameter.

In what follows, we first briefly survey the experimental linear rheology data we draw from the literature. Then we describe briefly the pointer algorithm and the correlations derived from it. Next, we continue our validation of the pointer algorithm predictions by comparing them against those of slip-spring simulations for micelles whose average lengths range from $Z = 3$ to $Z = 9$ entanglements per micelle, using the same micelle parameters in both models. We then apply the pointer algorithm to experimental data, both by fitting its predictions to the data through iterative prediction, thereby extracting "best-fit" micelle parameters, and by extracting the parameters more simply through use of the correlations, and then using these parameters to predict directly the linear rheology from the pointer algorithm. Finally, we check how well the

latter predictions agree with the experimental data and how similar the parameters obtained from the correlations are to those obtained by iteratively fitting the predictions of the pointer algorithm to the data. These processes help check and confirm the ability of the pointer algorithm to fit the linear rheological data for a wide variety of experimental micellar solutions, and the ability of the simple correlations to calculate fairly accurately micellar parameters that are very difficult to measure in any other way. An important and unique output of this paper is a tabulation of micelle parameters, including micelle length, breakage time, and persistence length, at various surfactant and salt concentrations, for the most commonly studied micellar solutions, information that had not heretofore been assembled in a systematic way.

Experimental Data from Literature

The main experimental data analyzed in this work comes from multiple sources. The first set of solutions, from Helgeson *et al.* [14], contain cetyltrimethylammonium bromide (CTAB) at a constant surfactant concentration of 0.1 M and $NaNO_3$ salt concentrations of 0.1, 0.2, and 0.3 M, giving salt to surfactant ratios of R =1, 2, and 3. The data were obtained from mechanical rheometry at 25°C. We compare the linear rheology of these solutions to that of a series of SLE1S solutions at a surfactant volume fraction $\varphi = 0.05$ and NaCl salt concentrations of 4.6, 5.1, and 5.3 wt%. The rheology of these SLE1S solutions at 25°C was measured using mechanical and high-frequency diffusing wave spectroscopy (DWS), with mechanical and DWS data merged as described in previous work [17].

We also consider the rheology of 0.1 M cetylpyridinium chloride (CPyCl)/0.06 M sodium salicylate (NaSal) solutions from Oelschlaeger *et al.* [40] at temperatures varying from 20-40°C, again from a merger of mechanical and DWS data.

The last experimental data set considered here in detail is from a 0.1 M CTAB solution at 22°C with 0.04 M NaSal taken from Galvan-Miyoshi *et al*. [13], which includes DWS and mechanical data. These data represent a sample of commonly studied surfactants and salts having micelle parameters that span several orders of magnitude, showing the applicability of the pointer algorithm and its underlying theory to micelles that range from short and weakly entangled, that relax faster than they break, to ones that are long, highly entangled, and break multiple times before relaxing.

A few other less systems with less complete data, or less favorable for application of the pointer algorithm, are considered briefly at the end of this paper and in Appendix F.

Methods

For each set of rheology curves from the literature, we calculate the predicted micelle parameters from our previously determined correlations, as detailed below. We then compare the rheological properties predicted by the pointer algorithm using these parameters to the experimental rheology, to verify the consistency of the correlations. When possible, we also fit directly the experimental data using the pointer algorithm to compare the fitted micelle parameters with those calculated from the correlations.

In previous work [15], we fitted experimental rheological data for SLE1S and CAPB solutions with NaCl and found that the extracted parameters could be described well by correlations for the micelle length and breakage time. These correlations provide a method for determining micelle parameters from rheology that is much faster and more convenient than fitting them by iteratively running a full pointer-algorithm simulation. Below we review briefly the correlations and other formulas that relate micelle parameters to each other, whose derivation

is presented in detail in previous work [15,16], and show how to use these equations to calculate the micelle parameters necessary to run a predictive pointer algorithm simulation.

The pointer algorithm involves various time scales, length scales, and dimensionless parameters, although only a few of these are completely independent. To run a single-iteration, predictive, pointer algorithm simulation, the independent parameters required are the diameter d, persistence length l_p, semi-flexibility factor α, average micelle length $\langle L \rangle$, and dimensionless breakage rate ζ, as well as some experimental and rheological parameters. The semi-flexibility factor is defined as $\alpha = l_e/l_p$, where l_e is the entanglement length, and the dimensionless breakage rate as $\zeta = \frac{\tau_{br}}{\tau_{rep}}$, where τ_{br} and τ_{rep} are the breakage and reptation times respectively. We have found that the diameter cannot be determined from rheology, so it is treated as an input parameter that must be obtained from other experimental methods (such as neutron scattering [25,41,42]) or from simulations [43]. Without high-frequency data, the persistence length also cannot be extracted from rheology and must be determined from another method such as small-angle neutron scattering (SANS) [25], simulations [43], or rheo-optics [14]. If high-frequency data are available, the persistence length can be calculated along with the other independent parameters through the equations and correlations below.

Firstly, the experimental temperature T, solvent viscosity η_s, and volume fraction φ are required, as well as the rheological parameters G'_{min}, G''_{min}, and ω_{c1}, which are, respectively, the values of G' and G'' at the minimum in G'' and the first crossover frequency ω_{c1}. These values are known, physical, properties of the solution that will be used in the calculations that follow.

From G'_{min} and G''_{min}, the plateau modulus G_0, which is related to l_e and l_p and is necessary to determine α, is calculated from the correlation given in Appendix A,

$$\frac{G_0}{G'_{min}} = \frac{4.75}{(G'_{min}/G''_{min})} + 0.625 \qquad \text{(Eq. 3.1)}$$

for $G'_{min}/G''_{min} < 10$ or $G_0 \approx G'_{min}$ for $G'_{min}/G''_{min} > 10$. The plateau modulus is also defined by a "crossover formula" (Eq. 3.2 below) in the pointer algorithm that spans between "loose" and "tight" entanglement regimes, defined, respectively, by $l_e/l_p > 2$ and by $l_e/l_p < 1$ [16].

$$G_0 = \frac{\alpha^3}{3+\alpha^3} 9.75 \frac{k_b T}{\alpha^{1.8} l_p^3} + \frac{3}{3+\alpha^3} \frac{28}{5\pi} \frac{\phi k_b T}{d^2 \alpha l_p} \qquad \text{(Eq. 3.2)}$$

If no high-frequency data, such as from diffusive wave spectroscopy, are available, one must pre-specify the value of l_p, which is input into Eq. 3.2 along with the other known parameters, and Eq. 3.2 can then be solved for l_e, which is finally used with l_p to obtain $\alpha = l_e/l_p$. If there are high-frequency data, both l_p and l_e (and thus α) can be taken as unknowns in Eq. 3.2 and another equation, derived from the high-frequency data, is necessary. Such an equation has been used by Willenbacher *et al*. [26], derived from high-frequency relaxation of micelles through bending modes [21] (Eq. 3.3 below), which leads to a 3/4 power law for the loss modulus at high frequency.

$$G'' - \omega\eta_s = Im\left[\frac{1}{15}\rho\kappa l_p \left(\frac{-2i\varsigma_\perp}{\kappa}\right)^{3/4} \omega^{\frac{3}{4}}\right] \qquad \text{(Eq. 3.3)}$$

Here, the area density of micelles ρ, is defined by $\rho = \frac{\phi}{\pi d^2/4}$, the bending modulus by $\kappa = k_B T l_p$, and the lateral drag coefficient by $\varsigma_\perp = \frac{4\pi\eta_s}{\ln(0.6\xi/d)}$ with the mesh size $\xi = l_e^{0.6} l_p^{0.4}$. Because the unknown values in both Eqs. 3.2 and 3.3 are l_p and l_e, the two equations have to be solved simultaneously to determine the persistence and entanglement lengths, thereby yielding the two independent parameters l_p and α.

Once l_e is known, the average micelle length $\langle L \rangle$ can then be calculated from our correlation obtained from running the pointer algorithm [15]:

$$\frac{G'_{min}}{G''_{min}} = 0.317 \left(\frac{\langle L \rangle}{l_e}\right)^{0.82} \qquad \text{(Eq. 3.4)}$$

We note that this correlation is similar to the "Cates scaling law" proposed initially by Granek and Cates [11], with exponent revised from 1.0 to 0.8 by Granek [37] but without giving a prefactor; our fits to the predictions of the pointer algorithm supply the prefactor of 0.317 in Eq. 3.4. Previous authors used the Cates scaling with exponent unity and prefactor unity, i.e., $\frac{G_0}{G''_{min}} = \frac{\langle L \rangle}{l_e}$, and l_e given by assuming the loose-entanglement limit, i.e., $G_0 = \frac{k_b T}{\xi^3}$, instead of our Eq. 3.3, which accounts for the crossover to the tight-entanglement regime. The accuracy of the pointer algorithm's predictions of the effect of micelle length on rheology was supported by our recent work showing agreement of the linear rheology predicted by the pointer algorithm with that predicted by the more microscopic "slip-spring" simulations [15,23].

Lastly, the dimensionless breakage rate $\zeta \equiv \tau_{br}/\tau_{rep}$ can be determined by calculating the reptation time τ_{rep} and then getting τ_{br} from the following semi-empirical correlation, again obtained from G' and G" predicted by the pointer algorithm:

$$\tau_R = 0.484 \tau_{br}^{0.63} \tau_{rep}^{0.37} \qquad \text{(Eq. 3.5)}$$

where the longest rheological relaxation time τ_R is taken as the inverse of the first crossover frequency of G' and G" and the reptation time is calculated from theory as $\tau_{rep} = \frac{2\langle L \rangle^3}{\pi^2 \alpha D_0}$. The micelle translational diffusivity within the tube is given by $D_0 = \frac{k_B T}{\varsigma}$ with the drag coefficient given by $\varsigma = \frac{2\pi\eta_s}{\ln(\xi/d)}$.

These calculations produce the required independent parameters needed as input to the pointer algorithm – α from Eq. 3.2, l_p from Eq. 3.3 (solved simultaneously with Eq. 3.2 if high-frequency data are available), $\langle L \rangle$ from Eq. 3.4, and $\zeta = \frac{\tau_{br}}{\tau_{rep}}$ from Eq. 3.5. (As shown above, other parameters that may be of interest, such as G_0 or τ_{br}, are related to the four independent

parameters by the formulas given.) The experimental parameters (T, η_s, φ) and the independent micelle parameters (d, l_p, α, $\langle L \rangle$, ζ) can then be input into the pointer algorithm and a predictive simulation run to compare to the experimental data.

If an iterative pointer algorithm simulation is run to fit experimental data with high-frequency data, the experimental parameters T, η_s, and φ and the micelle diameter are required inputs. Without high-frequency data, the persistence length l_p is also a required input parameter.

Results and Discussion

Slip-spring simulations

Before applying the pointer algorithm to a variety of surfactant solutions, we first want to validate the pointer algorithm simulations. Because the pointer algorithm predictions, or correlations based on the pointer algorithm, are fit to experimental data, there is the possibility that the fitting is compensating for errors in the theory and approximations used to derive the method. To provide an independent check on the pointer algorithm, the much more resolved slip-spring model, developed and validated for entangled polymers, was modified in previous joint work with our group [23] by the addition of random breakage and rejoining of micelles. We earlier found good agreement between predictions of the pointer algorithm and slip-spring simulations for $Z = 3$ and $Z = 5$ entanglements per micelle, where $Z \equiv \langle L \rangle / l_e$. Since such lightly entangled micelles would not have easily measurable rheology, it is important to extend the comparison to higher numbers of entanglements, which we do here for $Z = 9$. The other micelle parameters are $\langle L \rangle = 2.52$ μm, $l_p = 20$ nm, $\alpha = 14$, and $\zeta = 0.01$, 0.1, 1 in both the slip-spring simulations and the pointer algorithm, so that there are no adjustable parameters, with results shown in Figure 3.1. In these predictions of the pointer algorithm, the bending modes are left out

because they are not included in the slip-spring simulations (although they could easily be added to them, in the same way that they are added to the predictions of the pointer algorithm), and the "full" Rouse modes are included, as discussed in the earlier work.

As with the less entangled $Z = 3$ and 5 simulations, we again see excellent agreement between the results for the pointer algorithm and the slip-spring simulations. The micelle length (>1-2 μm) and average number of entanglements (~10) in this comparison are similar to values seen in the rheology of more dilute solutions (such as in Figure 3.1a and 3.7 below). We note that the slip-spring simulations become very expensive for larger Z, since an entire ensemble of micelles must by simulated, as described in detail in [23]. But the attainment of micelle lengths comparable with those in some experimental micellar solutions is an important result that bridges the gap between the earlier slip-spring simulations for dilute, weakly entangled micelles and the semi-dilute, high entangled solutions often studied in literature. Since we find that the pointer algorithm and slip-spring simulations match well at the experimentally relevant entanglement value of $Z = 9$, this result helps to support our use of the pointer algorithm to fit the experimental data in the sections that follow.

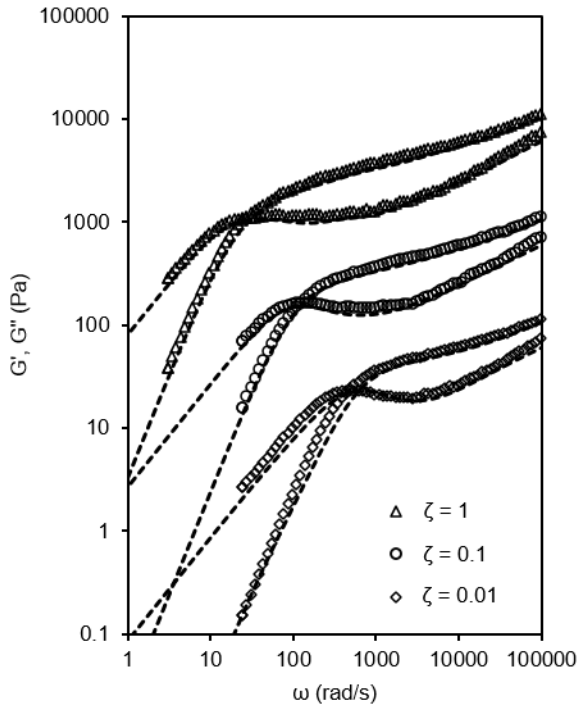

Figure 3.1: Predictions of pointer algorithm (dashed lines) and slip-spring simulations (symbols) compared at $Z = 9$ and varying ζ. The top two sets of curves have been shifted upwards by 1 and 2 orders of magnitude for readability

Effect of salt concentration

Three solutions of 0.1 M CTAB with added $NaNO_3$ from Helgeson *et al.* [14] were studied with the pointer algorithm and its derived correlations. First, the correlations were used to predict micelle parameters and a non-iterative pointer algorithm simulation was run with those calculated parameters to produce rheology curves for comparison with the experimental data. Since no high frequency data were available, the persistence lengths used were the experimentally derived values that Helgeson *et al*. determined from flow birefringence. For the solution with the lowest salt concentration, 0.1 M, the maximum value of G'(ω)/G"(ω) was used in calculations because there was no minimum in G"(ω). Since the solution rheology for salt/surfactant molar ratio R = 1 also lacked high-frequency data, we were unable to use the

pointer algorithm to fit these data. For the R = 2 and R =3 solutions, the micelle parameters were calculated using the procedure outlined in the methods section, then these parameters were verified with a non-iterative pointer-algorithm simulation, and the parameters were also obtained by fitting with the pointer algorithm without use of the correlations. When fitting with the pointer algorithm, a simulation is said to be "converged" if the G' and G" curves produced by the pointer algorithm match the experimental data with an average error of less than 10%. Pointer algorithm results from simulations that do not converge to within this tolerance are referred to as the "best-fit" results.

As Figure 3.2 shows, both the calculated and fitted micelle parameters produce G' and G" curves that match the experimental data reasonably well for all three solutions. The pointer algorithm results for the R = 1 solution have the greatest deviation from the experimental data, but this might be expected because the data have few defining features. Overall, we note that the experimental data are similar in shape and have comparable features (ω_{c1}, G'_{min}/G''_{min}) to those for SLE1S and SLE1S + CAPB solutions that we previously fit with the pointer algorithm, and so we obtain similar micelle parameters. The plateau moduli are 10-100 Pa, micelle lengths are 1-10 μm, and breakage to reptation time ratios are 0.01-10. The calculated and fitted parameters (from converged simulations) for selected micelle parameters are provided below in Table 3.1. We see general agreement between the fitted micelle parameters and those obtained from the correlations, although the micelle lengths differ somewhat and the breakage times change by a factor of more than two to compensate.

In previous work [17,44], and in Appendix D, we carried out extensive sensitivity analyses to assess the error in the parameters inferred from rheology, such as those in Table 3.1. While errors are of course sensitive to the particular data sets, we can say that, in general, one

can infer that the errors are comparable to the differences between parameter values inferred from the correlations and those from fitting the pointer algorithm. An exception is the persistence length, whose value and its accuracy depends strongly on the existence and accuracy of high-frequency data, such as that obtained by DWS, and on the accuracy of the value of the micelle diameter, as discussed below, and studied in detail in Appendix D.

The micelle parameters obtained from either the correlations or from fitting by the pointer algorithm differ significantly from those published by Helgeson *et al*. because of the methods used to estimate them. The published breakage times of Helgeson *et al.* were derived from the inverse of the frequency at which G" has a minimum while the pointer algorithm treats τ_{br} as an independent fitting parameter used to optimize the fit of G' and G" over the entire frequency range. The differences in plateau moduli reported by Helgeson *et al.* and those reported in Table 3.1arise because the pointer algorithm fits the low frequency reptation data with multiple Maxwell modes as necessary and uses a modulus crossover formula that bridges loosely and tightly entangled micelles, instead of assuming 1 or 2 Maxwell modes and loosely entangled micelles, as Helgeson's fits do. Lastly, the micelle length, as we discussed in our previous work, is underestimated by both the Cates scaling and by SANS measurement, which are the two methods used by Helgeson *et al*. At concentrations high enough that viscoelastic rheology can be reliably measured, the micelles overlap and screening makes it difficult to determine accurately the micelle lengths from SANS. The values of $\langle L \rangle$ = 0.431 μm and l_e = 88.6 nm (number of entanglements $Z = \langle L \rangle / l_e = 5$) published by Helgeson *et al*. for the R = 2 solution, if input into the slip-spring calculation, would *not* produce rheology similar to Figure 3.2b. We infer this, since even for longer micelles (1.4 μm) with $Z = 5$, the first crossover frequency from the slip-spring predictions is an order of magnitude higher than in the R = 2 experimental data,

and lacks the minimum in G" present in the experimental data. (See Fig. 8 in Sato *et al.* [23]) Thus the shorter micelle length suggested by Helgeson *et al*. would results in even greater deviations between the predictions of the pointer algorithm and experimental data. Given the reliability of the slip-spring model for polymer chains and likely also for wormlike micelles, these differences imply that the micelles in these solutions are at least several microns long, not less than a micron in length, which had been surmised by Helgeson *et al*.

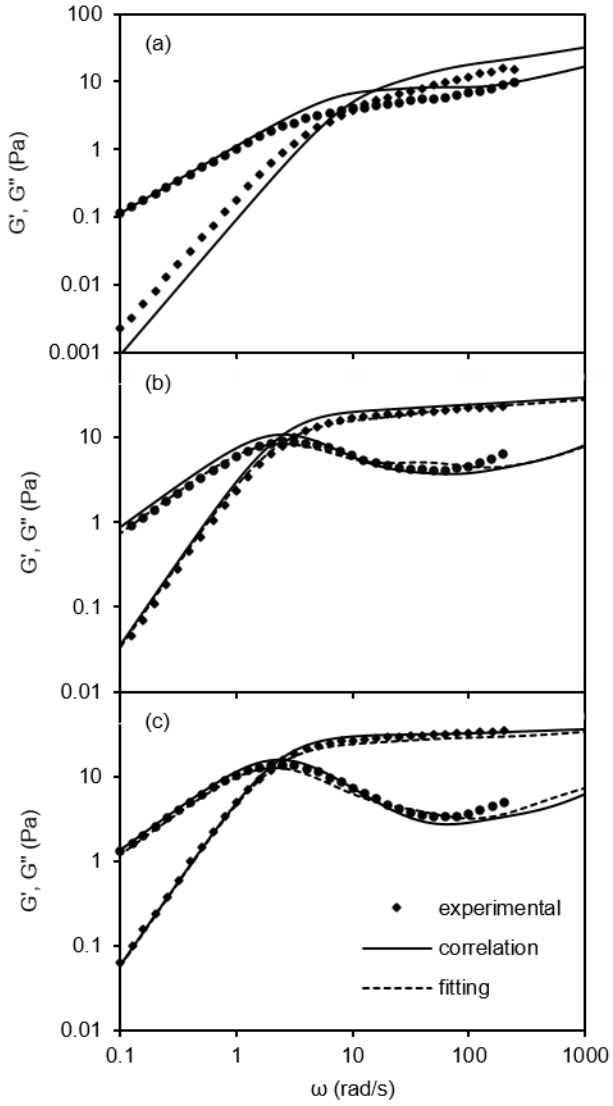

Figure 3.2: Rheology curves generated from the pointer algorithm with parameters calculated from correlations (solid lines) and fitting (dashed lines) compared to experimental data for 0.1 M CTAB solutions with (a) 0.1 M (R = 1), (b) 0.2 M (R = 2), and (c) 0.3 M (R = 3) $NaNO_3$. (Data

from Helgeson *et al*. [14]. As discussed in the text, pointer algorithm predictions could not be obtained for R = 1

Table 3.1: Micelle parameters for 0.1 M CTAB solutions at varying $NaNO_3$ concentration obtained from the correlations and from fittings by the pointer algorithm

$[NaNO_3]$		ζ	τ_{br} (s)	G_0 (Pa)	$\langle L \rangle$ (μm)	l_e (nm)	l_p (nm)
0.1 M	corr.	4.5	0.33	38.6	1.38	167	56
0.2 M	corr.	0.063	0.26	30.2	7.36	251	32
	fit	0.47	0.66	30.5	5.07	250	32
0.3 M	corr.	0.0024	0.098	33.9	17.5	277	25
	fit	0.016	0.20	31.9	12.0	286	25

Most of the micelle parameters are more sensitive to the salt concentration than to the surfactant concentration. In particular, the micelle length grows much more quickly with increasing salt concentration than for a similar relative increase in surfactant concentration. The mean field theory predicts that micelle length grows with surfactant volume fraction φ as $\langle L \rangle \sim \phi^{0.5}$ or as $\langle L \rangle \sim \phi^{0.6}$ if excluded volume is considered in the latter case [31], where these predictions ignore the effects of electrostatics. Mackintosh *et al*. [45], on the other hand, predicted that, because of electrostatic effects, the micelle length should transition from slow growth at dilute surfactant concentration to faster growth with a power-law exponent greater than 0.5 in the semi-dilute concentration regime. Previously, we found a scaling-law exponent close to 0.5 for the dependence on surfactant concentration of micelle length for SLE1S+CAPB/NaCl solutions at constant sodium ion concentration [15]. For the CTAB solutions of Helgeson *et al.* [14], the micelle length obtained from the correlations scales as $[NaNO_3]^{2.3\pm0.1}$ and as $[NaNO_3]^{2.4}$ from fits of the pointer algorithm to the rheological data, where the former is based on three data

points and the latter on only two points. Both of these scaling laws show significantly steeper increase of length with salt concentration than with surfactant concentration. For a series of SLE1S/NaCl solutions with varying salt concentration, we found the scaling $\langle L \rangle \sim [\mathrm{NaCl}]^{3.6 \pm 0.7}$. Because of the limited data – i.e., 3 data points for both the CTAB/$NaNO_3$ and SLE1S/NaCl solutions – and narrow range of salt concentration, there is significant uncertainty in the magnitude of the power law exponent, but it is safe to conclude that micelles grow faster with salt concentration than with surfactant concentration.

In contrast, the plateau modulus is less sensitive to the salt concentration than to the surfactant concentration. Neither CTAB/$NaNO_3$ nor SLE1S/NaCl, considered in this section, show any clear dependence of the plateau modulus on salt concentration. The pointer algorithm, using either the fits or the correlation, gives a plateau modulus that remains approximately constant or increases slightly as the salt concentration increases. Previous work on the SLE1S+CAPB/NaCl system over a wider range of salt concentrations may show a moderate increase in the plateau modulus with salt based on a visual inspection of the rheology curves [17]. Other work with SLES/NaCl [46], CPyCl/NaSal, and CTAB with $NaNO_3$, $NaCO_3$, or KBr [47] also generally show a modest increase in G_0 with increasing salt concentration.

Effect of temperature

Next, we analyze a solution of 0.1 M CPyCl/0.06 M NaSal at temperatures ranging from 20-40°C at 5° increments obtained by Oelschlaeger *et al.* [40] using a combination of rotational rheometry, oscillatory squeeze flow, and DWS. As with the CTAB/$NaNO_3$ solutions from the previous section, we both predict the micelle parameters using our correlations and fit the data using iterations of the pointer-algorithm simulations. For these data, at higher temperatures, the

results are similar to those for the CTAB/$NaNO_3$ solutions, where the parameters calculated from the correlations and the iterative best-fit parameters show general agreement, although they do not match exactly. The micelle parameters and example fits to the experimental data are shown in Table 3.2 and Figure 3.3. As the temperature decreases, the micelles grow to lengths greater than 10-20 μm, increasing the time per iteration of the simulation and making it difficult to run enough iterations to reach convergence. Hence, the best-fit parameters are not appreciably different from the initial input parameters, calculated from the correlations, and only the T = 40°C simulation "converges," in the sense defined earlier.

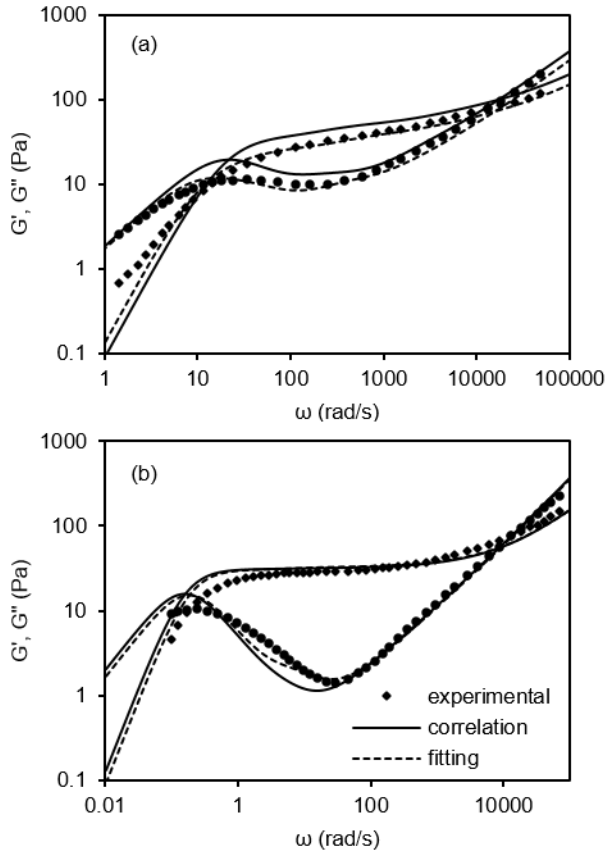

Figure 3.3: Comparison of results from the pointer algorithm with micelle parameters calculated from correlations (solid lines) or fitted (dashed lines) to experimental data for 0.1 M CPyCl/0.06 NaSal solutions at (a) 40°C and (b) 20°C. Additional rheology curves for 35, 30, and 25°C can be found in Appendix B.

Table 3.2: Micelle parameters for 0.1 M CPyCl/0.06 NaSal solutions at various temperatures

T (C)		ζ	τ_{br} (s)	G_0 (Pa)	$\langle L \rangle$ (μm)	l_e (nm)	l_p (nm)
40	corr.	0.14	0.051	61.0	2.36	154	105
	fit	0.55	0.13	46.1	2.01	161	85.2
35	corr.	0.091	0.15	50.5	3.80	160	96
	fit	0.29	0.32	41.2	3.32	178	100.
30	corr.	0.038	0.45	39.6	7.00	173	91
	fit	0.056	0.51	39.6	6.41	173	91
25	corr.	0.0037	0.61	33.5	16.6	178	82
	fit	0.0019	0.41	25.2	19.0	202	83.7
20	corr.	0.001	0.92	31.7	29.2	178	72
	fit	0.00088	0.79	31.7	29.0	178	72

Additionally, particularly for the data at lower temperature and low frequency in Figure 3.3, the shapes of the rheology curves from the pointer algorithm do not match the experimental data well. We believe this may be the result of the way the mechanical and DWS data were merged together. The difference between the mechanical and DWS data can be seen in Willenbacher *et al*. [26] for the solution at 20°C and is discussed further in Appendix C. DWS provides a way to access high-frequency data for surfactant solutions, but results have varied from system to system. In general, mechanical rheology and DWS data produce rheology curves that are similar in shape, but sometimes vertical shifting of the DWS data is required to match the magnitude of the mechanical data. The CPyCl/NaSal system explored by Oelschlaeger *et al.* exhibited this behavior; they saw agreement between the shapes of the mechanical and DWS

data but the magnitude of the DWS data differed from the mechanical data. Cardinaux *et al.* [48] also found that a scaling factor of 1.5-2 was needed to match the DWS data to mechanical rheometry for hexa-ethylene glycol mono *n*-hexadecyl ether ($C_{16}E_6$) solutions. In our previous work [17] with SLE1S+CAPB/NaCl, we used a similar merging procedure to combine mechanical and DWS data. In contrast, Bellour *et al*. [49] did not need to scale their DWS data to match mechanical rheology for solutions of either hexane sulfonate cetyltrimethylammonium ($CTAC_6SO_3$) or heptane sulfonate cetyltrimethylammonium ($CTAC_7SO_3$), and neither did Galvan-Miyoshi *et al*. [13] for CTAB/NaSal solutions. Even when the shapes of the DWS and mechanical rheology curves agree well without vertical shifting, there can still be significant deviation in the micelle parameters extracted separately from each of the methods. The overall relaxation time τ_R, taken as the inverse of the first crossover frequency, and the plateau modulus, taken as the value of G' at the minimum in G", can differ between DWS and mechanical rheology by more than a factor of 2 [13,40]. These differences between the mechanical and DWS data have been hypothesized to be caused by properties of the probe particles used in DWS [49], either because they do not accurately follow the generalized Stokes-Einstein relation [48], or because of interference from free ions [13], but the deviations have not been definitively explained.

We can use high-frequency data to calculate the persistence length, but results from our pointer algorithm differ from those obtained by Oelschlaeger *et al*. [40] primarily because of the micelle diameter, d = 2.6 nm, used by Oelschlaeger *et al.* Assuming an average carbon-carbon bond length of 1.54 Å and a bond angle of 109.5°, CPyCl's 16-carbon tail, fully extended, would be about 1.8 nm. Even allowing for some coiling of the tail, it seems unlikely that the micelle radius $d/2$ would be only 1.3 nm after the pyridine head group is added. Both SLE1S and CTAB

have similar tails – 12 carbons plus an ether group and 16 carbons respectively – and have been found to have diameters closer to ~4 nm. The SLE1S/NaCl system was studied using SANS and the micelle diameter was determined to be 3.5-3.8 nm over a range of surfactant concentrations [25]. Other SANS studies for CTAB/NaSal gave diameters of 4 nm [41] and 4.4 nm [42]; SANS performed on CTAB/$NaNO_3$ yielded a diameter of 4.06 nm [14]; and a coarse-grained molecular dynamics simulation for CTAC/NaSal determined a diameter of approximately 5 nm [43]. A SANS study of CPyCl/NaSal found d = 4.4 nm [50]. It therefore seems likely that CPyCl has a micelle diameter of around 4 nm, which we use when calculating micelle parameters from our correlations and as an input parameter for the iterative pointer algorithm simulations. Increasing the diameter, when fitting high-frequency rheology data, leads to an increase in the persistence length, from ~30-50 nm when d = 2.6 nm to ~70-100 nm, when d = 4 nm, similar to what we found for SLE1S solutions. This increase in the persistence length calculated from G" is due to the dependence of G" on d and l_p captured by retaining only these dependences in Eq. 3.3 for high-frequency bending modes, namely $G'' \sim \frac{l_p^{1.25}}{d^2}\left[\frac{1}{\ln(l_p^{0.6}/d)}\right]^{0.75}$; thus, increasing d increases l_p.

The micelle length ranges from around 2-30 μm, and grows exponentially with inverse temperature, as predicted theoretically, and shown in Figure 3.4. These micelle lengths correspond to scission free energies E_{sc} of 49-59 kJ/mol, as calculated from $E_{sc} = 2RT \ln\left(\frac{\langle L\rangle \rho_s \pi d^2 N_A}{8 M_s X^{0.5}}\right)$, where R is the molar gas constant, ρ_s and M_s are the surfactant micelle density and molecular weight respectively, and X is the surfactant mole fraction [30]. Alternatively, E_{sc} can be calculated from a similar equation $E_{sc} = 2RT \ln\left(\frac{\langle L\rangle \rho_s \pi d^2 N_A}{4 M_s \phi^{0.5}}\right)$ based on the surfactant volume fraction φ instead of the mole fraction [25]. The difference between the two equations derives from whether one assumes the mixing entropy to be ideal, or given by a

Flory-Huggins expression, neither of which is rigorous. From the volume fraction equation, E_{sc} = 38-48 kJ/mol, which is about 20% lower than that obtained using the ideal solution assumption. Either equation produces scission free energies for this system that are similar to the scission free energies of 55-71 kJ/mol found for SLE1S [25] and SLE1S/CAPB [17,30] solutions with NaCl.

The enthalpy of scission H_{sc} can be extracted from the slope of ln ($\langle L \rangle$) plotted against the inverse of temperature (as in Figure 3.4), giving H_{sc} = 200±10 kJ/mol or H_{sc} = 230±27 kJ/mol using the micelle lengths calculated from the correlations or fitted using the pointer algorithm respectively. Again, these values are similar to what has been found for SLE1S micelles [25].

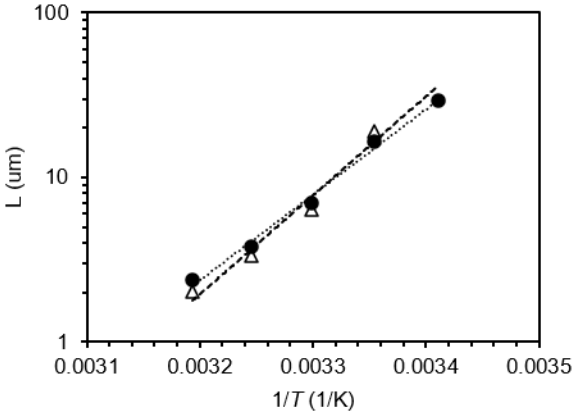

Figure 3.4: Micelle length from correlation (solid circles) and fitting (open triangles) plotted against the inverse of absolute temperature. Lines represent best-fit exponential functions.

Overall, for this system we find that the pointer algorithm and the correlations derived from it seem to be able to describe the rheology well. The discrepancies between the micelle parameters based on the pointer algorithm and the published values are because the published values were obtained from the original Cates method, which underestimates the micelle length [15], and also assumed a micelle diameter that was too small, as discussed above, leading to a too-small persistence length. We believe that our estimates of these parameters are significantly

more realistic than previous estimates for this micelle solution. Further discussion of how the other micelle parameters are affected by changing the micelle diameter can be found in Appendix D.

Micelles of Unusual Size

The last system that we examine in detail is a CTAB/NaSal solution from Galvan-Miyoshi *et al*. [13]. This system exhibits two peaks in the curve of viscosity as a function of the concentration of intercalating salt (Sal^-). Our solution of interest, namely 0.1 M CTAB/0.04 M NaSal solution at 22°C, lies in the region before the first viscosity peak, where micelles should be mostly linear; i.e., unbranched. From the rheology shown in Figure 3.5, the first crossover frequency is very low, ~0.01 rad/s, corresponding to an overall relaxation time of ~100 s, in contrast to some of the solutions above, where the relaxation time is 1 s or less. Moreover, the ratio G'/G" at the minimum in G" is also higher than previously seen, which, like the long relaxation time, indicates unusually long, entangled micelles. In fact, when we calculate the micelle parameters from our correlations, we find a predicted micelle length of 90 μm and a persistence length of 161 nm. Both the micelle length and persistence length are longer than found for the other systems discussed above. When we run a pointer algorithm simulation with the calculated parameters, we see good agreement with the experimental data, except that the prediction of the second crossover frequency is three-fold lower than in the experiments, as shown in Table 3.3. If, instead of extracting the persistence length from the high frequency data, we use a more "typical" surfactant micelle persistence length of 30 nm and the corresponding calculated micelle length of 89 μm, Figure 3.5 shows that the second crossover frequency from the pointer algorithm simulation matches the experimental value better, but the magnitudes of G'

and G" at high frequency are considerably underestimated. Table 3.3 compares features of the experimental rheology curves to the ones from the pointer algorithm simulations and shows how the longer persistence length better matches the magnitudes of G' and G" at intermediate to high frequency while the shorter persistence length agrees better with the second crossover frequency.

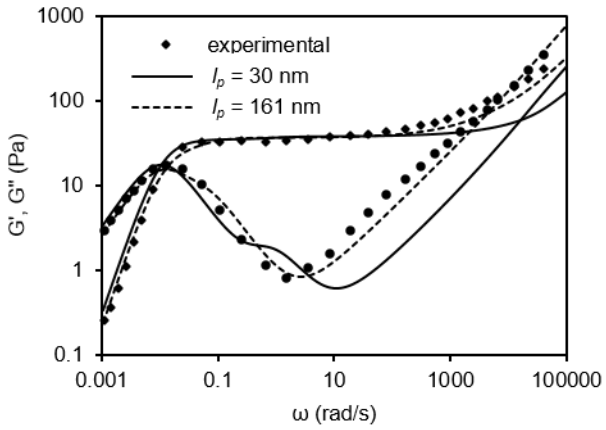

Figure 3.5: Experimental rheology for an 0.1 M CTAB/0.04 M NaSal solution compared to predictions of pointer algorithm simulations with parameters calculated from correlations that use the two different persistence lengths. Data from Galvan-Miyoshi *et al.* [13]

Table 3.3: Experimental rheology features compared to predictions of the pointer algorithm

	ω_{c1} (rad/s)	G'_{min}/G''_{min}	ω_{min} (rad/s)	ω_{c2} (rad/s)
experimental	0.0125	42.0	1.47	12300
l_p = 161 nm	0.0122	44.0	2.65	4370
l_p = 30 nm	0.0102	61.6	10.4	15800

Because l_p is determined from the magnitude of high-frequency data obtained from DWS, which (as discussed above) is sometimes vertically shifted to overlap the mechanical rheology, the procedure used to merge the data can affect the persistence length calculated. This may be part of the reason the persistence we extract from the data is higher than expected. Other

experimental and simulation methods indicate that l_p is usually in a range of about 20-50 nm, with most values being near 30 nm, which is why we choose this as our "typical" persistence length. For example, SANS studies on SLE1S/NaCl produced persistence lengths of 25-32 nm [25], flow birefringence gave l_p = 25-56 nm for CTAB/$NaNO_3$ [14], and coarse-grained molecular dynamics simulations of CTAC/NaSal showed l_p ~ 10-30 nm [43]. For the SLE1S+CAPB/NaCl solutions we studied earlier, the addition of longitudinal or full Rouse modes allowed both the second crossover frequency and magnitudes of G' and G" at high frequency to be fit well by the pointer algorithm, using a persistence length of l_p ~80 nm. The CTAB/NaSal solution of Galvan-Miyoshi *et al*. differs, however, from the SLE1S+CAPB system in that the former cannot have both its high-frequency data and second crossover frequency fit by a single persistence length. A longer persistence length of 161 nm fits the magnitude of the experimental data and a shorter persistence length of ~30 nm better agrees with the second crossover frequency. Extracting the micelle persistence length from high-frequency rheology is thus an area that still requires study, to determine if the variance in persistence lengths is due to inaccuracies in the experimental data, or perhaps to high-frequency relaxation modes that are not accounted for in the pointer algorithm. Appendix D contains simulations that explore how the value of the persistence length affects the other parameters when fitting rheology with the pointer algorithm.

The very long, "Brobdingnagian," micelle length for CTAB/NaSal, on the other hand, namely 90 μm when the persistence length is taken to be 161 nm, and 89 μm when it is taken to be 30 nm, seems plausible. The zero-shear viscosity of this CTAB solution is greater than 1800 Pa·s, which is over a million times greater than the viscosity of water, and 10-1000 times greater than that of other surfactant solutions that we have maintained should contain micelles that are at

least several microns long [15]. Although quantitative measurements of the micelle length are difficult to determine from cryo-TEM experiments, micrographs of CTAC/NaSal [51], CTAB/NaSal [52], and CTAB/salicylic acid [53], even at surfactant concentrations less than the 0.1 M CTAB solution considered here, show micelles that are very much longer than the field of view (i.e., greater than 100s of nm) since very few ends are visible in the micrographs, which is consistent with micelles being multiple microns long. Because of the long micelle length required to fit the rheological data, it would require too much computer time to run iterative pointer algorithm simulations to find the best-fit micelle parameters, but the correlations provide a way to estimate the parameters, which can then be checked by using them in a single, non-iterative simulation. The results from this simulation, in Figure 3.5 and Table 3.4, show good agreement with the experimental data, supporting a micelle length approaching 100 μm, as also indicated by the high zero-shear viscosity, long relaxation time, and large number of entanglements per micelle, given by $\langle L \rangle / l_e$. As with the systems above, differences between the parameters from the pointer algorithm and the published ones mainly come from the differences between our Eqs. 3.2 and 3.4 and the corresponding formulas from the Cates scaling with unit prefactor (namely $G_0 = \frac{k_b T}{\xi^3}$ and $\frac{G_0}{G''_{min}} = \frac{\langle L \rangle}{l_e}$), which likely underestimates the micelle length. The micelle length that Galvan-Miyoshi *et al*. calculated from the Cates scaling is over a micron (2.8 μm) but considering the high zero-shear viscosity and long relaxation time as compared to other solutions discussed above, these micelles are likely much longer.

Table 3.4: Micelle parameters for 0.1 M CTAB/0.04 M NaSal solution

l_p (nm)		ζ	τ_{br} (s)	G_0 (Pa)	$\langle L \rangle$ (μm)	l_e (nm)
161	corr.	0.00025	4.9	36.5	90.2	233

30	corr.	0.0019	16	37.8	89.0	230

Other Surfactant Systems

The sections above demonstrate that the pointer algorithm can be used to model the rheology of various surfactant solutions besides SLE1S+CAPB/NaCl, which was the focus of our earlier work. Through the use of correlations derived from the pointer algorithm, we also provide a way to estimate micelle parameters from experimental data that does not require running an iterative pointer algorithm simulation. This allows insight into a wider range of surfactant solutions, including solutions that approach the dilute regime, with micelles too short and weakly entangled to provide stresses high enough and relaxing slow enough for conventional rheometers to measure as well as ones that are so long and strongly entangled that a prohibitive amount of time is required to fit their rheology with the pointer algorithm.

Although the solutions we have examined so far represent some of the commonly studied surfactants and salts, rheological data for many other systems are found in literature. Additionally, besides surfactant and salt [47,54], cosurfactants and other additives, such as perfumes or oils commonly used in consumer products, can be added to the solutions [30,32]; a different solvent can be used [55]; or the temperature [40], salt concentration [13,14], or surfactant concentration [15] can be varied. Thus, the literature contains a wide variety of rheological studies performed on surfactant solutions that use different experimental methods and that change different experimental parameters than those considered here thus far. While in the sections above we explored a few systems in depth, here we look briefly at others and discuss how micelle parameters can be estimated for them. For these additional solutions we only calculate the micelle parameters using the correlations derived from the pointer algorithm, and

then run a forward predictive simulation for comparison with the experimental data. Since the determination of the persistence length is still uncertain, we calculate parameters using both 30 nm as an "average" value and 100 nm as an approximate upper bound for l_p.

First we consider an additional CPyCl/NaSal solution [56]. This is the same system as studied by Oelschlaeger *et al*. [40], at the same surfactant and salt concentration (0.1 M CPyCl/0.06 M NaSal, T = 20°C) as the earlier data of Oelschlaeger *et al*. examined above (in Figure 3.3), but with only mechanical data available in the data of Rehage and Hoffmann (Figure E1 in Appendix E shows the Rehage and Hoffmann data plotted on the same graph as the Oelschlaeger *et al*. data for comparison.) Both the earlier data set and the one presented in Figure 3.6 are generally in agreement with predictions of the pointer algorithm using parameters from the correlations, but with some variance around G''_{min}, which is usually the most difficult part of the rheology to fit. Unlike the merged Oelschlaeger data (containing both mechanical and DWS data), we get a good match at and around the first crossover frequency (similar to the fit obtained to the mechanical data of Willenbacher *et al*. [26] without the DWS data as shown in Appendix C), further showing the difference between the mechanical and DWS data for this solution.

The extracted micelle parameters (Table 3.5) are similar but do not agree exactly with those extracted from the nominally identical solution of Oelshlaeger *et al*. The micelle length extracted from the data of Oelschlaeger *et al*. and Willenbacher *et al*. is about 30 μm for the merged data, 20 μm for the mechanical data alone, and 40 μm for the DWS data alone; for the Rehage data it is around 50 or 60 μm depending on the persistence length used. These differences mostly come from disparities in the experimental data around G''_{min}, which besides sometimes being difficult to fit, also have a large effect on the micelle length. It is possible that a micelle length that better fits the experimental data might be found by iteratively running the

pointer algorithm, but the micelles are at or approaching a length that makes each iteration of the pointer algorithm fairly long. Given the variation in experimental data, we can at least conclude that we can fit the low-frequency data of Rehage and Hoffmann well and the intermediate frequency data somewhat well. We can also conclude that the micelles are a few 10s of microns long. These results are important in that to date, rheological measurements from different labs are essentially never compared, so that good "reference" data for solutions of threadlike micelles are essentially unknown, unlike the situation for entangled polymers. The comparisons carried out here thus help to establish the level of reproducibility of at least one set of rheological data in the literature. They also set a precedent for necessary future work aimed at establishing benchmark data sets for wormlike micellar solutions, and obtaining estimates of micellar parameters for those solutions and their dependence on salt concentration and temperature.

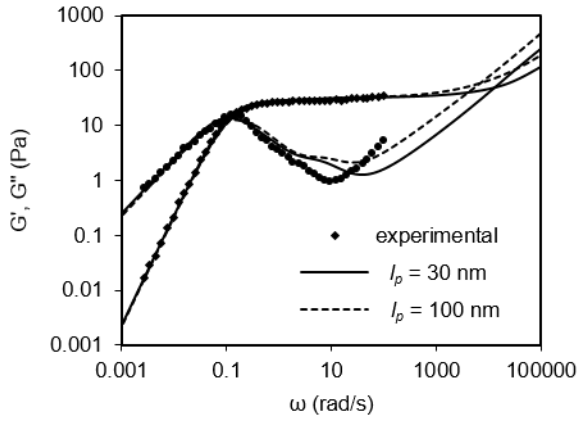

Figure 3.6: Predictions of pointer algorithm compared to experimental rheology for 0.1 M CPyCl/0.06 M NaSal solution at T = 20°C. Data from Rehage and Hoffmann [56]

Table 3.5: Micelle parameters for 0.1 M CPyCl/0.06 M NaSal solution

l_p (nm)		ζ	τ_{br} (s)	G_0 (Pa)	$\langle L \rangle$ (μm)	l_e (nm)
30	corr.	0.00027	0.81	31.5	64.3	253

100	corr.	0.00012	0.56	31.5	47.5	187

Finally, we extract micelle parameters for a few more solutions: 0.05 M NaOA in 0.6 M KCl [57], 1 wt% cetyltrimethyl tosylate (CTAT)/sodium dodecylbenzene sulfonate (SDBS) (at a 97/3 weight ratio) in 0.25 wt% sodium tosylate (NaTos) organic salt [27], 3 wt% sodium oleate (NaOA)/C_8TAB (at a 70/30 weight ratio) [54] with no added salt, 0.015 M CPyCl in 0.011 M NaSal [58], and 0.1 M CTAB in 0.0275 M NaSal [52]. These solutions contain a variety of surfactants and salts and have micelle lengths spanning over an order of magnitude, but most of which can be described well by the pointer algorithm. In all of these, the micelle parameters were obtained from the correlations in Eqs. 3.2-3.5, and then used in the pointer algorithm to predict the rheology.

All micelle parameters calculated from the correlations at the two persistence lengths of 30 nm and 100 nm are given in Table 3.6, but only the pointer algorithm predictions for the 0.05 M NaOA/0.6 M KCl solution are shown in Figure 3.7. Pointer algorithm predictions for the other solutions can be found in Appendix F along with additional commentary about fitting those solutions. In general, the good quality of the fit indicates that the correlations and the pointer algorithm can be used both to obtain micelle parameters and to fit rheological data for multiple surfactant solutions, including ones other than those we have concentrated on in previous work, such as the SLE1S or SLE1S+CAPB in NaCl solutions.

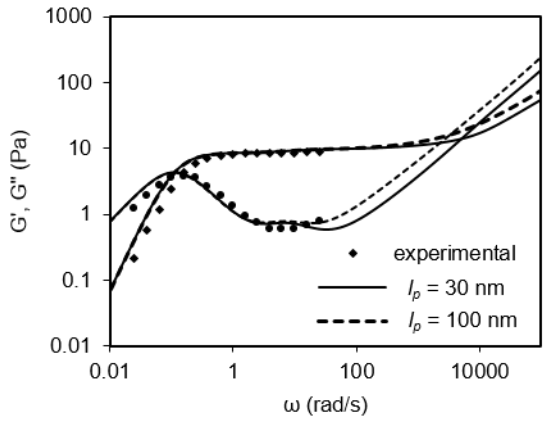

Figure 3.7: Predictions of pointer algorithm, with parameters based on correlations, compared to experimental rheology for 0.05 M NaOA/0.6 M KCl solution. Data taken from Kalur and Raghavan [57]

Table 3.6: Micelle parameters for additional surfactant solutions, all obtained from correlations in Eqs. 3.2-3.5.

l_p (nm)	ζ	τ_{br} (s)	G_0 (Pa)	$\langle L \rangle$ (μm)	l_e (nm)
		0.05 M NaOA/0.6 M KCl			
30	0.0033	2.0	9.45	51.1	499
100	0.0037	2.0	9.45	27.3	267
		1 wt% CTAT/SDBS/0.25 wt% NaTos			
30	0.0084	0.11	2.50	19.1	1040
100	0.014	0.13	2.50	8.93	487
		3 wt% NaOA/C_8TAB			
30	0.0038	23	22.7	90.9	307
100	0.002	18	22.7	63.7	215
		0.1 M CTAB/0.0275 NaSal			
30	105	5.0	22.4	1.8	309
30	105	22	22.4	3.0	309

0.015 M CPyCl/0.011 M NaSal					
30	0.077	0.80	0.5	23.5	2530
100	0.14	0.98	0.5	10.6	1140

The above demonstrates that the pointer algorithm describes reasonably well the linear rheology of a variety of surfactant solutions. However, the pointer algorithm is only able to predict linear rheology, leaving the nonlinear rheology of surfactant solutions without an accurate theory. On the other hand, the slip-spring model is able to model both linear and nonlinear rheology. Since we have shown that rheology predictions from the pointer algorithm and slip-spring simulations agree with each other, this would now allow one to measure the linear rheology of a surfactant solution, obtain the micelle parameters using the pointer algorithm, and then input those parameters into the slip-spring model to predict the nonlinear rheology. This combination of simulation methods would thus take advantage of the pointer algorithm's ability to extract micelle parameters from linear rheology and the slip-spring model's capability of modeling nonlinear rheology to achieve greater insight into surfactant solution rheology. In the future, such a strategy could be used to test the modeling by predicting complex nonlinear rheology, perhaps along with other properties such as SANS patterns, in large amplitude oscillatory shearing, for example [59].

Conclusions and Future Directions

We found that the pointer algorithm can fit the rheology of, and extract micelle parameters from, a variety of surfactant systems, ranging from CTAB in NaCl or NaSal solutions, known to form long, well-entangled micelles; to SLE1S/CAPB in NaCl solutions, commonly found in consumer products like soaps and shampoos. We also showed that

correlations derived from the pointer algorithm provide estimates of the micelle parameters that yield similarly good predictions of the rheology, and can be used in place of the fitting procedure, which is especially useful when fits are hard to perform because of the length of the micelles. The simulations also provide guidelines for how and when to apply the pointer algorithm and correlations.

Moreover, we have shown that the pointer algorithm gives predictions of linear rheology that are almost identical to that of the slip-spring simulation, up to the highest entanglement density we can attain with the latter. The slip-spring simulation method has been well validated by comparisons of its predictions with well-characterized entangled polymer solutions. Since micelle parameters such as length and breakage time cannot readily be obtained except through fits to rheological data, the validation of the pointer algorithm through its agreement with the slip spring model is essential to confirm that micelle parameters obtained from the pointer algorithm are reasonable.

At lower concentrations, where the micelles are weakly entangled, if high frequency data that include the second crossover frequency are available, the pointer algorithm can be used to fit the data and extract micelle parameters. Without high frequency data, the micelle parameters can be calculated from our correlations but the data cannot be fit by the pointer algorithm using the automated fitting procedure. However, because of greater uncertainty in the values used to estimate the micelle parameters (primarily in how the ratio G'_{min}/G''_{min} is approximated), the fits and parameter values may not be as accurate as for more entangled micelles. The rheological data at low surfactant or salt concentrations have no minimum in G" and have a first crossover frequency that is greater than 1 rad/s, which usually corresponds to a micelle length of a few microns or less.

As the surfactant or salt concentration increases, the micelles grow in length and become well-entangled; the first crossover frequency then decreases to around 0.1-10 rad/s, and the minimum in G" becomes pronounced, with G'_{min}/G''_{min} ratios of ~5-15 and micelle lengths of ~3-25 μm. For these solutions, the micelle parameters can be determined either from a fit to the rheology by the pointer algorithm or from the correlations, although for a few cases, usually at lower surfactant concentrations, the correlations can produce parameters and G' and G" curves that differ significantly from the data and from the best-fit by the pointer algorithm.

At still higher concentrations, where the micelles are highly entangled, the first crossover frequency further decreases to 0.01-0.1 rad/s, and the ratio G'_{min}/G''_{min} increases to values greater than 15. The micelle length then ranges from 20-100 μm. At the lower end of this range, it is still possible to fit the rheology using the iterative pointer-algorithm simulations, but this can be time consuming. For the longest micelles, it is more practical to estimate the micelle parameters from the correlations and then run a single iteration of the pointer algorithm with those parameters to check the predicted linear rheology curves against the experimental data. Results are generally in good agreement with experimental data, with the greatest deviations occurring in the G" curve near the minimum.

Overall, the pointer-algorithm simulations and correlations seem to do a good job of matching surfactant micelle rheology across a variety of different surfactants, salts, and concentrations that span more than two orders of magnitude in the micelle length. This indicates universal behavior in the rheology of these solutions, although some uncertainties remain, particularly with the high-frequency data. In particular, the shift factor that is sometimes required to match the magnitudes of mechanical and DWS data has not been fully explained. There are also variations in the shapes of the mechanical and DWS data which can have a significant effect

on the extracted micelles parameters. When the persistence length is extracted from the high-frequency data, for some more entangled solutions the magnitude of the curves and the frequency of the second crossover frequency cannot always be fit – the persistence length calculated to match the magnitude of the moduli can be 3-5 times longer than the persistence length that fits the second crossover frequency. These disparities remain in need of explanation and correction. In general, however, the pointer algorithm and the theories it combines are consistent with surfactant wormlike micelle rheology and the correlations we developed provide a relatively simple way to extract micelle parameters from rheology.

Despite some remaining uncertainties, the results for several surfactant systems indicate "universality" in the rheology of entangled wormlike micelles that can be captured by an adaptation of polymer entanglement theory, with a limited number of micelle parameters that can be obtained by fits to linear rheological data. These micelle parameters are the micelle length, micelle breakage time, plateau modulus, and persistence length, along with the other known inputs of solvent viscosity and micelle diameter. The difficulty of correlating rheology with micelle parameters, such as micelle length, has been hindered by inability to control, or accurately measure, these parameters a priori, thus requiring fitting by a rheological model to convert those measurements into estimates of the micelle parameters. The consistency of micelle solution rheology with predictions of the pointer algorithm suggest that this model is accurate enough to provide useful estimates of these parameters. Further steps are required to confirm or correct these estimates from a combination of experimental data and molecular dynamics simulations, and to develop correlations and theories for how the micelle parameters depend on salt concentration and other additives. Ultimately, an ability to link both linear and nonlinear

rheological properties to concentrations of surfactant, salt, and other additives would be highly desirable to enable rational design of these important solutions.

Acknowledgements: The authors thank Takeshi Sato for providing the slip-spring simulations at $Z = 9$ used for comparison with the pointer algorithm. Funding was provided by Procter and Gamble, as well as the National Science Foundation under grant CBET-1907517. Any opinions, findings, and conclusions or recommendations expressed in this material are those of the authors and do not necessarily reflect the views of NSF.

Chapter 4: The Pointer Algorithm User Manual

Now that the pointer algorithm has been validated using slip-spring simulations and has been shown to be applicable to a variety of surfactant systems, we want to make the pointer algorithm simulation code and correlations available for use by other researchers. To that end, in what follows, we provide instructions for setting up and running pointer algorithm simulations. This user manual, the mentioned Excel spreadsheet, and the pointer algorithm simulation code will be archived in the University of Michigan's Deep Blue digital repository and publicly accessible.

Introduction

The "pointer algorithm" is a mesoscopic simulation method that models the linear rheology of surfactant solutions containing wormlike micelles. It can be used for the following purposes:

1) to extract micelle parameters (e.g. micelle length, plateau modulus, and breakage time) from experimental small amplitude oscillatory shear rheology
2) to predict G' and G" rheology curves from a given set of micelle parameters
3) to compare the G' and G" curves from specified micelle parameters to an experimental data set.

The pointer algorithm is based on the Cates theory [5] that states that micelles, like entangled polymers, relax by diffusing through a tube formed by surrounding micelles, a process also known as reptation. However, unlike polymers, micelles can reversibly break and rejoin. In the pointer algorithm, reptation, breakage, and rejoining are simulated for an ensemble of micelles.

High frequency relaxation modes, namely Rouse [60] and bending [21] modes, are also added analytically to the pointer algorithm, and the effects of contour length fluctuations and constraint release (double reptation) are considered in the simulation as well. A detailed explanation of the pointer algorithm can be found in [16].

Version history

The pointer algorithm was originally developed in the Larson lab by Weizhong Zou, and has been modified by Grace Tan. It is written in Fortran (F90) and several notable versions are described below.

[unmerged] – This version of the pointer algorithm models the relaxation of well-entangled micelles. It was shown to be able to match the rheology of a couple common surfactant/salt systems from literature [16] and was fit to several SLE1S+CAPB/NaCl solutions [30,44]. A full description of this version is found in Ref. [16].

v3.1 – In this version of the pointer algorithm, additional contributions to relaxation from unentangled micelles (shorter than the entanglement length) are added to the simulation. These added relaxation mechanisms, explained in Ref. [17], allow the pointer algorithm to be applied to surfactant solutions at lower concentrations than previously possible.

v3.3 – After a comparison of the pointer algorithm with the more highly resolved slip-spring model [23], we found that the assumption that longitudinal (slow) Rouse modes can be neglected because entanglements impede relaxation along the micelle seems to be incorrect. Instead, for

well-entangled micelles (an average of >15 entanglements per micelle), both fast and longitudinal Rouse modes must be considered, and if micelles are weakly entangled (an average of <15 entanglements per micelle), an unfractionated, full spectrum of Rouse modes best describes the high-frequency data. These additional Rouse modes were added to the pointer algorithm in this version, as described in Ref. [15], which also shows improved fits to SLE1S+ CAPB/NaCl rheological data.

Preparing the simulation input file

To run a pointer algorithm simulation, there is a single input file, titled INPUT_[version].DAT. The instructions shown here will be for version 3.3 and are mostly, but not exactly, applicable to earlier versions. Figure 4.1 below shows a sample input file for reference. In the sections below, inputs are referenced as [line number].[column number] and "yes" and "no" are designated as "Y" and "N" respectively. This section provides general instructions for creating an input file; examples with sample numerical calculations and results are given below in the "Example simulations" section.

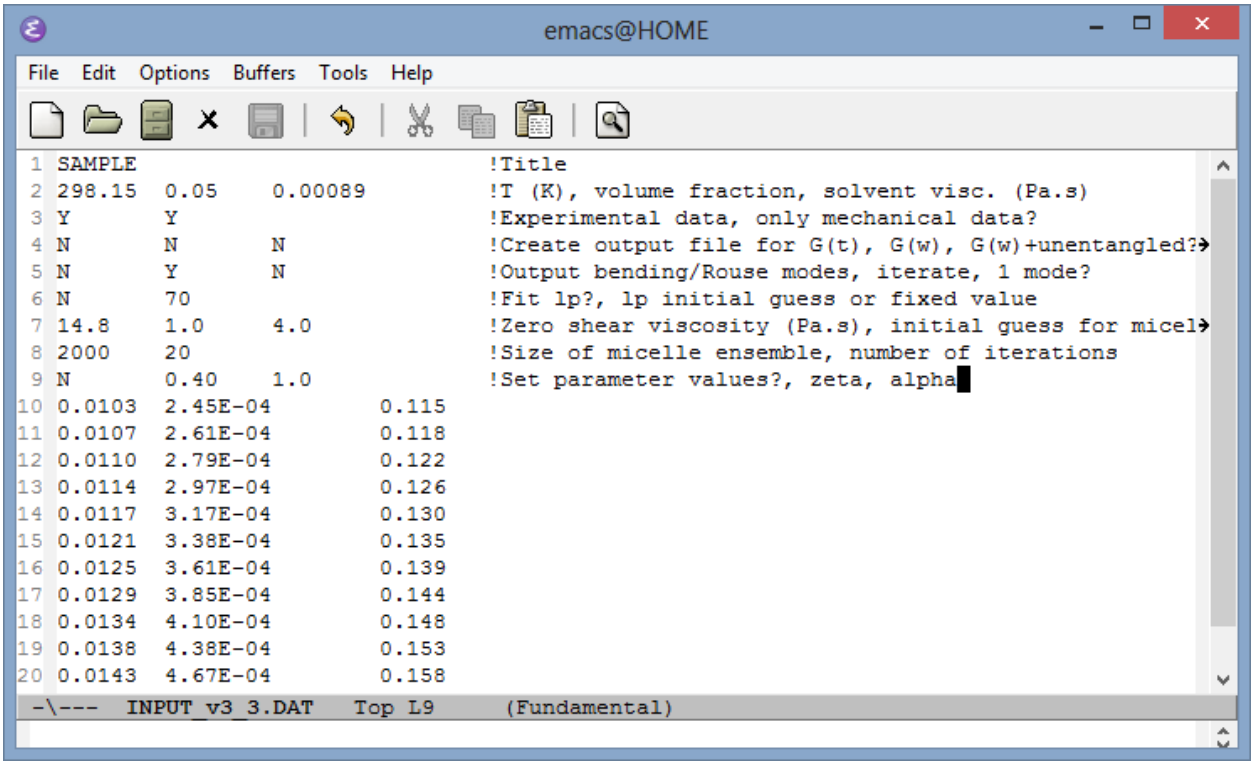

Figure 4.1: Sample input file for v3.3 of the pointer algorithm

1. Title – This can be the sample ID, a description of the surfactant/salt and concentration, or any other kind of identifier. It has no effect on how the simulation runs.

2.1. Temperature [K] – The temperature at which the experimental data were collected or at which you want to generate predictive rheology curves.

2.2. Micelle volume fraction ϕ – Ratio of the micelle volume to the total solution volume. For most systems that we've investigated, the volume fraction is within 10% of the weight fraction, so weight fraction can be used if volume fraction cannot be calculated or estimated another way.

2.3. Solvent viscosity η_s [Pa·s] – The solvent viscosity can either be that of the salt solution without surfactant, if measured separately, or if not, the viscosity of pure water at the appropriate temperature.

3.1. Are experimental data present? [Y/N]

- Y to run an iterative pointer algorithm simulation that fits the experimental data and extracts micelle parameters or a simulation that compares input micelle parameters to experimental data without iterating to fit the experimental rheology
- N to run a predictive pointer algorithm simulation for a given set of micelle parameters without comparing them to any experimental data

3.2. Are only mechanical data present? [Y/N]

- Y if the data are from a mechanical rheometer and go up to ~100-200 rad/s (also select yes if no data are present at all)
- N if there are high-frequency data (up to or greater than ~100,000 rad/s) from DWS or another experimental method

4.1. Should a file containing G(t) from reptation be generated? [Y/N] – If this option is selected, a file containing the G(t) curve from reptation and its best fit from the genetic algorithm (fitting with multiple Maxwell modes) for the current iteration will be outputted.

4.2. Should a file containing G'(ω) and G"(ω) from reptation be generated? [Y/N] – This option outputs a file containing the G(t) (reptation) curve for the current iteration transformed into the frequency domain.

4.3. Should the simulation output G'(ω) and G"(ω) with the contribution of unentangled micelles in a separate file? [Y/N] – This file contains G' and G" from reptation with relaxation from unentangled micelles (rotary relaxation, Rouse modes, and bending modes) added.

5.1. Should the simulation output the contributions to G'(ω) and G"(ω) from high frequency relaxation modes in separate files? [Y/N] – If this option is selected, the simulation will generate separate files with G' and G" for 1) rotary relaxation of unentangled micelles, 2) Rouse modes for unentangled micelles, 3) bending modes for unentangled micelles, 4) Rouse modes for entangled micelles, and 5) bending modes for entangled micelles.

5.2. Is an iterative simulation being run? [Y/N]

- Y if fitting to experimental data
- N if predicting the rheology of a specific set of micelle parameters (either independently of experimental data or to compare to experimental data)

5.3. Should the simulation try to fit G(t) from reptation with a single Maxwell mode? [Y/N] – The genetic algorithm that converts G(t) from the time to frequency domain allows a minimum of 2 Maxwell modes. With this option, the simulation will first try to fit G(t) with a single Maxwell mode. If the error is low enough, the simulation continues with the 1 Maxwell mode; if the error is too high it uses the genetic algorithm to find a better fit.

6.1. Is the persistence length a fitting parameter? [Y/N]

- Y if high frequency data are available and you want the simulation to extract the persistence length from the data
- N if no high frequency data are available or you want to set the persistence length yourself

6.2. Initial guess or fixed value for the persistence length l_p [nm] – For iterative simulations without high frequency data or predictive simulations, the persistence length is a required input parameter that would have to come from another experimental method or literature. For iterative simulations with high frequency data, the value for l_p entered here is either the starting value of l_p for the first iteration or chosen to be fixed depending on what was entered for input 6.1.

7.1. Zero shear viscosity η_0 [Pa·s] – If the zero shear viscosity was not measured for the solution of interest, it can be extracted from the slope of G" at low frequency. This value will not affect how the simulation converges, but the simulation may not think it's converged even if it has and keep running. The zero shear viscosity is not required as an input to run a predictive pointer algorithm simulation but can help in judging how well the predicted rheology curves match experimental data if making such a comparison.

7.2. Initial guess or value of the average micelle length $\langle L \rangle$ [μm] – For iterative fitting simulations, a better initial guess for $\langle L \rangle$ can decrease the number of iterations it takes before convergence. As a general estimate, for solutions with $\eta_0 < 10$ Pa·s, $\langle L \rangle_0 = 1$ μm is a reasonable starting guess, increasing to $\langle L \rangle_0 = 5\text{-}10$ μm for 10 Pa·s $< \eta_0 <$ 100 Pa·s.

7.3. Micelle diameter d [nm] – This input parameter cannot be determined from rheology. The literature value for a variety of systems is ~4 nm.

8.1. Number of micelles N in the simulated ensemble – The number of micelles in the ensemble needs to be large enough that the length distribution is not overly discretized, but more micelles take more time to simulation. From tests of the ensemble size, we have determined

that 2000 micelles balances getting a good length distribution with simulation time. [Note that fewer micelles can be used, but certain parameters may be under or overestimated. If not running an iterative simulation and the micelles are very long the ensemble size can be decreased to ~500 micelles without overly affecting the predicted rheology curves to get the simulation to finish in a reasonable amount of time.]

8.2. Number of iterations – Our standard for an average set of experimental data is 20 iterations and 5 days of compute time on a high-performance computing cluster.

9.1. Is the simulation being started with all parameters specified? [Y/N] – Out of the five independent micelle parameters (d, l_p, $\langle L \rangle$, ζ, α), d cannot be determined from rheology and must be specified, l_p can be extracted from high-frequency data but at least requires a starting value, $\langle L \rangle$ needs a starting value as input, and ζ and α can both either start from user-input values or from simulation-estimated values.

- Y if running an iterative simulation and all parameters have been pre-calculated or restarting a simulation from a previous set of parameters. Also enter yes if running a predictive pointer algorithm simulation, for which all independent micelle parameters must be inputted. (See "Calculating micelle parameters" below for how to extract micelle parameters from experimental rheology using previously developed correlations.)
- N if running an iterative pointer algorithm simulation with no initial guesses for ζ and α

9.2. Initial guess or value for dimensionless breakage time ζ (not required if input 9.1 = N)

9.3. Initial guess or value for semi-flexibility factor α (not required if input 9.1 = N)

10-EOF. Experimental rheology data in three columns, in the order ω [rad/s], G'(ω) [Pa], G"(ω) [Pa]. See Figure 4.2 below about preparing experimental data for input. In particular, especially when using mechanical data only, watch for poor data at the lowest frequencies where the modulus may be lower than the physical limits of the rheometer and the highest frequencies where inertial effects can begin to affect the data.

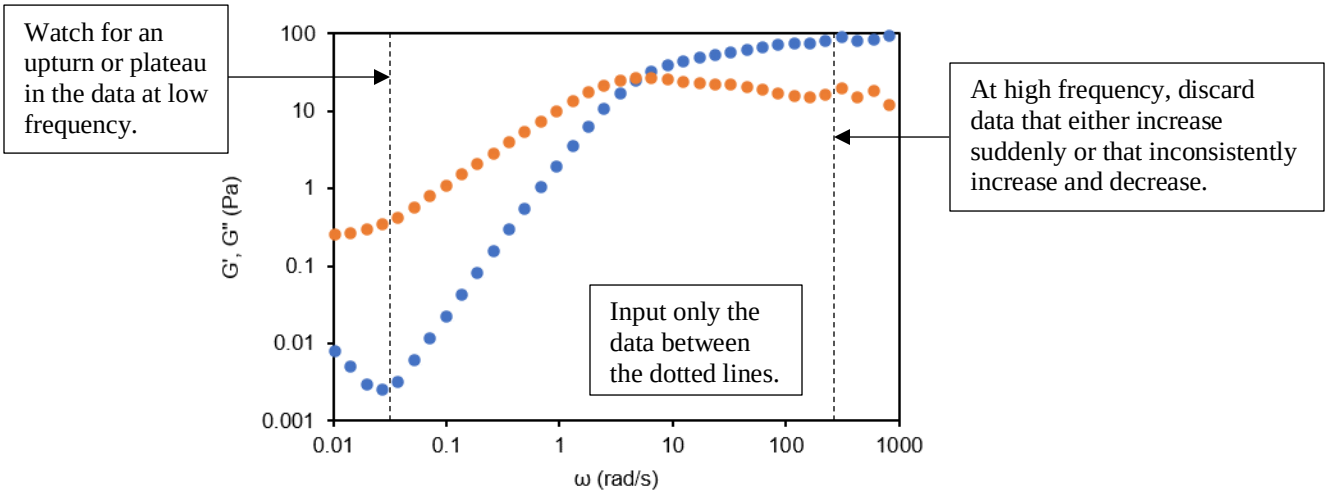

Figure 4.2: Example experimental rheology data

Calculating micelle parameters

The independent fitting parameters α, l_p, $\langle L \rangle$, and ζ can be estimated from experimental rheological data using correlations derived from pointer algorithm simulations. The process was detailed in Chapter 3 and is also summarized below.

1) Obtain solution parameters T (K), ϕ, and η_s (Pa·s).

2) Get experimental parameters G'_{min} (Pa), G''_{min} (Pa), and ω_{c1} (rad/s) from the rheology data. G'_{min} and G''_{min} are the values of G' and G" at the frequency where G" has a minimum. If there is no minimum in G", either the maximum of the ratio G'(ω)/G"(ω) or the limit of 1 can be used in the calculations below. ω_{c1} is the first crossover frequency, where the G' and G" curves intersect at low frequency.

3) Calculate G_0 (Pa) from the correlation

$$\frac{G_0}{G'_{min}} = \frac{4.25}{G'_{min}/G''_{min}} + 0.625 \text{ if } G'_{min}/G''_{min} < 10 \text{ or take}$$

$$G_0 \approx G'_{min} \text{ if } G'_{min}/G''_{min} > 10. \qquad (4.1)$$

4.1) If l_p (m) is known or will be specified, calculate α from the crossover formula

$$G_0 = \frac{\alpha^3}{3+\alpha^3} 9.75 \frac{k_B T}{\alpha^3 l_p^{1.8}} + \frac{3}{3+\alpha^3} \frac{28}{5\pi} \frac{\phi k_B T}{d^2 l_e} \qquad (4.2)$$

4.2) To extract l_p from the high-frequency data, perform steps 4.1 and 4.2 simultaneously to determine α and l_p, solving the crossover formula while minimizing the error of fitting bending modes to the G" high-frequency data at the same time. Equation for bending modes:

$$G'' - \omega\eta_s = Im\left[\frac{1}{15}\rho\kappa l_p\left(\frac{-2i\varsigma_\perp}{\kappa}\right)^{3/4}\omega^{\frac{3}{4}}\right] \qquad (4.3)$$

where the area density of micelles $\rho = \frac{\phi}{\pi d^2/4}$,

the bending modulus $\kappa = k_B T l_p$,

and the lateral drag coefficient $\varsigma_\perp = \frac{4\pi\eta_s}{\ln(0.6\xi/d)}$

5) Calculate $\langle L\rangle$ (m) from the correlation

$$\frac{G'_{min}}{G''_{min}} = 0.317\left(\frac{\langle L\rangle}{l_e}\right)^{0.82} \qquad (4.4)$$

using l_e as calculated from $\alpha \equiv \frac{l_e}{l_p}$

6) Calculate $\xi \equiv \tau_{br}/\tau_{rep}$ from the correlation

$$\tau_R = \frac{1}{\omega_{c1}} = 0.484\tau_{br}^{0.63}\tau_{rep}^{0.37} \qquad (4.5)$$

where the reptation time $\tau_{rep} = \frac{2\langle L\rangle^3}{\pi^2\alpha D_0}$,

in which the translational diffusivity within the tube $D_0 = \frac{k_B T}{\varsigma}$

and the drag coefficient $\varsigma = \frac{2\pi\eta_s}{\ln(\xi/d)}$

[Note: We have provided an Excel spreadsheet that can be used to aid in calculating the micelle parameters as outlined above.]

Running a pointer algorithm simulation

The pointer algorithm can be compiled using the gfortran compiler and run locally in a command line or IDE, or run remotely on a computing cluster.

Understanding the output files

RESULT.DAT – At the end of the simulation, this file will contain the final extracted micelle parameters and G' and G" curves. For a noniterative pointer algorithm simulation, the parameters should match the inputs and the G' and G" curves are the predicted rheology. For an iterative simulation, the output is either the converged results or the results from the final (unconverged) iteration, in which case you may decide to restart the simulation with the final micelle parameters.

result_fit.dat – After every iteration, the simulation checks the error between the G' and G" curves from the current iteration and the experimental data. If the error has decreased from previous iterations, the current best-fit parameters and rheology curves are recorded in this file.

GF_t.DAT – This file contains the stress relaxation curve from reptation and its fit using the genetic algorithm assuming multiexponential relaxation of the form $\mu(t) = \sum_i \mu_i e^{t/\tau_i}$. These data are normalized by the plateau modulus and are in the form [time (s), μ(t) from simulation, μ(t) fitted with the genetic algorithm].

GW.DAT – The contents of the above file transformed into the frequency domain, scaled by the plateau modulus. The columns of this file are [ω (rad/s), G'(ω) (Pa), G"(ω) (Pa)] with $G'(\omega) = \sum_i G_0 \mu_i \frac{\omega\tau_i}{1+\omega^2\tau_i^2}$ and $G''(\omega) = \sum_i G_0 \mu_i \frac{(\omega\tau_i)^2}{1+\omega^2\tau_i^2}$.

rotary.dat, rouse_u.dat, bending_u.dat, rouse.dat, bending.dat – These files contain contributions to relaxation from rotary relaxation, Rouse modes of unentangled micelles, bending modes of unentangled micelles, Rouse modes of entangled micelles, and bending modes of entangled micelles respectively. All of these files contain data in the format [ω (rad/s), G'(ω) (Pa), G"(ω) (Pa)].

NEW_INPUT.DAT – This file tracks the best-fitting iteration and creates a new input file with those parameters in case the simulation does not converge and you want to restart it from the best-fit parameters. Note that it does not contain the experimental data that were input.

result_in.dat – The predicted G' and G" values are output to this file at the same frequencies as the experimental data for the best-fit iteration. Certain features of the experimental and pointer algorithm rheology such as the first crossover frequency are also output to this file. This information can be useful to manually compare the pointer algorithm predictions to the experimental data at the same frequencies.

<u>Other files:</u>

SIMULATION OUTPUT.DAT – This is an intermediate file that records the micelle parameters and the calculated error between the pointer algorithm G' and G" curves and the experimental

data at each iteration. If the simulation is not converging, this file may be useful. You can look for iterations with lower error and restart the simulation from those parameters as an alternative to using the simulation-determined best-fit parameters.

INTRADATA.DAT – This file contains the micelle parameters and G' and G" curves for every iteration. It can be used to manually compare any iteration to the experimental data after potential iterations of interest have been identified in the SIMULATION OUTPUT file.

TEMP.DAT – The unrelaxed fraction of micelles $\mu(t)$ is written to this file in the format [time step (#), time (s), $\mu(t)$].

TIME_FREQUENCY TRANSFORMATION.DAT – This file has the results from fitting $\mu(t)$ to a multiexponential expression with the genetic algorithm. The data pairs are [μ_i, τ_i].

SIMULATION MONITOR.DAT – This file tracks the step of the pointer algorithm currently being performed (reptation, the genetic algorithm, etc.).

Example simulations

Example 1: An iterative pointer algorithm simulation

This example shows how to set up an iterative pointer algorithm simulation and the simulation results. The solution considered is a SLE1S + CAPB/NaCl solution with merged mechanical and high-frequency DWS rheology shown in Figure 4.3 below. The rheology was measured at 25°C, the salt solution (solvent) has a viscosity of η_s = 0.0011 Pa.s, the zero shear viscosity of the

surfactant solution was measured to be 26.1 Pa.s, and the surfactant concentration was calculated to give a volume fraction of 0.06.

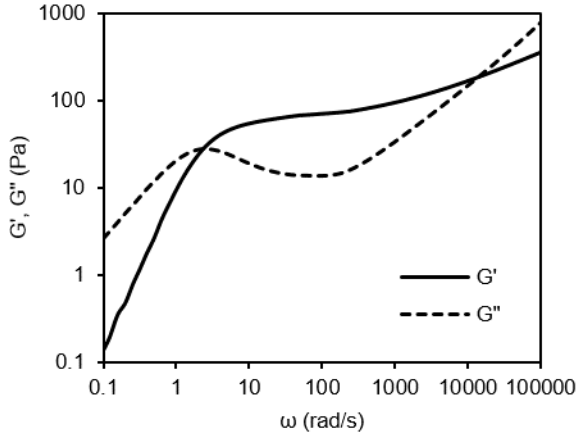

Figure 4.3: Experimental rheology for example SLE1S/CAPB solution.

Along with those known experimental parameters, we also need to estimate starting values for the micelle parameters and select options for the simulation. In this case, if we opt not to pre-calculate the micelle parameters before beginning the simulation, we only need to make guesses for the starting persistence length and the micelle length. For the persistence length, because high-frequency data are available, we choose to have the simulation fit the persistence length and estimate a starting value of 80 nm, close to values we previously found for other SLE1S/CAPB solutions. For the micelle length, the experimental data do show a minimum in G", but the ratio of G' to G" at the frequency where G" has its minimum is only moderately high (~5) so we don't expect the micelle length to be extremely long and guess 3 μm as a starting value for the micelle length. After choosing starting values for the micelle and persistence lengths, we can generate the input file for the simulation, shown in Figure 4.4.

In Figure 4.4 below, the experimental parameters T, ϕ, η_s, and η_0 (units given in the "preparing the simulation input file" section) are entered in lines 1 and 7 (column 1). The estimated micelle parameters, the persistence length and micelle length, are inputs 6.2 and 7.2 respectively. If we had also wanted to estimate the other independent fitting parameters α and ζ, those would have been entered in line 9 (and Y entered for input 9.1).

Line 3 contains the information about the form of the experimental data. Input 3.1 (Y) signifies that experimental rheological data are available, and 3.2 (N) means that high-frequency data are present. Since we entered Y for all items in line 4, the simulation will generate the output files GF_t.DAT, GW.DAT, and a file containing the contribution to relaxation from unentangled micelles added to the data in GW.DAT for the most recent iteration. See the above section for more information on the contents of GF_t.DAT and GW.DAT.

Input 5.1 is the switch for generating separate output files for the contributions to relaxation from Rouse, bending, and rotary modes for entangled and unentangled micelles. For the example simulation in Figure 4.4, these files will be output. Input 5.2 (Y) tells the simulation to iterate and fit the experimental data, not run a single-iteration predictive pointer algorithm simulation. The last input on line 5 (N) means that the simulation will not try to fit the stress relaxation curve from reptation with a single Maxwell mode, but will use the Genetic Algorithm to fit the stress relaxation curve with an appropriate number of modes.

As mentioned above, input 6.2 is the starting value of the persistence length in nanometers. Input 6.1 (Y) is the option for the pointer algorithm to fit the high-frequency data and extract the

persistence length as a fitting parameter. We can choose this option because high-frequency data are present in this example.

The final input in line 7 is the micelle diameter in nanometers. We usually use a value of 4.0 nm here, but if a separate measurement of the micelle diameter is available from SANS or another experimental method, the diameter can be input here.

Line 8 contains the inputs for the number of micelles and number of iterations. From a series of simulations fitting experimental rheology with different ensemble sizes, we determined that 2000 micelles is the smallest ensemble size that gives the same results as larger ensembles (see Appendix D). For the number of iterations, we find that 20 is a good number to allow enough iterations and time for the parameters to converge.

Line 9 was described above, and finally, lines 10 to the end of the file contain the experimental rheology in the order [ω(rad/s), G' (Pa), G"(Pa)].

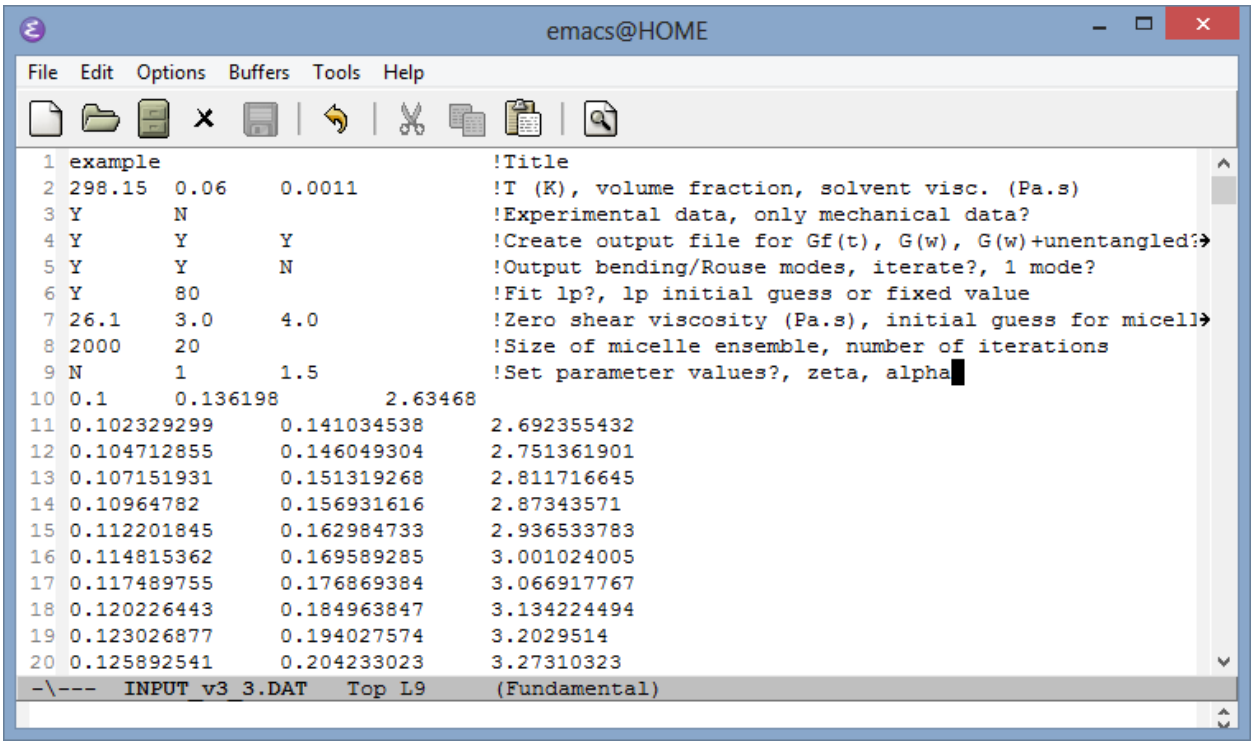

Figure 4.4: Example input file for data shown in Figure 4.3.

After completing the input file, we transferred the input file, the simulation code, and a submission script to the University of Michigan's high-performance computing cluster. [The simulations can be run locally, but their length often makes it more practical to run them remotely.] The simulation was given 5 days of wall time, but converged after 16 hours and the results are shown in Figure 4.5 and Table 4.1.

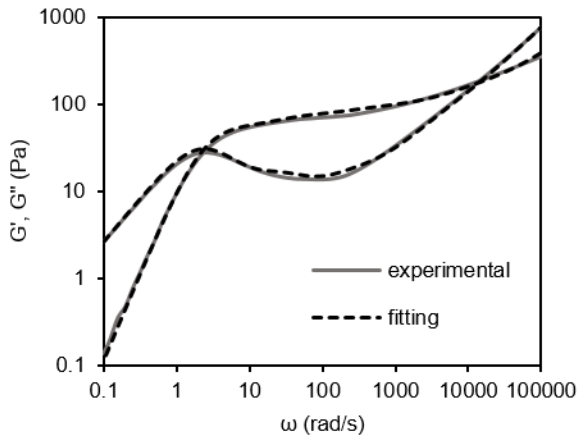

Figure 4.5: Example simulation results showing the fitted pointer algorithm rheology curves compared to the experimental data.

Table 4.1: Fitted micelle parameters extracted from experimental rheology

parameter	value
ζ	0.2
τ_{rep} (s)	3
τ_{br} (s)	0.4
$\langle L \rangle$ (μm)	3.7
G_0 (Pa)	98
l_e (nm)	140
l_p (nm)	91
$\alpha \equiv l_e/l_p$	1.6
$Z \equiv \langle L \rangle / l_e$	26

From Figure 4.5, we see good agreement between the pointer algorithm results and the experimental data.

Example 2: A predictive pointer algorithm simulation

If in the above example we had chosen to pre-calculate our micelle parameters, thought the micelles were very long, or didn't want to wait for an iterative simulation to converge, we could

instead have run a predictive pointer algorithm simulation. To run a predictive simulation, we need to have better estimates of the micelle parameters, which can be obtained from the correlations in the "Calculating micelle parameters" section.

First, we need the experimental parameters T = 298 K, ϕ = 0.06, and η_s = 0.0011 Pa.s and the experimental rheological parameters G'_{min}, G''_{min}, and ω_{c1}. For this data set, G'_{min} = 69.9 Pa, G''_{min} = 13.8 Pa, and ω_{c1} = 2.34 rad/s.

The ratio G'_{min}/G''_{min} = 5.06 is less than 10 so Eq. 1 is used to calculate G_0 and

$$G_0 = G'_{min}\left(\frac{4.25}{G'_{min}/G''_{min}} + 0.625\right) = 69.9\ Pa\left(\frac{4.25}{69.9\ Pa/13.8\ Pa} + 0.625\right) = 102\ Pa$$

Next, because we want to extract the persistence length from the high-frequency rheology, Eqs. 4.2 and 4.3 must be solved simultaneously. Here we use an Excel spreadsheet that has been set up for this purpose. Part of the spreadsheet is shown in Figure 4.6. Columns M, N, and O are the experimental data. Column P is the right-hand side (RHS) of Eq. 4.3, calculated from the experimental data and column R is the LHS of Eq. 4.3, initially calculated from the known micelle parameters and placeholder values for l_e and l_p. We are interested in the high-frequency data when the slope is 0.75, so we calculate the slope of column P on a log-log scale in column Q. We look for where the slope of the RHS of Eq. 4.3 is close to 0.75 and sum the differences (error) between columns P and R, the left and right sides of Eq. 4.3. The spreadsheet is also simultaneously calculating the plateau modulus from Eq. 4.2 and comparing it to G_0 determined earlier from Eq. 4.1, 102 Pa. We then use solver to minimize the two sources of error (from fitting to high frequency data and from the already calculated G_0) by varying l_e and l_p. The solver

solution for this experimental data set is l_e = 141 nm and l_p = 92.5 nm, so $\alpha = \frac{l_e}{l_p} = \frac{141\ nm}{92.5\ nm} =$ 1.52.

M	N	O	P	Q	R	S
Experimental data			RHS			
ω (rad/s)	G' (Pa)	G" (Pa)	G"-ηs.ω (Pa)	slope	LHS	error
75857.76	322.3717	631.219	545.1963215	0.727341	545.6441	-0.4478
77624.71	324.9301	642.4478	554.4214016	0.728707	555.1489	-0.7275
79432.82	327.5093	653.8931	563.8163013	0.729764	564.8192	-1.00294
81283.05	330.1099	665.5613	573.3863309	0.730971	574.658	-1.2717
83176.38	332.733	677.4594	583.1374097	0.732357	584.6682	-1.5308
85113.8	335.3766	689.5866	593.0675951	0.733329	594.8528	-1.78517
87096.36	338.0445	701.9581	603.1908119	0.735052	605.2147	-2.02391
89125.09	340.7325	714.5666	613.4987032	0.735893	615.7572	-2.25847
91201.08	343.4428	727.4227	624.000669	0.737141	626.4833	-2.48261
93325.43	346.1748	740.5302	634.6991273	0.738285	637.3962	-2.69709
95499.26	348.9317	753.9033	645.6071364	0.740042	648.4993	-2.89212
97723.72	351.7086	767.5323	656.7136413	0.740772	659.7957	-3.08206
100000	354.51	781.4361	668.036062	0.742387	671.2889	-3.25286
						0.009121

Figure 4.6: Portion of Excel spreadsheet showing fitting to Eq. 4.3, scrolled to the high-frequency data where the slope is close to 0.75.

$\langle L \rangle$ can now be calculated from Eq. 4.4, $\frac{G'_{min}}{G''_{min}} = 0.317 \left(\frac{\langle L \rangle}{l_e}\right)^{0.82}$ and

$$\langle L \rangle = l_e \left[\frac{1}{0.317}\left(\frac{G'_{min}}{G''_{min}}\right)\right]^{\frac{1}{0.82}} = 0.141\ \mu m \left[\frac{1}{0.317}(5.06)\right]^{\frac{1}{0.82}} = 4.13\ \mu m$$

Lastly, the ratio of breakage to reptation time is determined from Eq. 4.5,

$$\tau_R = \frac{1}{\omega_{c1}} = 0.484 \tau_{br}^{0.63} \tau_{rep}^{0.37},$$

where the reptation time $\tau_{rep} = \frac{2\langle L \rangle^3}{\pi^2 \alpha D_0}$,

in which the translational diffusivity within the tube $D_0 = \frac{k_B T}{\varsigma}$

and the drag coefficient $\varsigma = \frac{2\pi\eta_s}{\ln(\xi/d)}$.

Starting from the drag coefficient and working upward, $\varsigma = \frac{2\pi(0.0011\ Pa.s)}{\ln(141^{0.6} * 92.5^{0.4}/4)} = 0.0021\ Pa.s$,

$$D_0 = \frac{1.38 * 10^{-23}\ J/K\ (298\ K)}{0.0021\ Pa.s} = 1.96 * 10^{-18}\ \frac{m^3}{s}$$

$$\tau_{rep} = \frac{2(4.13 * 10^{-6}\ m)^3}{\pi^2(1.52)(1.96 * 10^{-18}\ m^3/s)} = 4.80\ s$$

$$\tau_{br} = \left(\frac{1}{2.34/s\ (0.484) 4.80\ s^{0.37}}\right)^{1/0.63} = 0.326\ s$$

and $\zeta = \frac{\tau_{br}}{\tau_{rep}} = \frac{0.326\ s}{4.80\ s} = 0.0678.$

With the independent micelle parameters calculated, the input file can be filled in much like the example above except with the calculated values in inputs 6.2, 7.2, 9.2, and 9.3 (persistence length, micelle length, zeta, and alpha respectively). Additionally, make sure Y is entered for input 9.1 so that the simulation uses the calculated values of zeta and alpha.

An example result is shown in Figure 4.7. Note that the calculated parameters are close to the fitted parameters given in Table 4.1, and although the simulation rheology curves do not match the experimental data as well as the fitted curves (compare with Figure 4.5), the agreement is still reasonably good.

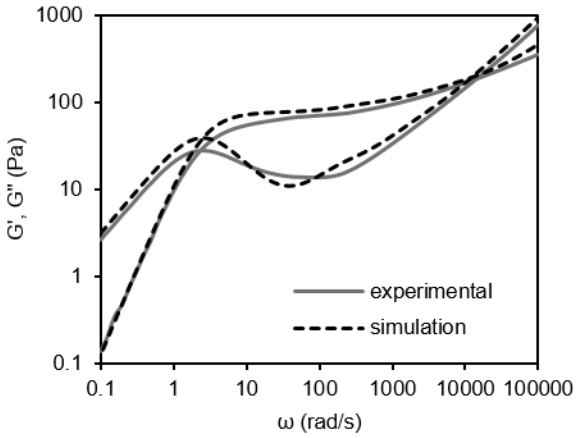

Figure 4.7: Rheology curves predicted by the pointer algorithm using micelle parameters calculated from correlations (Eqs. 4.1-4.5).

Troubleshooting

The simulation does not run:

If running a predictive pointer algorithm simulation (or a single iteration to compare to experimental data), the format or units of the input parameters may have been entered incorrectly, causing an error.

If running an iterative pointer algorithm simulation, you should still double check the input parameters, but there are also minimum requirements for the experimental data. The data need to contain a minimum in G" or if there is no minimum in G", high-frequency data that include the second crossover frequency must be available. Without either of these rheological features, an iterative fitting simulation cannot be run, but the micelle parameters can still be estimated from the rheology, as detailed in "Calculating micelle parameters."

The simulation does not finish:

For a predictive pointer algorithm simulation, you may just need to increase the wall time if running the simulation on a computation cluster. However, if the micelles are very long (greater than ~40-50 μm), even with an increased simulation time the simulation may take an excessive amount of time to finish. In this case, the number of micelles can be decreased to a minimum of ~500 micelles.

An iterative simulation may not finish because it also wasn't given enough time to complete all the iterations. Again, the wall time can be increased, but long micelles may make more than a few iterations difficult to complete in a reasonable amount of time. The options here are to increase the simulation time, use less iterations, or estimate the micelle parameters from the rheology and switch to a predictive simulation.

The simulation does not converge:

Although we have made an effort to test the pointer algorithm with a variety of surfactant/salt systems, the pointer algorithm may not be able to fit every single set of data. There may be a feature in your experimental data that the pointer algorithm cannot handle well. If the best-fit rheological curves look close to the experimental data, you can restart the simulation with the best-fit parameters and see if more iterations would allow the simulation to converge. If the best-fit G' and G" curves do not match the experimental data well, you may want to switch to a predictive simulation with the parameters calculated from the experimental data.

Chapter 5: Conclusion

In this work, we investigated the use of a mesoscopic simulation method, the pointer algorithm, to extract micelle parameters from the rheology of surfactant solutions and better understand the relation between solution composition and rheology. The pointer algorithm, previously developed in the Larson lab, is based on polymer theory adapted for micelles and combines several relaxation mechanisms, namely reptation, contour length fluctuations, constraint release, Rouse modes, and bending modes, to model surfactant solution rheology. The simulation had been shown to fit a SLE1S+CAPB/NaCl solution at varying surfactant and salt concentrations and with perfume raw materials added, and here we extend the use of the pointer algorithm to general surfactant systems from literature.

We began by validating the pointer algorithm simulations with the slip-spring model modified for micelles in Chapter 2. The comparison between the two simulation methods led us to reevaluate the treatment of Rouse modes in the pointer algorithm and to the interesting result that the initial assumption of ignoring the longitudinal Rouse modes was incorrect. Instead, we found that the Rouse modes transition from a full Rouse spectrum to fractionated Rouse modes (including both fast and longitudinal Rouse modes) as solutions become more concentrated and the micelles go from locally relaxing as if they were in a dilute solution to being restricted as a confining tube of surrounding micelles forms. Once we modified the Rouse modes in the pointer algorithm, we saw good agreement between the two simulation methods over a range of micelle lengths and breakage ratios. This result helps to verify that the micelle parameters that we extract from rheology are accurate, in particular the micelle length that can be an order of magnitude

longer than what is calculated from the Granek and Cates scaling relation but seems more consistence with the high solution viscosities.

After comparing the pointer algorithm with the slip-spring model, we used the pointer algorithm to fit the rheology of a series of SLE1S+CAPB/NaCl solutions in which the surfactant concentration was systematically varied while the counterion concentration was held constant. From the micelle parameters that were determined from the rheology, we calculated scaling laws for the micelle parameters to quantify how they change with surfactant concentration. The scaling laws we found were consistent with theoretical predictions. We were also able to use the fitted micelle parameters to recover Cates-like correlations that directly relate the micelle length and breakage time, two parameters that are otherwise difficult to determine, from rheology. The correlations make it possible to quickly estimate micelle parameters from experimental data without running a full iterative pointer algorithm simulation.

Next, the pointer algorithm and our derived correlations were applied to a variety of surfactant systems from literature. Since the pointer algorithm doesn't contain any properties of the surfactants or salts in the solution, it should be valid for any general surfactant solution, which we confirm in Chapter 3. In Chapter 3, we fit several sets of rheology data for CTAB/$NaNO_3$ and CPyCl/NaSal solutions, use the correlations to extend the range of concentrations for which the pointer algorithm can be used, and test the correlations' ability to estimate micelle parameters without fitting. We find that for solutions with micelles of intermediate length, the pointer algorithm can fit the experimental data similarly to the SLE1S+CAPB/NaCl solutions we previously worked with. For more dilute solutions where the rheology doesn't have enough features to fit, or for more concentrated solutions with very long micelles where the time per iteration is computationally prohibitive, the correlations still allow

the micelle parameters to be estimated. Overall, the pointer algorithm is able to describe the rheology of a variety of surfactant systems well, showing that the relaxation mechanisms of surfactant micelles are similar across different systems.

In Chapter 4, we document the pointer algorithm to make it generally usable. We provide a user manual that gives instructions for running iterative pointer algorithm simulations as well as predictive simulations. The correlations that we developed in Chapter 2 and tested in Chapter 3 increase the accessibility of the pointer algorithm, both by expanding the range of concentrations encompassed in the simulation and by providing a relatively quick and simple way to estimate the micelle parameters without a full iterative simulation.

With the pointer algorithm validated by the slip-spring model and shown to be applicable to surfactant solutions in general, future work can focus on developing a deeper understanding of the relationship between the surfactant solution composition and the rheology as well as combining results from the pointer algorithm with different simulation and experimental methods. In Chapter 2, we began to study the effect of surfactant concentration on the micelle parameters and calculated scaling laws for the micelle parameters as a function of surfactant concentration. In general, however, unlike for polymers, surfactant micelles lack comprehensive reference sets of rheological data in which both surfactant and salt concentration are varied systematically. The effect of salt, in particular the counterion, and other additives is also still not fully understood. Although some work has been done to quantify the effect of counterion binding efficiency [47], it uses the original Cates scaling relations and we would like to apply the pointer algorithm to similar data, in which salt curves and rheology for varied salts and a chosen surfactant are obtained. The rheology could then be fit with the pointer algorithm and we would ascertain how the micelle parameters are affected by the counterion and if those changes are

consistent with what we might expect based on the Hofmeister series. We are also interested in the effect of additives like perfumes that are common in consumer products. Previous work [30] combined dissipative particle dynamics (DPD) simulations with pointer algorithm simulations to relate how additives alter the packing of surfactant molecules to changes to the rheology. It was found that the octanol/water partition coefficient roughly correlates to the location of additives in and around the micelle and to the zero-shear viscosity, but further work can be done to find a better predictor of how additives will affect rheology as well as look at the effect of multiple additives in the same solution.

Additionally, further development of the pointer algorithm has added branched micelles to the simulation, allowing exploration of a different range of solutions past the peak of the salt curve. It is generally accepted that the peak in the salt curve signifies an onset of branching, which has been qualitatively visualized using cryo-TEM [14,25]. Branching is predicted to speed up relaxation, but its effect on rheology has not been quantified. With this addition to the pointer algorithm, we would be able to investigate both sides of a salt curve, and compare the rheology of two solutions with similar viscosities, which would aid in understanding the effect of branched micelles on the micelle parameters and could be useful for product formulation.

Finally, so far we have concentrated on the linear rheology of linear micelles. Although the pointer algorithm is not designed to model nonlinear rheology, the comparisons to the slip-spring model open up an interesting possibility. Our more recent comparisons with the slip-spring model (in Chapter 3) approach rheologically relevant concentrations, where micelles are long and entangled enough to have measurable rheology. As discussed in Chapter 3, this means that it could be possible to use the pointer algorithm to extract micelle parameters from experimental data, then use those parameters in the slip-spring model to predict the nonlinear

rheology. For surfactant solutions, stress controlled experiments in which the shear rate is measured as the stress is increased have found that the solutions have a maximum stress [12,61,62] that is related to the plateau modulus but the experimental value often differs from the theoretically predicted value. If the stress is ramped up, then down, hysteresis is seen for these solutions [63]. Under shear startup, the rheology can exhibit a stress plateau, a stress overshoot, or oscillations depending on the shear rate [64]. Where possible, we could run slip-spring simulations for these rheological experiments and see which of these phenomena can be captured or predicted by the slip-spring model. The results could help explain the underlying physics of some of these phenomena and why experimental results differ from theoretical predictions.

Extensional rheology is another area that the slip-spring simulations could explore. Various experiments using capillary breakup extensional rheometers (CaBER) and filament stretching extensional rheometers (FiSER) [63,65–67] indicate that the viscosities and relaxation times extracted from these methods differ from each other and from results from linear rheology. It also seems that the initial step size in CaBER affects the rheology of surfactant solutions, unlike polymer solutions, where the viscosity is relatively insensitive to the step strain [65,66]. Slip-spring simulations could provide insight into the differences between the measured viscosities and relaxation times and determine the effect of micelle breakage on extensional rheology. As we continue to build on the pointer algorithm and use it in combination with other simulation methods, we work toward our goal of gaining a more comprehensive understanding of surfactant solution rheology.

Appendix A: Parameters for 60 mM CTAB/120 mM $NaNO_3$ Solution from Helgeson *et al.*

The experimental data in Figure 2.8 drawn from Helgeson *et al.* show no minimum in G", but other data in Helgeson *et al.* show that an increase in either surfactant concentration or salt concentration produces a minimum in G". Thus, we take the data in Figure 2.8 to be at the threshold of having a minimum in G". (We can also see that the data are near this threshold by examining the two-mode fit to these data in Fig. 5 of Helgeson *et al.*) Thus, we take our scaling relation $\frac{G\prime_{min}}{G^{"}_{min}} = 0.317\left(\frac{\langle L\rangle}{l_e}\right)^{0.82}$ in the limit $G'_{min}/G''_{min} = 1$ and thereby obtain $\langle L\rangle = 4.06 l_e$. To get l_e, we assume loosely entangled micelles, which is usually true of less concentrated/entangled solutions, and our crossover formula then reduces to

$$G_0 = 9.75\frac{k_bT}{\xi^3}, \text{ where } \xi = l_e^{0.6} l_p^{0.4}. \qquad \text{(A1)}$$

The plateau modulus is estimated by $G_0 = 4.88 G'_{min}$, which comes from fitting pointer algorithm results to the equation

$$\frac{G_0}{G'_{min}} = \frac{4.25}{G'_{min}/G^{"}_{min}} + 0.625 \qquad \text{(A2)}$$

(shown in Figure A1) and again taking $G'_{min}/G''_{min} = 1$. We can also estimate from *Figure 2.8* that the storage modulus at the frequency where this incipient minimum will appear, G'_{min}, is approximately twice its value at the crossover frequency. Then from Figure 2.8, we find G'_{min} = 4.54 Pa and therefore Eq. A2 gives G_0 = 22.2 Pa. From the persistence length of 32 nm from Helgeson *et al.*, and Eq. A1, the entanglement length is 298 nm. Then, from $\langle L\rangle = 4.06 l_e$, we find $\langle L\rangle$ = 1.2 μm. For a solution well outside the fast breakage regime, we use a large value of ζ

= 200, so that results are insensitive to ζ . These calculations have given us all the independent input parameters needed for the pointer algorithm, namely G_0 = 22.2 Pa, $\langle L \rangle$ = 1.2 μm, l_p = 32 nm, and ζ = 200. (Other calculated parameters used in the pointer algorithm are derived from these, namely $\alpha = l_e/l_p = 9.30$, $Z = 5.1$, and l_e = 298 nm.) Using these input parameters, the pointer algorithm predicts the G' and G" curves shown by the dotted lines in Figure 2.8.

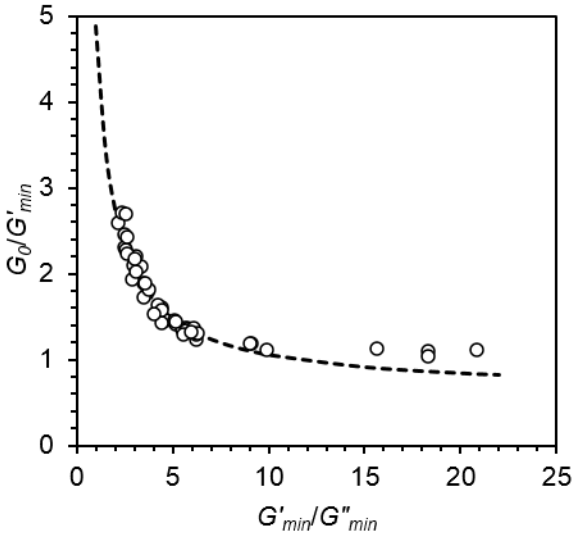

Figure A1: Plot of ratio G_0/G'_{min} vs. G'_{min}/G''_{min} , which is used to calculate G_0. Dashed line shows best fit inverse function $\frac{G_0}{G'_{min}} = \frac{4.25}{G'_{min}/G''_{min}} + 0.625$, which we recommend when $G'_{min}/G''_{min} < 10$. For $G'_{min}/G''_{min} > 10$, G_0 can be approximated as G'_{min}.

Appendix B: Additional Experimental and Pointer Algorithm Rheology for 0.1 M CPyCl/0.06 M NaSal

Figures B1-B3 below show the experimental rheology compared to pointer algorithm predictions from calculated correlation parameters and from fitting for 0.1 M CPyCl/0.06 M NaSal at 35, 30, and 25°C. The comparisons for 20 and 40°C are given in the main text and these additional figures show similar results, with the rheology curves from both the correlation and fitted parameters matching the experimental data well at high and intermediate frequencies and less well at low frequency.

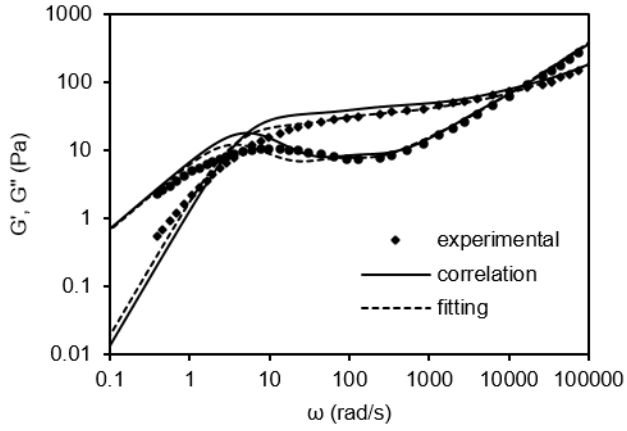

Figure B1: Experimental rheological data for 0.1 M CPyCl/0.06 M NaSal at 35°C compared to pointer algorithm curves from calculated correlation parameters (solid lines) and fitting by the pointer algorithm (dashed lines).

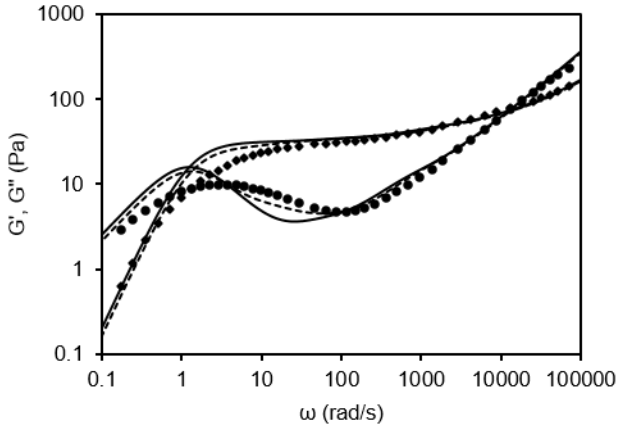

Figure B2: The same as Figure B1 except at 30°C.

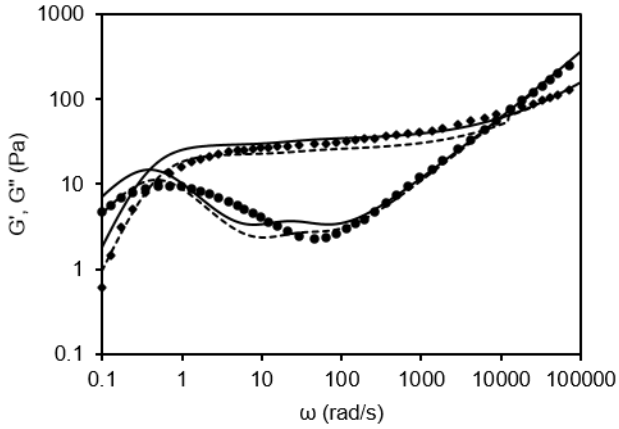

Figure B3: The same as Figure B1 except at 25°C.

Appendix C: Separately Fitted DWS and Mechanical Data for 0.1 M CPyCl/0.06 M NaSal at 20°C

Figures C1 and C2 show rheology for the same solution measured by mechanical rheometry (Figure C1) and DWS (Figure C2). The overall form and magnitude of the two data sets are similar, although the DWS data have a different shape around the first crossover frequency and a deeper minimum in G". For each of the two data sets, micelle parameters were calculated using our correlations in Eqs. 3.2-3.5. The plateau modulus and persistence length extracted from the mechanical and DWS data agree well with each other while the micelle length from DWS is about twice the length from mechanical rheology because of the greater G'_{min}/G''_{min} ratio in the former data. To compensate for the difference in lengths, the breakage times also change to fit the shape of the rheological curves at lower frequencies. A pointer algorithm simulation was run with the parameters calculated from the correlations and results compared to the experimental data. The mechanical data are matched well by the pointer algorithm curves over the entire frequency range. For the DWS data, the high frequency data are matched well, but there is a deviation near the minimum in G" and at the first crossover frequency. These results demonstrate that although the data look fairly similar, the details are significant, since the difference in the minimum in G" doubles the micelle length, as shown in **Error! Reference source not found.**. The results also help to explain the pointer algorithm's poor fit around the first crossover frequency for the CPyCl//NaSal rheology above and show the importance of developing a

consistent procedure for merging DWS and mechanical data, which seems to remain an outstanding problem for experimentalists to address.

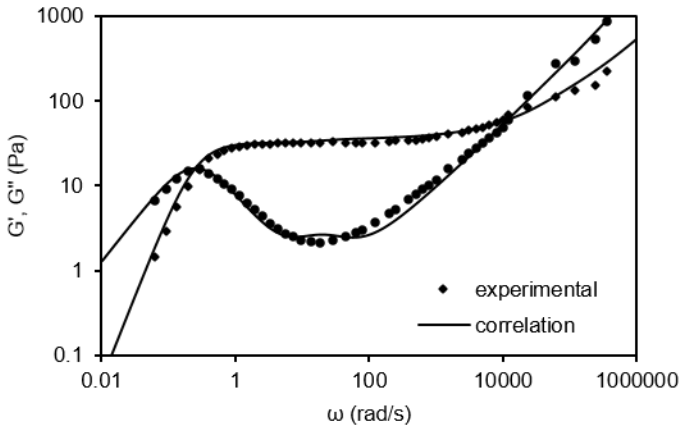

Figure C1: Mechanical rheology of 0.1 M CPyCl/0.06 M NaSal solution at 20°C compared to pointer algorithm prediction with micelle parameters calculated from correlations.

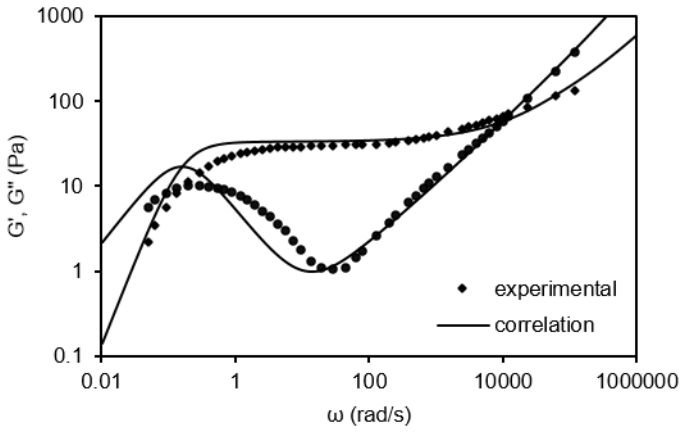

Figure C2: The same as Figure C1, except for DWS rheology.

Table C1: Calculated micelle parameters for 0.1 M CPyCl/0.06 M NaSal solution at 20°C

T (C)		ζ	τ_{br} (s)	G_0 (Pa)	$\langle L \rangle$ (μm)	l_e (nm)	l_p (nm)
Mech.	corr.	0.004	0.91	35.5	19.2	170.	58
DWS	corr.	0.0002	0.56	33.6	42.9	173	66

Appendix D: Effect of Ensemble Size, Diameter, and Persistence Length on Pointer Algorithm Simulations

For the studies below, each set of simulations was performed for one data set containing only mechanical data (no high frequency data) and one data set with merged mechanical and DWS data that includes high frequency data. These solutions were chosen as examples of fitting with a fixed persistence length and of fitting with the persistence length left as an additional fitting parameter. The data set without high frequency data is a 16 wt% SLE1S/CAPB solution with 2.1% NaCl and the data set with high frequency data is a SLE1S/CAPB solution with a surfactant volume fraction of $\varphi = 0.04$ and NaCl added so that $[Na^+] = 0.7$ M. All rheological data were measured at 25°C.

Effect of ensemble size on fitted micelle parameters

Since the time per iteration of the pointer algorithm is directly proportional to the number of micelles in the simulation, it is advantageous to use a smaller ensemble size. However, because the micelle lengths are discretized in the simulation, the length distribution for a given average micelle length is affected by the number of micelles. In this study we vary the ensemble size and compare the converged micelle parameters to find the minimum number of micelles we need to simulate. At each ensemble size, five simulations were run and the average values of the best fit parameters are plotted and tabulated below. All simulations converged, in that the average deviation between measured and predicted moduli is less than 10%.

For the data set without high frequency data, the plateau modulus and entanglement length are approximately constant over the range of ensemble sizes tested, as can be seen in Figure D1. The time scales and micelle length are dependent on the ensemble size up to around 1000 micelles, where the change in these parameters slows and the parameters plateau by around 2000 micelles. The average values of the micelle parameters are given in Table D1.

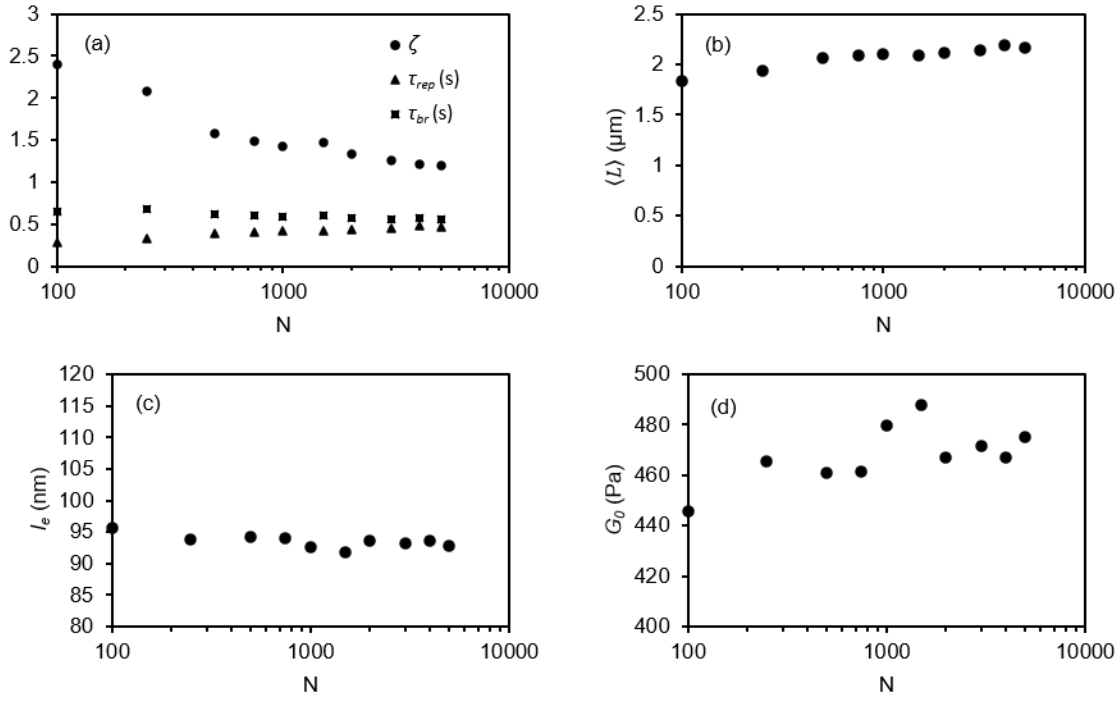

Figure D1: Variation of micelle parameters with number N of micelles in the ensemble, at fixed persistence length of 70 nm for pointer algorithm fits to data for 16 wt% SLE1S/CAPB solution with 2.1% NaCl.

Table D1: Micelle parameters, averaged over 5 runs, at different ensemble sizes N, at fixed persistence length of 70 nm

N	ζ	τ_{rep} (s)	τ_{br} (s)	$\langle L \rangle$ (μm)	G_0 (Pa)	l_e (nm)	α	Z
100	2.39	0.281	0.644	1.83	446	95.7	1.37	19.2
250	2.08	0.331	0.676	1.94	465	93.8	1.34	20.7
500	1.58	0.397	0.612	2.06	461	94.2	1.35	21.9
750	1.48	0.410	0.606	2.08	462	94.1	1.34	22.1
1000	1.43	0.425	0.592	2.10	480	92.5	1.32	22.7
1500	1.47	0.413	0.597	2.08	488	91.8	1.31	22.7
2000	1.34	0.432	0.574	2.12	467	93.6	1.34	22.6
3000	1.26	0.444	0.558	2.14	472	93.2	1.33	22.9
4000	1.21	0.477	0.568	2.19	467	93.6	1.34	23.4
5000	1.20	0.460	0.552	2.16	475	92.9	1.33	23.3

For the merged data (Figure D2 and Table D2), because the persistence length is now also a fitting parameter, its variation with the ensemble size causes the plateau modulus and entanglement length to also vary along with the time scales and micelle length. As in the case for mechanical data only, the change in the parameters with increasing ensemble size slows down significantly once 1000 micelles are used, and plateaus once around 2000 micelles are present. Our recommendation therefore is to run simulations with at least 2000 micelles when fitting experimental data with the pointer algorithm. Smaller ensembles can be used, as long as it is recognized that the breakage time will be overestimated and the micelle length underestimated and if high-frequency data are also being fit, the persistence length will also be underestimated and the plateau modulus slightly overestimated.

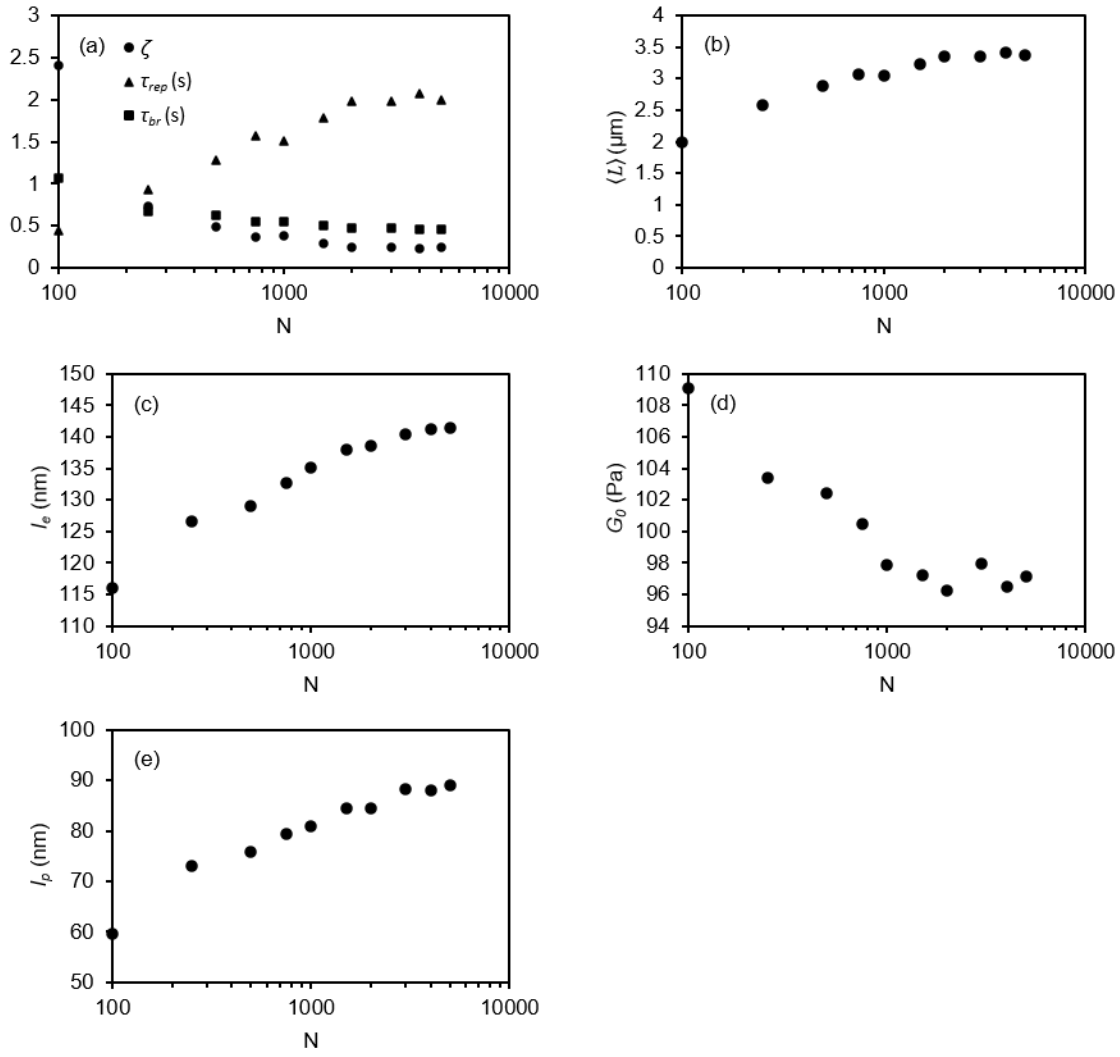

Figure D2: Variation of micelle parameters with ensemble size N, including persistence length as a fitting parameter for pointer algorithm fits to data for SLE1S+CAPB with a surfactant volume fraction of φ = 0.04 and [Na^+] = 0.7 M.

Table D2: Micelle parameters, averaged over 5 runs at different ensemble sizes N, with persistence length as a fitting parameter

N	ζ	τ_{rep} (s)	τ_{br} (s)	$\langle L \rangle$ (μm)	G_0 (Pa)	l_e (nm)	l_p (nm)	α	Z
100	2.41	0.447	1.069	1.99	109	116.1	59.7	1.95	17.1
250	0.73	0.936	0.676	2.58	103	126.7	73.0	1.74	20.4
500	0.49	1.281	0.627	2.88	102	129.0	75.7	1.71	22.3
750	0.36	1.563	0.550	3.08	101	132.7	79.5	1.67	23.2
1000	0.37	1.506	0.551	3.05	98	135.2	81.0	1.67	22.5
1500	0.28	1.775	0.503	3.23	97	138.0	84.4	1.64	23.4
2000	0.24	1.974	0.476	3.35	96	138.6	84.4	1.64	24.2
3000	0.24	1.973	0.476	3.36	98	140.4	88.2	1.59	23.9
4000	0.23	2.068	0.463	3.41	97	141.2	88.1	1.60	24.1
5000	0.24	1.995	0.463	3.37	97	141.4	88.9	1.59	23.8

Effect of persistence length on fitted micelle parameters

Even when the persistence length can be extracted from high-frequency rheology (if such data are available), doubts remain about the fitting process and the accuracy of the persistence length. Thus, it is important to assess how the fitted, or assumed, value of the persistence length affects the other micelle parameters that emerge from the fitting process. To determine this effect, we ran a series of simulations fitting experimental data with the persistence length fixed at a series of different values, while the other parameters were allowed to vary to achieve a best fit.

Pointer-algorithm simulations were run with persistence lengths ranging from 40-110 nm in 10-nm intervals, centered around the previously determined value of 70 nm for this system. When the high-frequency data were lacking, simulations with a persistence length l_p greater than 70 nm converged while shorter persistence lengths did not converge within an average error of 10%, and the parameters given are the best fits to the experimental data attained before runs

terminated. For the simulations that did not converge, the average error is around 15% at low frequency and up to 25% at intermediate frequency. Figure D3 below shows that the predictions for both l_p = 70 and 100 nm match the experimental data well although with slight differences at high frequency (greater than the maximum frequency of the experimental data). The curves for l_p = 40 nm fit the experimental data at low frequency but deviate significantly starting at intermediate frequencies so that this simulation does not converge, as can be seen in Figure D3.

In the range of persistence lengths over which the simulations do converge, the other parameters vary linearly with the persistence length, with micelle length and breakage time varying most strongly (see Figure D4 and Table D3). Thus, the ~50% increase in the persistence length from 70 to 110 leads to an increase of ~50% in the micelle length, a ~50% decreases in the breakage time, and ~20% decrease in the plateau modulus. Hence, when fitting without high frequency data in Figure D3, there is a range of persistence lengths over which the pointer algorithm converges, but the other micelle parameters obtained from the fit vary proportionately to the change in the persistence length. Thus, uncertainty in the value of the persistence length implies an uncertainty in the micelle parameters (such as micelle length) that, for micelle length, can easily be around a factor of two or so. This illustrates the importance of having high-frequency data from DWS to help determine the value of the persistence length.

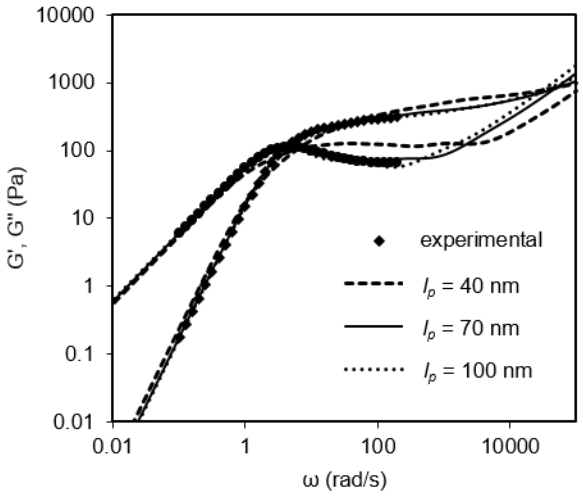

Figure D3: Predictions of pointer algorithm compared to experimental rheology for l_p = 40 nm (best fit), l_p = 70 nm (converged), and l_p = 100 nm (converged) for 16 wt% SLE1S/CAPB solution with 2.1% NaCl.

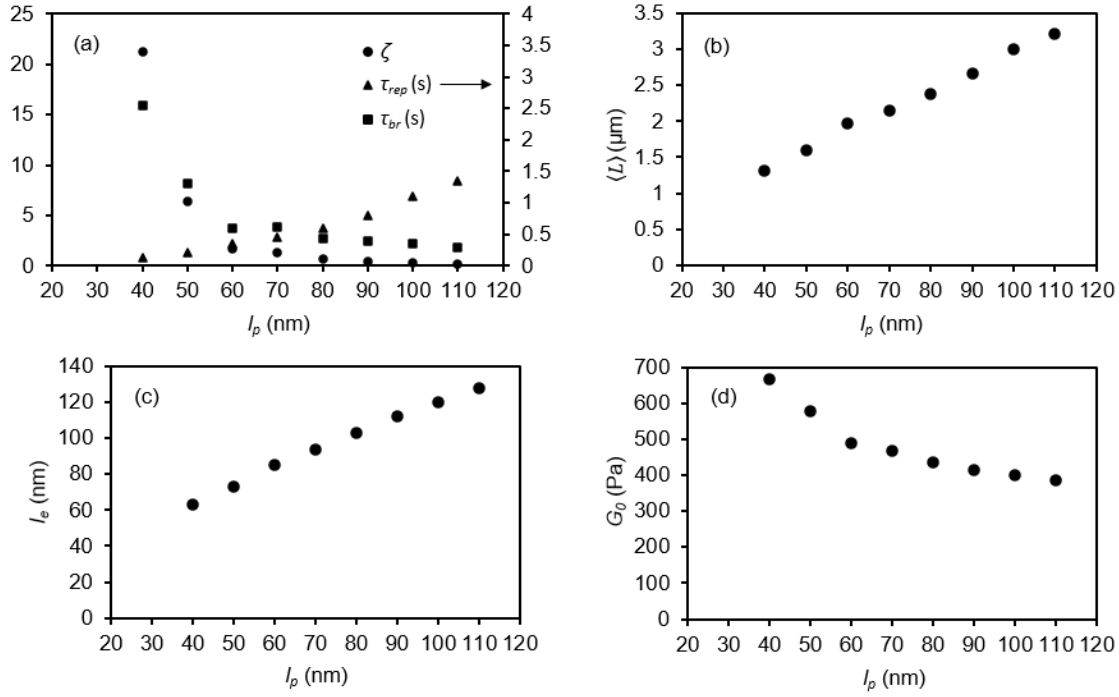

Figure D4: Variation of micelle parameters at fixed persistence lengths (parameters are "best fits" as described in the text at l_p = 60 nm and below and from "converged simulations" at l_p = 70 nm and above) for mechanical data only, for pointer algorithm fits to data for 16 wt% SLE1S/CAPB solution with 2.1% NaCl.

Table D3: Micelle parameters at imposed persistence lengths, obtained from mechanical data only

l_p (nm)	ζ	τ_{rep} (s)	τ_{br} (s)	$\langle L \rangle$ (μm)	G_0 (Pa)	l_e (nm)	α	Z
40	21.1	0.120	2.54	1.31	665.4	62.9	1.57	20.8
50	6.41	0.202	1.29	1.59	577.0	73.0	1.46	21.9
60	1.65	0.357	0.592	1.97	487.0	85.4	1.42	23.0
70	1.35	0.452	0.612	2.15	467.1	93.6	1.34	23.0
80	0.718	0.590	0.424	2.38	435.2	103.2	1.29	23.1
90	0.480	0.808	0.388	2.67	414.8	111.8	1.24	23.9
100	0.308	1.11	0.342	2.99	400.2	119.8	1.20	25.0
110	0.211	1.34	0.284	3.22	386.4	127.6	1.16	25.2

When high frequency data are included, convergence is only obtained in the simulation when the persistence length is close to the fitted value obtained when it is allowed to freely vary (88 nm). Persistence lengths less than or equal to 80 nm, or greater than or equal to 100 nm, are unable to fit the experimental data at the minimum in G" and at high frequency. The converged simulation curves and examples of unconverged simulations at a shorter and longer persistence length are shown in Figure D5 below. The average error for unconverged simulations is about 5-15% at low to intermediate frequencies and rises to 25% at high frequency. Figure D6 and Table D4 give the best-fit micelle parameters for all persistence lengths, but as can be seen in Figure D5 only the simulation with l_p = 90 nm converged. Thus, the added constraint of fitting the high frequency data severely limits the values of the persistence length that permit convergence of simulation predictions to the experimental data.

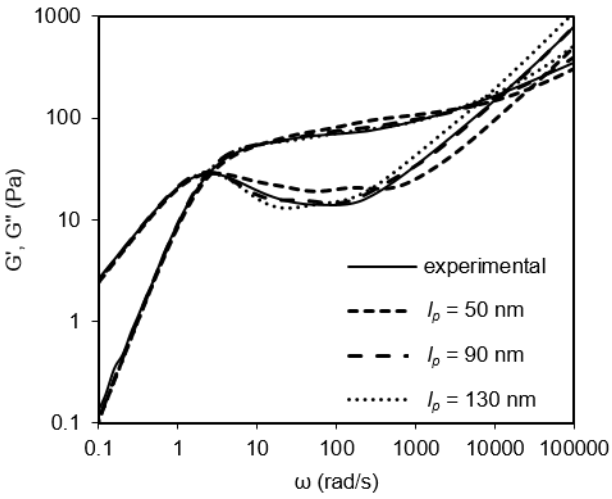

Figure D5: Predictions of pointer algorithm compared to experimental rheology for l_p = 50 nm, 90 nm, and 130 nm. Only the simulation with l_p = 90 nm converged For SLE1S+CAPB with a surfactant volume fraction of φ = 0.04 and [Na^+] = 0.7 M.

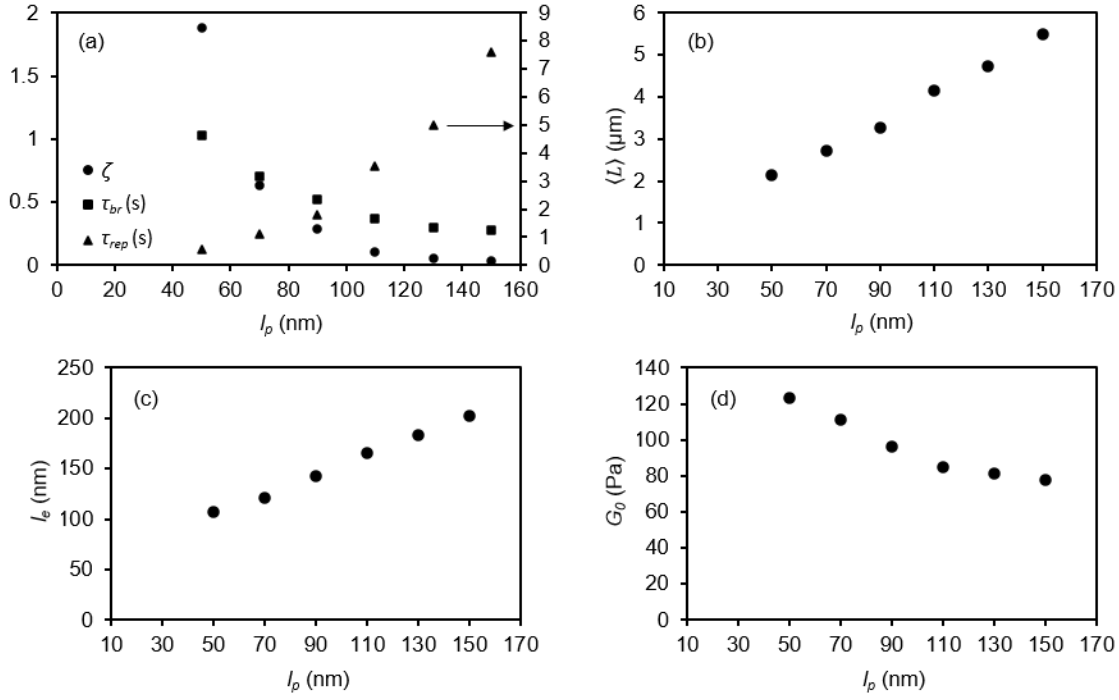

Figure D6: Variation of best-fit micelle parameters as functions of persistence lengths with high-frequency DWS data included in the rheology for pointer algorithm fits to data for SLE1S/CAPB with a surfactant volume fraction of φ = 0.04 and [Na^+] = 0.7 M.

Table D4: Micelle parameters at imposed persistence lengths, obtained from mechanical and high-frequency DWS data

l_p (nm)	ζ	τ_{rep} (s)	τ_{br} (s)	$\langle L \rangle$ (μm)	G_0 (Pa)	l_e (nm)	α	Z
50	1.88	0.55	1.03	2.15	123.5	107	2.13	20.2
70	0.63	1.11	0.70	2.72	111.3	121	1.73	22.5
90	0.29	1.79	0.52	3.26	96.0	143	1.59	22.8
110	0.10	3.54	0.36	4.16	84.7	166	1.51	25.0
130	0.059	5.00	0.29	4.72	81.5	184	1.41	25.7
150	0.036	7.62	0.27	5.49	77.7	202	1.35	27.1

Effect of diameter on fitted micelle parameters

The other parameter in the simulation that we can fix is the micelle diameter. As discussed in the main text, based on various studies, we usually set this parameter to 4 nm, but to assess the effect of possible inaccuracy in this parameter, we wish to determine its effect on the best-fit values of other micelle parameters. We therefore ran a series of simulations with the micelle diameter varying from 2-5 nm in 0.5 nm increments. From various SANS experiments and MD simulations, we don't expect the dimeter to be much greater than 4 nm, and we choose a minimum of 2 nm, since this value is close to that used by Oelschlaeger *et al*. [40] and Willenbacher *et al*. [26] in some of their work. All simulations converged.

Figure D7 and Table D5 show that the micelle diameter has a strong effect on the other parameters, similar to what was found when varying the persistence length. The parameters vary roughly linearly with the diameter, with the micelle length possibly showing two different scaling regimes. As the micelle diameter increases from 2 to 5 nm, the fitted micelle length decreases by approximately 60% while the breakage time increases by a factor greater than 5 and the plateau modulus increases by 50%. Because in these calculations the persistence length is set

to a constant value while the diameter is changed, the rheology curves differ from each other at high frequency, as seen in Figure D8.

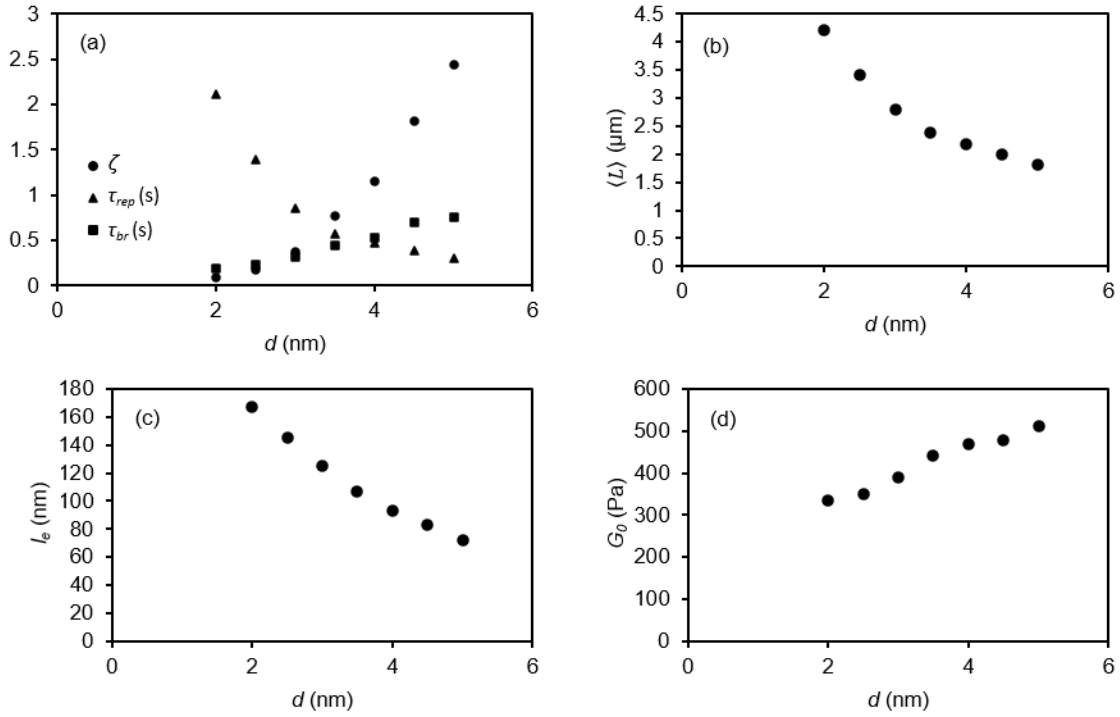

Figure D7: Variation of micelle parameters with micelle diameter, with mechanical data only for pointer algorithm fits to data for 16 wt% SLE1S/CAPB solution with 2.1% NaCl.

Table D5: Micelle parameters with varying micelle diameter, obtained from mechanical data only

d (nm)	ζ	τ_{rep} (s)	τ_{br} (s)	$\langle L \rangle$ (μm)	G_0 (Pa)	l_e (nm)	l_p (nm)	α	Z
2	0.087	2.12	0.19	4.22	334.5	168	70	2.39	25.2
2.5	0.17	1.40	0.23	3.41	351.2	145	70	2.07	23.5
3	0.37	0.85	0.32	2.79	388.7	125	70	1.78	22.3
3.5	0.77	0.57	0.44	2.38	440.4	107	70	1.53	22.2
4	1.15	0.47	0.53	2.17	469.4	93.4	70	1.33	23.3
4.5	1.82	0.39	0.70	2.00	477.7	83.2	70	1.19	24.0
5	2.44	0.31	0.75	1.81	509.8	71.9	70	1.03	25.2

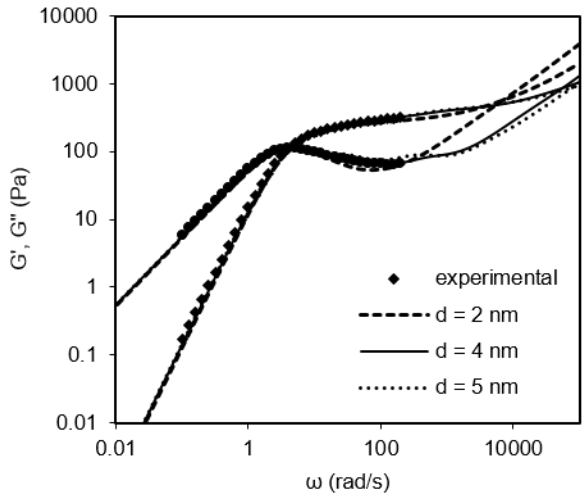

Figure D8: Predictions of pointer algorithm compared to experimental rheology at varying micelle diameter for 16 wt% SLE1S/CAPB solution with 2.1% NaCl.

With the persistence length now allowed to vary also, the effect of changing the diameter on the other parameters decreases and reverses the directions of the changes when compared to the simulations at a fixed persistence length. As an example, at a fixed persistence length, the micelle length *decreases* by over a factor of two when the diameter increases from 2 to 5 nm, but when the persistence length is also allowed to vary, the micelle length *increases*, but only by about 25%. Since the simulation has to fit the high frequency data to converge, the other parameters have to compensate for the changing diameter, and it seems that the persistence length is the main parameter that accomplishes that. Over the given range of diameters, the persistence length increases by close to a factor of 4; while the plateau modulus and breakage time decrease by factors of 2 and 1.2 respectively, and the length increases by a factor of 1.25. These changes can be seen in Figure D9 and Table D6 and Figure D10 shows that because the persistence length can vary to fit the high-frequency data, all the pointer algorithm curves match the data well and look similar across the range of micelle diameters.

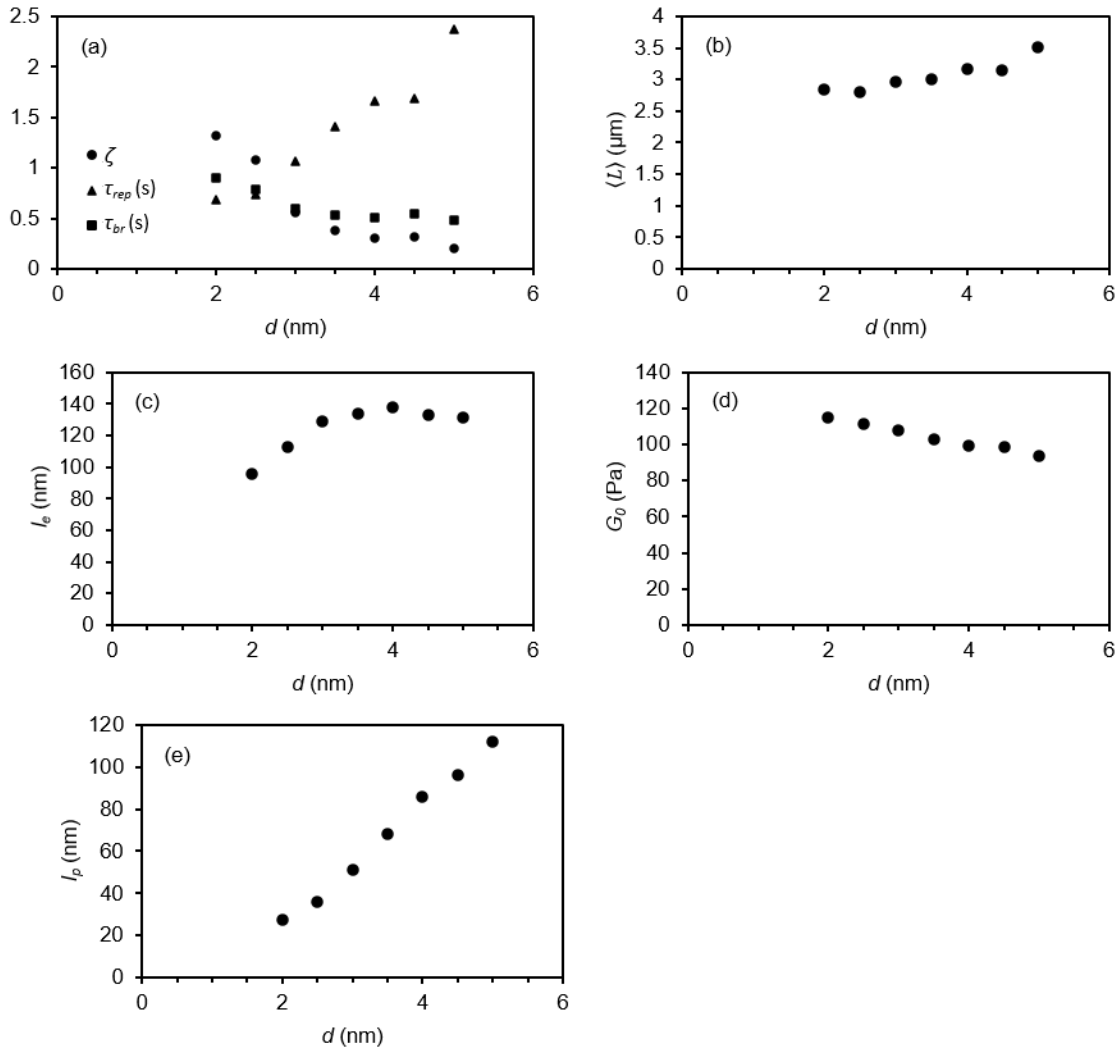

Figure D9:Variation of micelle parameters with micelle diameter, as in Figure D7, but with high-frequency data used in pointer algorithm fits for SLE1S+CAPB with a surfactant volume fraction of $\varphi = 0.04$ and $[Na^+] = 0.7$ M.

Table D6: Micelle parameters with varying micelle diameter, with high-frequency data

d (nm)	ζ	τ_{rep} (s)	τ_{br} (s)	$\langle L \rangle$ (μm)	G_0 (Pa)	l_e (nm)	l_p (nm)	α	Z
2	1.31	0.68	0.90	2.85	115	96.1	27.3	3.52	29.7
2.5	1.08	0.73	0.79	2.80	111	113	35.7	3.17	24.8
3	0.56	1.06	0.59	2.96	108	129	51.2	2.51	23.0
3.5	0.38	1.40	0.53	3.00	103	134	68.1	1.96	22.4
4	0.30	1.66	0.50	3.17	99.1	138	86.0	1.61	22.9
4.5	0.32	1.69	0.54	3.16	98.8	133	96.1	1.38	23.8
5	0.20	2.37	0.48	3.51	93.8	132	112	1.18	26.7

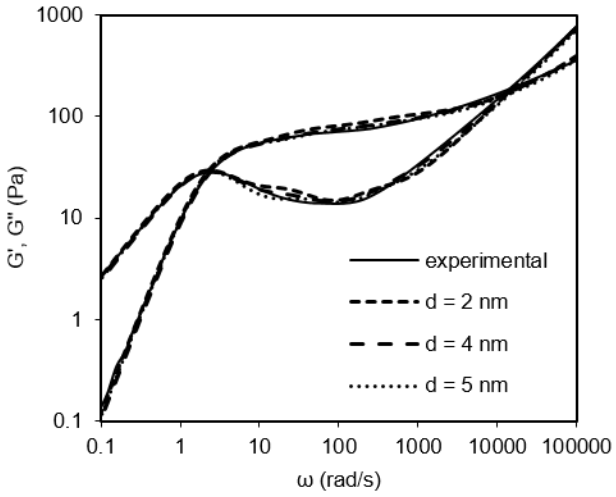

Figure D10: Experimental data and example pointer algorithm simulations for varying micelle diameters, for SLE1S+CAPB with a surfactant volume fraction of $\varphi = 0.04$ and $[Na^+] = 0.7$ M.

Thus, the persistence length and diameter are relatively important parameters that affect the other parameters in the simulation. However, as long as extreme values for the persistence length and diameter are avoided, the other parameters will lie within a "reasonable" range. For example, the length of the micelles in the two SLE1S+CAPB solutions considered above will be on the order of a few microns, not less than a micron as predicted by the Cates scaling or tens of microns long, as in like some of the other highly entangled solutions examined in this work.

Appendix E: Comparison of Rheology from Different References

Below, Figure E1 shows general agreement between the two rheology data sets measured by two different labs on the same surfactant formulation, with some disagreement around the first crossover frequency and the minimum in G".

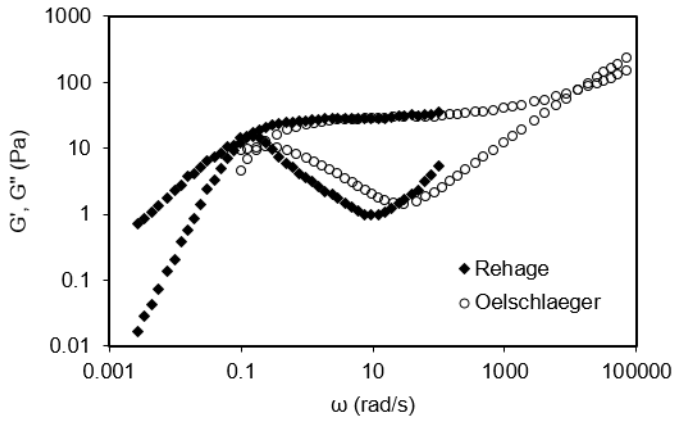

Figure E1: Comparison of rheology of 0.1 M CPyCl/0.06 NaSal solution at 20°C from Rehage and Hoffmann [56] (solid diamonds) and Oelschlaeger *et al.* [40] (open circles)

Appendix F: Additional Pointer Algorithm Predictions for Experimental Data

For the first two solutions considered in this section (Figure F1 and Figure *F2*), the rheology looks similar to other data we previously fit. Those solutions contain well-entangled micelles, and the pointer algorithm predictions match the experimental data well. However, the next two solutions (Figure F3 and Figure *F4*) are at lower salt and surfactant concentrations, and here we find that the predictions of the pointer algorithm predictions match poorly the experimental data. This disagreement reflects some of the difficulties in determining micelle parameters for more dilute solutions.

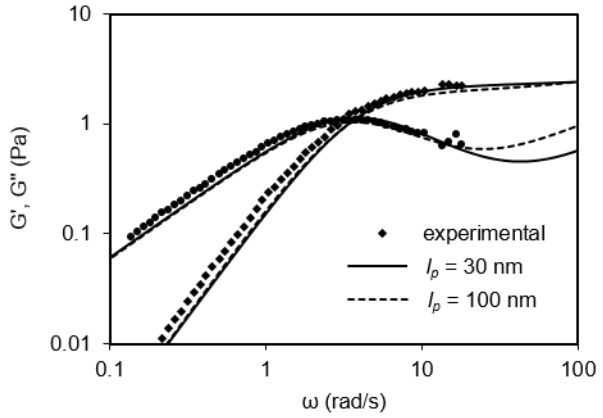

Figure F1: Predictions of pointer algorithm, with parameters based on correlations, compared to experimental rheology for 1 wt% CTAT/SDBS/0.25 wt% NaTos solution for two persistence lengths. Data taken from [27].

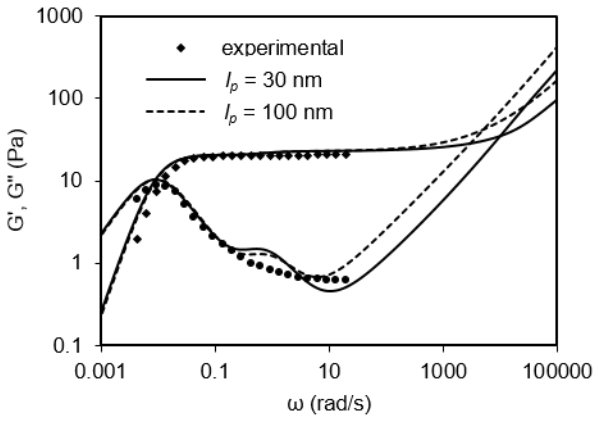

Figure F2: The same as Figure F1, except for 3 wt% NaOA/C_8TAB solution. Data from [54].

Because of the lack of rheological features, as mentioned above and discussed in earlier work, less concentrated solutions need high-frequency data that include the second crossover frequency to be fit with the pointer algorithm. If only mechanical data are available, we can approximate micelle parameters using the correlations (modified as discussed below), but these estimations tend to be less accurate than those for well-entangled micelles, for multiple reasons. Since the correlations normally require the value of the minimum in G", which does not exist for weakly entangled micelles, instead of the ratio G'_{min}/G''_{min}, the maximum value of $G'(\omega)/G''(\omega)$ can be used, or in the limiting case, simply be taken to be unity. However, this may be an underestimate that leads to a micelle length that is too short, especially if the maximum $G'(\omega)/G''(\omega)$ ratio is at the highest frequency at which experimental data are available. Additionally, for linear micelles, the magnitudes of G' and G" are lower for solutions at more dilute concentrations, and at low frequency may approach the physical limitations of the rheometer. For the 0.015 M CPyCl/0.011 M NaSal solution considered here (Figure F3), the terminal slopes of G' and G" are both close to 1, instead of 1 and 2 respectively, as expected for a Maxwell fluid, which typically describes surfactant solutions at low frequency. This uncertainty in the data and in the approximations

required to calculate micelle parameters evidently result in a poorer match between the experimental data and the predictions of the pointer algorithm.

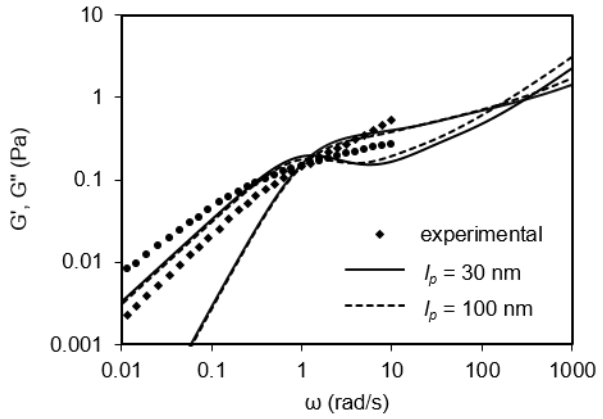

Figure F3: The same as Figure F1, except for 0.015 M CPyCl/0.011 M NaSal solution. Data taken from [58].

We obtain similar results for a CTAB/NaSal solution from Shikata and Hirata [52] (0.1 M CTAB/0.0275 M NaSal, T = 25°C) at lower salt concentration than that studied by Galvan-Miyoshi *et al*. [13]. In this rheological data set, in Figure F4, the maximum $G'(\omega)/G''(\omega)$ ratio is attained at the highest experimental frequency and the G' and G" curves appear to be still diverging at this frequency, so that a higher $G'(\omega)/G''(\omega)$ ratio would be attained if higher frequency data were obtained. Hence, using this maximum $G'(\omega)/G''(\omega)$ ratio attained within the experimental window in our correlation will likely produce an underestimation of the micelle length. The rheology curves predicted using the correlations, including this micelle length extracted from $G'(\omega)/G''(\omega)$, match the *shape* of the experimental data well, but the first crossover frequency is an order of magnitude too high, despite the fact that the cross-over frequency was used to estimate the parameters. This failure of the correlations to produce a good

fit is likely associated with the low surfactant concentration of this solution. By manually adjusting the micelle length to a longer value, we can get a better fit to the experimental data, shown in Figure F4 and Table 3.6 in the main text.

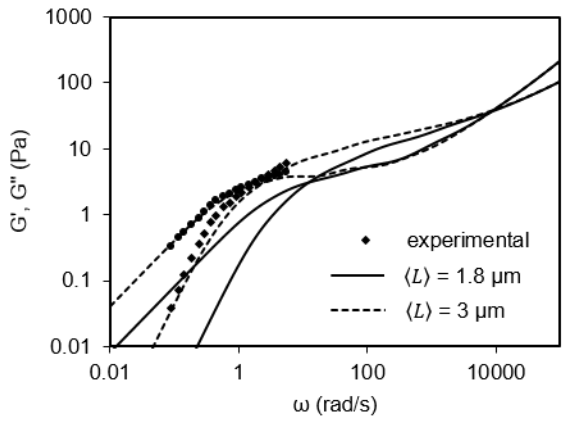

Figure F4: Comparison of predictions of the pointer algorithm to experimental rheology for 0.1 M CTAB/0.0275 M NaSal solution at 20°C for two different average micelles lengths, $\langle L \rangle$. Data from [52].

Fitting data from Shikata and Hirata [52] and from Galvan-Miyoshi *et al*. [13] with the pointer algorithm indicates that micelle lengths grow extremely quickly with the addition of salt; the zero shear viscosity increases from 3.8 Pa.s to over 1000 Pa.s as the salt-to-surfactant ratio R increases from 0.275 to 0.4 (which is near the first peak in the salt curve). For the 0.04 M NaSal solution, for which R = 0.4, the inferred micelle length is close to 100 μm, G" shows a clear minimum, and the first crossover frequency is near 0.01 rad/s (see Table 3.3 and Table *3.4*). The 0.0275 M NaSal solution, on the other hand, has no G" minimum, a first crossover frequency above 1 rad/s, and the inferred micelle length is about two orders of magnitude shorter.

References

(1) Yang, J. Viscoelastic Wormlike Micelles and Their Applications. *Curr. Opin. Colloid Interface Sci.* **2002**, *7* (5–6), 276–281. https://doi.org/10.1016/S1359-0294(02)00071-7.

(2) Kuperkar, K.; Abezgauz, L.; Danino, D.; Verma, G.; Hassan, P. A.; Aswal, V. K.; Varade, D.; Bahadur, P. Viscoelastic Micellar Water/CTAB/$NaNO_3$ Solutions: Rheology, SANS and Cryo-TEM Analysis. *J. Colloid Interface Sci.* **2008**, *323* (2), 403–409. https://doi.org/10.1016/j.jcis.2008.04.040.

(3) Croce, V.; Cosgrove, T.; Dreiss, C. A.; King, S.; Maitland, G.; Hughes, T. Giant Micellar Worms under Shear: A Rheological Study Using SANS. *Langmuir* **2005**, *21* (15), 6762–6768. https://doi.org/10.1021/la0479410.

(4) Shrestha, R. G.; Abezgauz, L.; Danino, D.; Sakai, K.; Sakai, H.; Abe, M. Structure and Dynamics of Poly (Oxyethylene) Cholesteryl Ether Wormlike Micelles : Rheometry, SAXS, and Cryo-TEM Studies. *Langmuir* **2011**, 12877–12883. https://doi.org/10.1021/la202879f.

(5) Cates, M. E. Reptation of Living Polymers: Dynamics of Entangled Polymers in the Presence of Reversible Chain-Scission Reactions. *Macromolecules* **1987**, *20* (9), 2289–2296. https://doi.org/10.1021/ma00175a038.

(6) De Gennes, P. G. Reptation of a Polymer Chain in the Presence of Fixed Obstacles. *J. Chem. Phys.* **1971**, *55* (2), 572–579. https://doi.org/10.1063/1.1675789.

(7) Doi, M.; Edwards, S. F. Dynamics of Rod-like Macromolecules in Concentrated Solution. Part 1. *J. Chem. Soc. Faraday Trans. 2 Mol. Chem. Phys.* **1978**, *74*, 1789–1801. https://doi.org/10.1039/F29787401789.

(8) Doi, M.; Edwards, S. F. Dynamics of Rod-like Macromolecules in Concentrated Solution. Part 2. *J. Chem. Soc. Faraday Trans. 2 Mol. Chem. Phys.* **1978**, *74*, 1802–1817. DOI https://doi.org/10.1039/F29787401802.

(9) Varchanis, S.; Dimakopoulos, Y.; Tsamopoulos, J. Evaluation of Tube Models for Linear Entangled Polymers in Simple and Complex Flows. *J. Rheol.* **2018**, *62* (1), 25–47. https://doi.org/10.1122/1.5009197.

(10) Turner, M. S.; Cates, M. E. Linear Viscoelasticity of Living Polymers: A Quantitative

Probe of Chemical Relaxation Times. *Langmuir* **1991**, *7* (8), 1590–1594. https://doi.org/10.1021/la00056a009.

(11) Granek, R.; Cates, M. E. Stress Relaxation in Living Polymers: Results from a Poisson Renewal Model. *J. Chem. Phys.* **1992**, *96* (6), 4758–4767. https://doi.org/10.1063/1.462787.

(12) Khatory, A.; Lequeux, F.; Kern, F.; Candau, S. J. Linear and Nonlinear Viscoelasticity of Semidilute Solutions of Wormlike Micelles at High Salt Content. *Langmuir* **1993**, *9* (6), 1456–1464. https://doi.org/10.1021/la00030a005.

(13) Galvan-Miyoshi, J.; Delgado, J.; Castillo, R. Diffusing Wave Spectroscopy in Maxwellian Fluids. *Eur. Phys. J. E* **2008**, *26* (4), 369–377. https://doi.org/10.1140/epje/i2007-10335-8.

(14) Helgeson, M. E.; Hodgdon, T. K.; Kaler, E. W.; Wagner, N. J. A Systematic Study of Equilibrium Structure, Thermodynamics, and Rheology of Aqueous CTAB/NaNO3 Wormlike Micelles. *J. Colloid Interface Sci.* **2010**, *349* (1), 1–12. https://doi.org/10.1016/j.jcis.2010.05.045.

(15) Tan, G.; Zou, W.; Weaver, M.; Larson, R. G. Determining Threadlike Micelle Lengths from Rheometry. *J. Rheol.* **2021**, *65* (1), 59–71. https://doi.org/10.1122/8.0000152.

(16) Zou, W.; Larson, R. G. A Mesoscopic Simulation Method for Predicting the Rheology of Semi-Dilute Wormlike Micellar Solutions. *J. Rheol.* **2014**, *58* (3), 681–721. https://doi.org/10.1122/1.4868875.

(17) Zou, W.; Tan, G.; Jiang, H.; Vogtt, K.; Weaver, M.; Koenig, P.; Beaucage, G.; Larson, R. G. From Well-Entangled to Partially-Entangled Wormlike Micelles. *Soft Matter* **2019**, *15* (4), 642–655. https://doi.org/10.1039/C8SM02223B.

(18) Rouse, P. E. A Theory of the Linear Viscoelastic Properties of Dilute Solutions of Coiling Polymers. *J. Chem. Phys.* **1953**, *21* (7), 1272–1280. https://doi.org/10.1063/1.1699180.

(19) Likhtman, A. E.; Mcleish, T. C. B. Quantitative Theory for Linear Dynamics of Linear Entangled Polymers. *Macromolecules* **2002**, *35*, 6332–6343. https://doi.org/10.1021/ma0200219.

(20) Wang, Z.; Chen, X.; Larson, R. G. Comparing Tube Models for Predicting the Linear Rheology of Branched Polymer Melts. *J. Rheol.* **2010**, *54* (2), 223–260. https://doi.org/10.1122/1.3301246.

(21) Gittes, F.; Mackintosh, F. C. Dynamic Shear Modulus of a Semiflexible Polymer Network. *Phys. Rev. E.* **1998**, *58* (2), 1241–1244. https://doi.org/10.1103/PhysRevE.58.R1241.

(22) Likhtman, A. E. Single-Chain Slip-Link Model of Entangled Polymers: Simultaneous

Description of Neutron Spin - Echo, Rheology, and Diffusion. *Macromolecules* **2005**, *38*, 6128–6139. https://doi.org/10.1021/ma050399h.

(23) Sato, T.; Moghadam, S.; Tan, G.; Larson, R. G. A Slip-Spring Simulation Model for Predicting Linear and Nonlinear Rheology of Entangled Wormlike Micellar Solutions. *J. Rheol.* **2020**, *64* (5), 1045–1061. https://doi.org/10.1122/8.0000062.

(24) Zana, R.; Kaler, E. W. *Giant Micelles: Properties and Applications*; CRC Press: Boca Raton, 2007.

(25) Vogtt, K.; Jiang, H.; Beaucage, G.; Weaver, M. Free Energy of Scission for Sodium Laureth-1-Sulfate Wormlike Micelles. *Langmuir* **2017**, *33* (8), 1872–1880. https://doi.org/10.1021/acs.langmuir.6b01169.

(26) Willenbacher, N.; Oelschlaeger, C.; Schopferer, M.; Fischer, P.; Cardinaux, F.; Scheffold, F. Broad Bandwidth Optical and Mechanical Rheometry of Wormlike Micelle Solutions. *Phys. Rev. Lett.* **2007**, *99* (6), 1–4. https://doi.org/10.1103/PhysRevLett.99.068302.

(27) Schubert, B. A.; Kaler, E. W.; Wagner, N. J. The Microstructure and Rheology of Mixed Cationic/Anionic Wormlike Micelles. *Langmuir* **2003**, *19* (10), 4079–4089. https://doi.org/10.1021/la020821c.

(28) Berret, J. F.; Appell, J.; Porte, G. Linear Rheology of Entangled Wormlike Micelles. *Langmuir* **1993**, *9* (11), 2851–2854. https://doi.org/10.1021/la00035a021.

(29) Rubenstein, M.; Colby, R. *Polymer Physics*; Oxford University Press: New York, 2003.

(30) Tang, X.; Zou, W.; Koenig, P. H.; McConaughy, S. D.; Weaver, M. R.; Eike, D. M.; Schmidt, M. J.; Larson, R. G. Multiscale Modeling of the Effects of Salt and Perfume Raw Materials on the Rheological Properties of Commercial Threadlike Micellar Solutions. *J. Phys. Chem. B* **2017**, *121* (11), 2468–2485. https://doi.org/10.1021/acs.jpcb.7b00257.

(31) Cates, M. E.; Fielding, S. M. Rheology of Giant Micelles. *Adv. Phys.* **2006**, *55*, 799-879. https://doi.org/10.1080/00018730601082029.

(32) Afifi, H.; Karlsson, G.; Heenan, R. K.; Dreiss, C. A. Solubilization of Oils or Addition of Monoglycerides Drives the Formation of Wormlike Micelles with an Elliptical Cross-Section in Cholesterol-Based Surfactants: A Study by Rheology, SANS, and Cryo-TEM. *Langmuir* **2011**, 7480–7492. https://doi.org/10.1021/la201026s.

(33) Francisco, K. R.; da Silva, M. A.; Sabadini, E.; Karlsson, G.; Dreiss, C. A. Effect of Monomeric and Polymeric Co-Solutes on Cetyltrimethylammonium Bromide Wormlike Micelles: Rheology, Cryo-TEM and Small-Angle Neutron Scattering. *J. Colloid Interface Sci.* **2010**, *345* (2), 351–359. https://doi.org/10.1016/j.jcis.2010.01.086.

(34) Peixoto, M. P. G.; Treter, J.; De Resende, P. E.; Da Silveira, N. P.; Ortega, G. G.; Lawrence, M. J.; Dreiss, C. A. Wormlike Micellar Aggregates of Saponins from Ilex Paraguariensis A. St. Hil. (Mate): A Characterisation by Cryo-TEM, Rheology, Light Scattering and Small-Angle Neutron Scattering. *J. Pharm. Sci.* **2011**, *100* (2), 536–546. https://doi.org/10.1002/jps.22283.

(35) Croce, V.; Cosgrove, T.; Maitland, G.; Hughes, T.; Karlsson, G. Rheology, Cryogenic Transmission Electron Spectroscopy, and Small-Angle Neutron Scattering of Highly Viscoelastic Wormlike Micellar Solutions. *Langmuir* **2003**, *19* (20), 8536–8541. https://doi.org/10.1021/la0345800.

(36) Kern, F.; Zana, R.; Candau, S. J. Rheological Properties of Semidilute and Concentrated Aqueous Solutions of Cetyltrimethylammonium Bromide in the Presence of Potassium Bromide. *Langmuir* **1991**, *7*, 1344–1351. https://doi.org/10.1021/la00038a020.

(37) Granek, R. Dip in G"(w) of Polymer Melts and Semidilute Solutions. *Langmuir* **1994**, *10* (7), 1627–1629. https://doi.org/10.1021/la00017a051.

(38) Kern, F.; Lemarechal, P.; Candau, S. J.; Cates, M. E. Rheological Properties of Semidilute and Concentrated Aqueous Solutions. *Langmuir* **1992**, *8* (2), 437–440. https://doi.org/10.1021/la00038a020.

(39) Candau, S. J.; Hirsch, E.; Zana, R. Light Scattering Investigations of the Behavior of Semidilute Aqueous Micellar Solutions of Cetyltrimethylammonium Bromide: Analogy with Semidilute Polymer Solutions. *J. Colloid Interface Sci.* **1985**, *105* (2), 521–528. https://doi.org/10.1016/0021-9797(85)90327-3.

(40) Oelschlaeger, C.; Schopferer, M.; Scheffold, F.; Willenbacher, N. Linear-to-Branched Micelles Transition: A Rheometry and Diffusing Wave Spectroscopy (DWS) Study. **2009**, *25*, 716–723. https://doi.org/10.1021/la802323x.

(41) Das, N. C.; Cao, H.; Kaiser, H.; Sokol, P. E.; Gladden, J. Shape and Size of Highly Concentrated Micelles in CTAB/NaSal Solutions by Small Angle Neutron Scattering (SANS). *Langmuir* **2012**, *28*, 11962-11968. https://doi.org/10.1021/la2022598.

(42) Aswal, V. K.; Goyal, P. S.; Thiyagarajan, P. Small-Angle Neutron-Scattering and Viscosity Studies of CTAB/NaSal Viscoelastic Micellar Solutions. *J. Phys. Chem. B* **2002**, *102* (14), 2469–2473. https://doi.org/10.1021/jp980181f.

(43) Mandal, T.; Koenig, P. H.; Larson, R. G. Nonmonotonic Scission and Branching Free Energies as Functions of Hydrotrope Concentration for Charged Micelles. *Phys. Rev. Lett.* **2018**, *121* (3), 38001. https://doi.org/10.1103/PhysRevLett.121.038001.

(44) Zou, W.; Tang, X.; Weaver, M.; Koenig, P.; Larson, R. G. Determination of Characteristic Lengths and Times for Wormlike Micelle Solutions from Rheology Using a Mesoscopic Simulation Method. *J. Rheol.* **2015**, *59* (4), 903–934. https://doi.org/10.1122/1.4919403.

(45) Mackintosh, F. C.; Safran, A.; Pincus, P. A. Self-Assembly of Linear Aggregates: The Effect of Electrostatics on Growth. *Epl* **1990**, *12* (8), 697–702. https://doi.org/10.1209/0295-5075/12/8/005.

(46) Parker, A.; Fieber, W. Viscoelasticity of Anionic Wormlike Micelles: Effects of Ionic Strength and Small Hydrophobic Molecules. *Soft Matter* **2013**, *9* (4), 1203–1213. https://doi.org/10.1039/c2sm27078a.

(47) Oelschlaeger, C.; Suwita, P.; Willenbacher, N. Effect of Counterion Binding Efficiency on Structure and Dynamics of Wormlike Micelles. *Langmuir* **2010**, *26* (10), 7045–7053. https://doi.org/10.1021/la9043705.

(48) Cardinaux, F.; Cipelletti, L.; Scheffold, F.; Schurtenberger, P. Microrheology of Giant-Micelle Solutions. *Eur. Lett* **2002**, *5* (57), 728–744. https://doi.org/10.1209/epl/i2002-00525-0.

(49) Bellour, M.; Skouri, M.; Munch, J. P.; Hébraud, P. Brownian Motion of Particles Embedded in a Solution of Giant Micelles. *Eur. Phys. J. E* **2002**, *8* (4), 431–436. https://doi.org/10.1140/epje/i2002-10026-0.

(50) Herle, V.; Kohlbrecher, J.; Pfister, B.; Fischer, P.; Windhab, E. J. Alternating Vorticity Bands in a Solution of Wormlike Micelles. *Phys. Rev. Lett.* **2007**, *99* (15), 1–4. https://doi.org/10.1103/PhysRevLett.99.158302.

(51) Clausen, T. M.; Vinson, P. K.; Minter, J. R.; Davis, H. T.; Talmon, Y.; Miller, W. G. Viscoelastic Micellar Solutions: Microscopy and Rheology. *J. Phys. Chem.* **1992**, *96* (1), 474–484. https://doi.org/10.1021/j100180a086.

(52) Shikata, T.; Hirata, H. Micelle Formation of Detergent Molecules in Aqueous Media: Viscoelastic Properties of Aqueous Cetyltrimethylammonium Bromide Solutions. *Langmuir* **1987**, *10*, 1081–1086. https://doi.org/10.1021/la00078a035.

(53) Shikata, T.; Sakaiguchi, Y.; Uragami, H.; Tamura, A.; Hirata, H. Enormously Elongated Cationic Surfactant Micelle Formed in CTAB-Aromatic Additive Systems. *J. Colloid Interface Sci.* **1987**, *119* (1), 291–293. https://doi.org/10.1016/0021-9797(87)90271-2.

(54) Raghavan, S. R.; Fritz, G.; Kaler, E. W. Wormlike Micelles Formed by Synergistic Self-Assembly in Mixtures of Anionic and Cationic Surfactants. *Langmuir* **2002**, *18* (10), 3797–3803. https://doi.org/10.1021/la0115583.

(55) Agrawal, N. R.; Yue, X.; Raghavan, S. R. The Unusual Rheology of Wormlike Micelles in Glycerol: Comparable Timescales for Chain Reptation and Segmental Relaxation. *Langmuir* **2020**, *36* (23), 6370–6377. https://doi.org/10.1021/acs.langmuir.0c00489.

(56) Rehage, H.; Hoffmann, H. Viscoelastic Surfactant Solutions:Model Systems for

Rheological Research. *Mol. Phys.* **1991**, *74* (5), 933–973. https://doi.org/10.1080/00268979100102721.

(57) Kalur, G. C.; Raghavan, S. R. Anionic Wormlike Micellar Fluids That Display Cloud Points: Rheology and Phase Behavior. *J. Phys. Chem. B* **2005**, *109* (18), 8599–8604. https://doi.org/10.1021/jp044102d.

(58) Rehage, H.; Hoffmann, H. Rheological Properties of Viscoelastic Surfactant Systems. *J. Phys. Chem.* **1988**, *92* (16), 4712–4719. https://doi.org/10.1021/j100327a031.

(59) Calabrese, M. A.; Wagner, N. J. Detecting Branching in Wormlike Micelles via Dynamic Scattering Methods. *ACS Macro Lett.* **2018**, *7*, 614–618. https://doi.org/10.1021/acsmacrolett.8b00188.

(60) Wang, Z.; Larson, R. G. Molecular Dynamics Simulations of Threadlike Cetyltrimethylammonium Chloride Micelles: Effects of Sodium Chloride and Sodium Salicylate Salts. *J. Phys. Chem. B* **2009**, *113* (42), 13697–13710. https://doi.org/10.1021/jp901576e.

(61) Spenley, N. A.; Cates, M. E.; Mcleish, T. C. B. Nonlinear Rheology of Wormlike Micelles. *Phys. Rev. Lett.* **1993**, *71* (6), 939–942. https://doi.org/10.1103/PhysRevLett.71.939.

(62) Aït-Ali, A.; Makhloufi, R. On the Nonlinear Rheology of a Wormlike Micellar System in the Presence of Sodium Salicylate Salt. *J. Rheol.* **1997**, *41* (2), 307–318. https://doi.org/10.1122/1.550878.

(63) Yesilata, B.; Clasen, C.; McKinley, G. H. Nonlinear Shear and Extensional Flow Dynamics of Wormlike Surfactant Solutions. *J. Nonnewton. Fluid Mech.* **2006**, *133* (2–3), 73–90. https://doi.org/10.1016/j.jnnfm.2005.10.009.

(64) Berret, J. F. Transient Rheology of Wormlike Micelles. *Langmuir* **1997**, *13* (8), 2227–2234. https://doi.org/10.1021/la961078p.

(65) Bhardwaj, A.; Miller, E.; Rothstein, J. P. Filament Stretching and Capillary Breakup Extensional Rheometry Measurements of Viscoelastic Wormlike Micelle Solutions. *J. Rheol.* **2007**, *51* (4), 693–719. https://doi.org/10.1122/1.2718974.

(66) Miller, E.; Clasen, C.; Rothstein, J. P. The Effect of Step-Stretch Parameters on Capillary Breakup Extensional Rheology (CaBER) Measurements. *Rheol. Acta* **2009**, *48* (6), 625–639. https://doi.org/10.1007/s00397-009-0357-9.

(67) Omidvar, R.; Wu, S.; Mohammadigoushki, H. Detecting Wormlike Micellar Microstructure Using Extensional Rheology. *J. Rheol.* **2019**, *63* (1), 33–44. https://doi.org/10.1122/1.5050387.